KU LEUVEN

ARENBERG DOCTORAL SCHOOL
FACULTY OF SCIENCE

DNA ANALYSIS WITH THE BIOLOGICAL NANOPORE CLYA

Lorenzo Franceschini

Supervisor:
Prof. dr. Giovanni Maglia

Dissertation presented in partial fulfillment of the requirements for the degree of Doctor in Science

February 2016

DNA ANALYSIS WITH THE BIOLOGICAL NANOPORE CLYA

Lorenzo FRANCESCHINI

Examination Committee:

Prof. dr. Marc De Maeyer[1], chair
Prof. dr. Giovanni Maglia[1-2], supervisor
Prof. dr. Johan Robben[1]
Prof. dr. Hideaki Mizuno[1]
Prof. dr. Enrico Carlon[1]
Prof. dr. David Rodriguez–Larrea[3]

1-University of Leuven
2-University of Groningen
3-University of the Basque Country

Dissertation presented in partial fulfillment of the requirements for the degree of Doctor in Science

February 2016

Uitgegeven in eigen beheer, Lorenzo Franceschini, Celestijnenlaan 200G box 2413, B-3001 Heverlee (Belgium)

Acknowledgement

My deepest thanks go to my family, my partner and friends. Your love inspired me and supported me through the many difficulties of this long journey. I'm blessed by your presence in my life and with you at my side I feel I can face any further challenge for the future.

Many thanks go to my supervisor and all the colleagues for contributing to my work and to IWT for funding my research.

A warm thank you to the many colleagues from the G building and to Belgium, thank you for your kindness and acceptance.

Leuven, February 2016.
Lorenzo Franceschini

In loving memory of my father,
Giovanni Franceschini, 1946-2013.

Abstract

The transport of nucleic acids through nano-scale pores is an important biological process that occurs in all-living cells and has received strong interest for the many possible applications that can be exploited, such as fast and inexpensive DNA sequencing. Nanopore-based sensors are attractive tools for low cost and high-throughput nucleic acids analyses at single molecule level and with atomic resolution. When a nanopore is reconstituted in an artificial lipid membrane, in aqueous solution and under an electrical applied potential, ions are conducted through the nanopore generating a net ionic current. Nucleic acids can enter the pore and provide a characteristic current signature, which can be used for their identification. The biological nanopores alpha haemolysin and porin A have been extensively employed for DNA analyses. However, their small inner lumen (<1.5 nm) allows the translocation of ssDNA molecules only. Enabling dsDNA translocation with biological nanopores is of particular importance for the future development of direct genomic applications such as DNA mapping analysis. In the present study we employed the Cytolysin A (ClyA) nanopore as a biosensor for the analysis of nucleic acids. The ClyA pore inner constriction (3.3 nm) is large enough for the translocation of both single and double-stranded DNA molecules. We demonstrated DNA translocation through ClyA nanopore at high salt concentration (2.5 M NaCl). We found that at this condition dsDNA molecules could be permanently captured inside the ClyA pore, while ssDNA capture was only transient. Exploiting this finding, we engineered the nanopore to build a nano-machine, which could recognize and selectively transport a specific DNA molecule across a biological membrane. In another implementation ClyA pores were engineered to translocate DNA through the pore also at lower ionic strengths. DNA translocation at physiological salt concentration could be advantageous for the investigation with nanopores of drugs or biomarkers that can specifically bind to DNA molecules only at low-salt conditions. The resulting ClyA mutant demonstrated translocation and single molecule detection of both ssDNA and dsDNA molecules at physiological salt concentration (0.15 M NaCl). The results obtained in this thesis describe the electrostatic and entropic barriers that regulate the transport of DNA molecules through the biological nanopore ClyA and might contribute to the further design of new applications for the analysis of nucleic acids with nanopore-based biosensors.

Beknopte samenvatting

Het transport van nucleïnezuren door nanoporiën is een belangrijk biologisch proces dat in alle levende cellen voorkomt en een sterke belangstelling heeft omwille van de vele mogelijke toepassingen zoals snelle en goedkope DNA sequentiebepaling. Nanoporie-gebaseerde sensoren zijn aantrekkelijke hulp-middelen voor goedkope en hogedoorvoeranalyse van nucleïnezuren op single-molecule niveau. Wanneer een nanoporie in een artificieel lipidemembraan ingebracht wordt, in een waterige oplossing en onder een elektrische potentiaal, worden ionen door de porie geleid wat een ionische stroom generert. Nucleïnezuren kunnen in de porie gaan en een karakteristieke stroom genereren die gebruikt kan worden voor hun identificatie. De biologische nanoporiën alpha hemolysin en porin A werden reeds uitvoerig gebruikt voor DNA-analyses. Hun kleine binnendiameter (<1.5 nm), laat echter enkel de translocatie van enkelstrengige (ssDNA) moleculen toe. Het toelaten van translocatie van dubbelstrengig DNA (dsDNA) met biologische nanoporiën is van bijzonder belang voor de ontwikkeling van directe genomische toepassingen zoals DNA-kartering. In dit onderzoek gebruikten we de nanoporie Cytolysin A (ClyA) als een biosensor voor de analyse van nucleïnezuren. De binnenste constrictie van ClyA (3.3 nm) is groot genoeg voor de translocatie van zowel enkel als dubbelstrengige DNA-moleculen. We toonden DNA-translocatie door de ClyA-nanoporie aan bij hoge zoutconcentratie (2.5 M NaCl). We ontdekten dat bij deze conditie dsDNA-moleculen permanent gevangen konden worden in de ClyA-porie, terwijl ssDNA slechts transiënt gevangen wordt. We gebruikten deze bevindingen om de nanoporie om te bouwen tot een nanomachine, die een specifiek DNA-molecule kon herkennen en selectief transporteren doorheen een biologisch membraan. In een andere implementatie werden ClyA-poriën gemanipuleerd om DNA ook bij lagere ionische sterkte te transloceren door de porie. DNA-translocatie bij fysiologische zoutconcentratie kan voordelig zijn voor het onderzoeken van geneesmiddelen of biomerkers die enkel specifiek binden aan DNA-moleculen in lagezoutcondities. De resulterende ClyA-variant toonde translocatie en single-molecule-detectie van zowel ssDNA-als dsDNA-moleculen bij fysiologische zoutconcentraties (0.15 M NaCl). De resultaten bekomen in deze thesis beschrijven de elektrostatische en entropische bijdragen die het transport van DNA-moleculen door de biologische nanoporie ClyA reguleren en kunnen bijdragen tot de verdere ontwikkeling van nanoporie-gebaseerde biosensoren voor de analyse van nucleïnezuren.

Table of Contents

Abbreviations

ClyA	Cytolysin A
αHL	Alpha haemolysin
MspA	*Mycobacterium smegmatis* porin A
φ29	Bacteriophage connector φ29
WT	Wild-type
PDB	Protein data bank
PFT	Pore-forming toxin
ssDNA	Single-stranded deoxyribonucleic acid
dsDNA	Double-stranded deoxyribonucleic acid
poly-$(dN)_n$	Homopolymeric (dT, dA or dC) ssDNA strand, n = length
DNAP	DNA polymerase
SSN	Solid-state nanopore
SCR	Single channel recording
Bio	Biotin moiety
NA	Neutravidin
I_O	Open pore current
I_B	Blocked pore current
I_{RES}	Residual pore current ($I_{RES} = I_B / I_O$)

$I_{RES\%}$	Percentage residual pore current ($I_{RES} \times 100$)
t_{OFF}	Dwell translocation time
t_{ON}	Inter-event translocation time
DPhPC	1,2-diphytanoyl-sn-glycero-3-phosphocholine
SDS−PAGE	Sodium dodecyl sulfate polyacrylamide gel electrophoresis
BN-PAGE	Blue native polyacrylamide gel electrophoresis
IPTG	Isopropyl β−D−1−thiogalactopyranoside
OD	Optical density
LB	Luria broth microbial growth medium
2xYT	Yeast Extract & Tryptone liquid microbial growth medium
Ni-NTA	Nichel-nitrilotriacetic acid
EDTA	Ethylenediaminetetraacetic acid
TAE	Tris base, acetic acid and EDTA buffer
SDS	Sodium dodecyl sulfate
DDM	N-Dodecyl-β-D-maltoside
HPLC	High-performance liquid chromatography
PCR	Polymerase chain reaction
IDT	Integrated DNA Technologies

List of Figures

List of Supplementary Figures

List of Tables

Chapter 1

Introduction

1.1 The Cytolysin A nanopore

1.1.1 Pore-forming toxins

Cytolysin A (ClyA) also known as hemolysin E (HlyE), silent hemolysin and locus A (SheA) is a pore-forming toxin (PFT), a protein assembly synthesized by many enteric bacteria such as *Escherichia coli, Salmonella enterica* and *Shigella flexneri*[1–4]. ClyA disrupts membrane cells, forming transmembrane holes (nanopores) and consequently inducing cellular lysing during infection[5]. Target cells are many: erythrocytes, mammalian cells and macrophages[6]. Pore-forming toxins are virulence factors, which play an important role in bacteria pathogenesis, constraining bacterial growth and thereby contributing to chronic infections[7]. Their expression in bacteria is complex and regulated in response to environmental signals such as oxygen and glucose starvation[8–10]. Regulation of ClyA expression might differ in different species. In *E. coli* K-12, the ClyA promoter includes a site for the binding of two transcription factors: the regulator of Fumarate Nitrate Reduction (FNR) factor, which enhances protein expression in response to oxygen starvation[11] and the cAMP receptor protein (CRP) regulatory protein, which enhances protein expression in response to glucose starvation [11]. FNR and CRP regulation is under control of the histone-like nucleoid-structuring protein (H-NS)[9]. H-NS promotes CRP activation and inhibits FNR regulation[9]. Moreover, H-NS is antagonized by the negative effects of a further transcriptional regulator the *E. coli* SlyA factor[9,10], which is activated in response to amino acid starvation[9]. In *Salmonella enterica* serovar Typhi, ClyA promoter is organized in one operon regulated by the virulence-associated regulator PhoPQ[7]. The two-component system PhoPQ is activated by PhoQ, which works as a sensor of the host environment by sensing specific signals encountered during infection as antimicrobial peptides, cAMP and acidic pH[12]. Regarding pore assembly, a common characteristic for PFTs is their conversion from a soluble monomeric state to a membrane-embedded oligomeric pore complex[6]. The interesting large conformational change, which monomeric proteins need to undergo for pore

assembly has been investigated in the last two decades by employing multiple bio- chemical and physical approaches[6,13–15]. Hereby, it is reported the current knowledge of ClyA structure and function respectively for the monomer, protomer and assembled pore.

Figure 1-1 Alignments of ClyA sequences.
ClyA protein sequences from *E. coli* K12 (*E. coli*), *Salmonella* Typhi (*S*.Typhi) and *Salmonella* Paratyphi (*S*. Para). The sequence alignment shows not conserved residues in bold black letters on a on a grey background. Two cysteine residues are present in each sequence and underlined in red. Percentage identity 97.36% between *Salmonella* sequences (*S*.typhi and *S*.para), 89.4% and 90.76% respectively for *E. coli* and Parathypi or Thypi. The alignment was generated from Alignment Annotator (Bioinformatics).

1.1.2 **Monomeric ClyA crystal structure**

The atomic resolution structure of ClyA monomeric protein from the water soluble form, it reveals a rod-shaped molecule (34 kDa) consisting of a bundle of long and short helices ordered in two main domains: (a) a large tail domain containing five α-helices and (b) a small head domain, including two short α-helices, *N* and *C- termini* and a hydrophobic β-hairpin element named β-tongue region, which is responsible for membrane insertion[6,16–18] (Figure 1-2). There are two cysteine residues close to each other, respectively at position 86 and 285 (Figure 1-1), in the tail region. Disulphide bond formation due to residues oxidation might affect pore oligomeric state. A recent work showed that both reduced and oxidized ClyA monomers are active[13,19]; furthermore other studies, where these two cysteines

have been substituted with other residues showed active pores[20–22]. We refer as monomer to the monomeric protein unit, which during the oligomerization process is activated by a structural rearrangement into the "protomer" in order to form the assembled pore[18]. During the monomer structural rearrangement, few α-helices from the tail domain shift to the head domain separating the N and the C-terminal end (Figure 1-2).

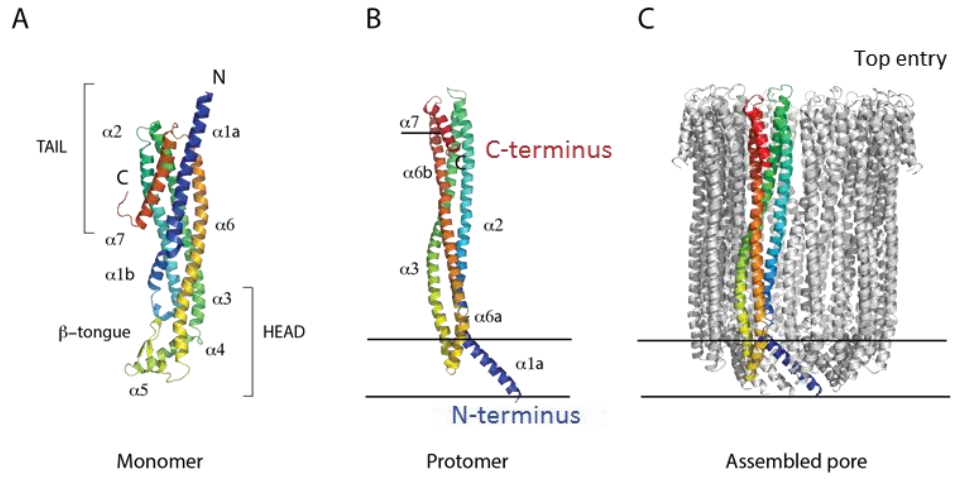

Figure 1-2 ClyA conformational states.
A Crystal structure of the ClyA water-soluble monomer. A ribbon representation shows a tail domain, presenting both C and N-terminal end of the protein, and a head domain containing the transmembrane region β-tongue. **B** During oligomerization the monomeric ClyA protein undergoes several conformational changes in order to form an assembled pore. The C and N-terminal end in the protomer are well separated comparing to the monomer structure and they are relocated in the assembled pore respectively at the pore top entrance and transmembrane side. **C** Single protomer representation (multicolor) embedded in a ClyA pore (grey). Figure are generated with PyMol from ClyA crystal structure (PDB code: 2WCD)[18].

1.1.3 ClyA assembled pores

Assembly of ClyA monomers into oligomer cylinder-shaped pores can be achieved *in vitro* by addition of detergents or membranes[14,17]. The Crystal structure for ClyA nanopores (Figure 1-3A, PDB code: 2WCD) shows a hollow cylinder-shaped pore with a height of 130 Å, an inner and outer diameter at the wider opening (top side) respectively of 70 and 105Å and at the narrowest opening (trans-membrane side) of respectively 40 and 90 Å[18] (Figure 1-3A). Electron microscopy micrographs of ClyA pores (Figure 1-3C) embedded into lipid membranes revealed that the pore is inserted perpendicular to the membrane with a central aperture of variable size for the internal diameter (75, 85 and 95 Å) and the pore three-dimensional reconstruction revealed a length of 140 Å for the height of the reconstituted pore[16]. These results suggest that the monomeric proteins (~100 Å height) undergo a large conformational change in order to form a functional pore (140 Å height) and moreover the assembly process generates a mixture of different oligomeric species (octameric, dodecameric, tridecameric pores)[6,13,14,22]. Tzokov et al.[14] and Hun et al.[23] were the first to propose a model which included monomeric conformational changes in order to form a functional pore.

The formation of cytolytic ClyA nanopores initiates with a structural rearrangement of the monomeric protein into a competent unit, leading to pore assembly[15]. The mechanisms of the large conformational change and pore formation are challenging to decode, due to the numerous and rapid transitional steps and involved intermediates. The latest proposed model for solving the monomeric conformational states and the pore assembly dynamics, employed a combination of single molecule fluorescence spectroscopy and complementary biophysical techniques, to gain precise information for each step involved in the pore formation[15]. Benke et al.[15] showed in their work the formation of a pathway intermediate resembling a molten globule[24,25], for the transition from the monomer to the protomer, which is the competent assembly unit for the pore formation. Förster resonance energy transfer (FRET) measurements[26] distinguished between

the monomer, intermediate, protomer and oligomer state, though could not discriminate between the different oligomeric species[15]. The oligomerization process was then investigated with photo-induced cross-linking assay[27]. According to the obtained results, protomers first assemble into low order structures as dimers or trimers, then into higher oligomers and complete assembled pores (Figure 1-3B). The assembly rate coefficient for the final association of oligomers into final pores is hundred times faster than the initially protomer oligomerization. Therefore, this ultimate model (Figure 1-3D) is supported by the combination of the data obtained from the Förster resonance energy transfer (FRET) analyses[26] for the monomer activation and from photo-induced cross-linking[27] and two-focus fluorescence correlation spectroscopy (2f-FCS) experiments[28] for the pore assembling. The model is based on the dodecameric ClyA structure from *E.coli K-12* deposited in the protein data bank (PDB code: 2WCD)[18], thus limited to a maximum number of 12 subunits for the complete pore. The model can be adjust considering a larger or smaller oligomeric state (than 12 subunits) for the final assembled pore[14], showing similar results[15].

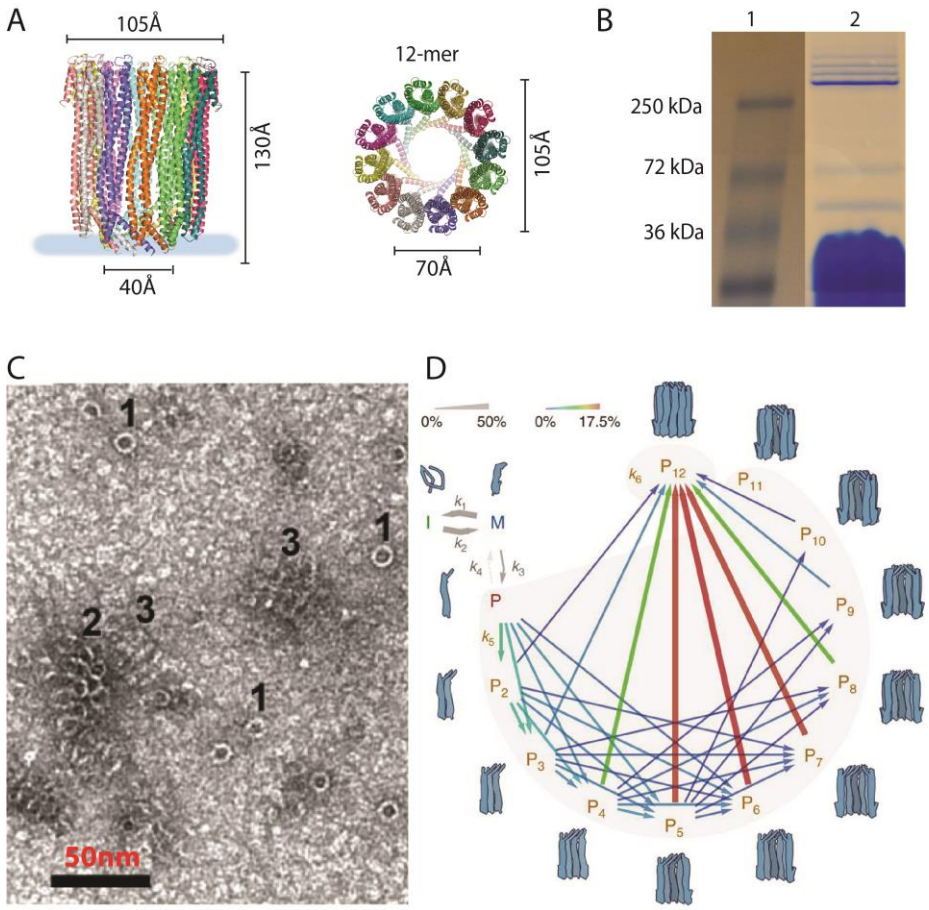

Figure 1-3 Assembled ClyA nanopores.
A Side and top view for ClyA nanopore. Each monomeric unit is represented in a different color. Size and protein sequence are based on the dodecameric ClyA (*E.coli* K- 12) crystal structure deposited in the protein data bank (PDB code: 2WCD)[18]. **B** ClyA monomer oligomerization bands from native blue gradient gel electrophoresis (4–15% polyacrylamide). **C** Electron microscopic micrograph of negatively stained HlyE pores in n-octyl-β-D-glucopyranoside. Individual pores (1) and small clusters in top view (2) are shown. Some clusters lie on the carbon film with the pores on their sides (3). Rare side views of individual ClyA pores are also captured. Pores (1) from three size groups (big, medium and small) were found. Scale bar_50 nm. **D** Pathways of ClyA pore formation. Arrows show the mass flux through the states of a non-sequential assembly model for a ClyA dodecamer nanopores. Grey arrows represent a conformational change between *I*, intermediate; *M*, monomer; *P*, protomer Colored arrows show oligomerization steps between P and Pi, oligomeric species. Widths and colors of the arrows correspond to the normalized flux from one state to another according to the scales shown at the top left. The relative fluxes in this model are independent to the ClyA concentrations tested (5 nM- 5 mM). Figures are reproduced from references 14, 15 and 18.

1.2 Biological nanopores

1.2.1 Small holes with great applications

Biological nanopores are nano-scale openings that form as protein channels in cell membranes. These membrane pores have been developed as biosensors in the last two decades (mid-'90s), for the detection and study of many analytes, such as nucleic acids and other biological or chemical compounds of biomedical interest [29–31]. Biological nanopores with different dimensions are constructed in nature and can be used for single molecule sensing analysis (Figure 1-4).

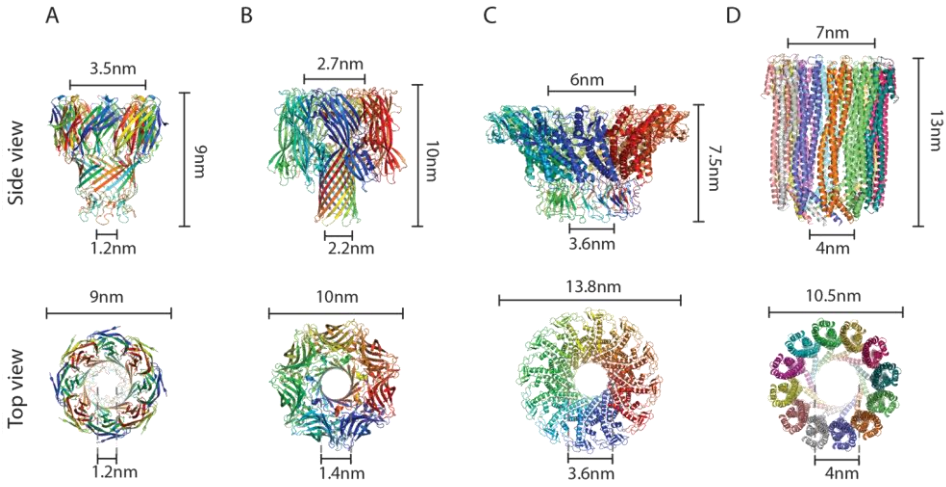

Figure 1-4 Biological nanopores.
Nanopores side and top view. **A** *Mycobacterium smegmatis* porin A (MspA, PDB code: 1UUN) its lower constriction at the pore bottom shows a narrow opening of 1.2 nm inner diameter. **B** Staphylococcal toxin alpha haemolysin (αHL, PDB code: 3ANZ), openings at the pore top and bottom are respectively 2.7 and 2.2 nm, a central narrowest constriction (1.4 nm) further reduces the inner pore diameter. **C** Bacteriophage φ29 connector (PDB code: 1IJG). It is the central component of a rotary motor that packages the genomic DNA during infection. The top and bottom openings show an inner diameter respectively of 6 and 3.6 nm. **D** *E. coli* K12 cytolysin A (ClyA, PDB code: 2WCD) the wide top opening 7 nm in diameter gradually reduces, outlining a funnel shaped inner pore lumen, down to the bottom opening 4 nm wide. Crystal structures are reproduced from references 18 and 32–34.

The technical principle of nanopore sensing is based on ion channels and the Coulter counter[35,36]. A single nanopore is reconstituted in an insulating planar lipid membrane separating two compartments (*cis* and *trans*) filled with electrolyte solution[37]. Ions are conducted through the pore and a net ionic current is generated under an applied electric potential. Single molecules added in solution can change this current when enter or translocate through the pore (Figure 1-5). It is possible to observe a specific current level when one molecule occupies the pore lumen. Each analyte can provide a characteristic change in the open pore current on the base of its size, structure and charge distribution. This specific modulating of the ionic current allows the identification and further discrimination of different molecules during translocation through the nanopore. Therefore, biological nanopores have been employed for sensing analysis for their ability to discriminate analytes at single molecule level[38]. Moreover, what makes these proteins attractive is that bacteria can produce large numbers of monomers (nanopore assembling unit) at low cost, which can assemble into nanopores with highly reproducible size and structure[32,33]. In addition, X-ray crystallography can provide information about the nanopore structure at nanometer scale, which can be used to tailor the physical and chemical properties of the nanopores by using simple mutagenesis techniques.

Among the many target analytes, nucleic acids are the most extensively studied[29,30,39–41]. Sequencing analysis with biological nanopores have attempted to provide a new tool for direct, fast and cheap sequencing of the human genome[42,43]. In particular, nanopores received strong interest for DNA sequencing applications, because they are reagent-free, amplification-free, label-free and promise long read lengths and high-throughput DNA analysis. The alpha haemolysin (αHL) nanopore first and afterwards porin A (MspA), from *Mycobacterium smegmatis*, have shown precise discrimination within nucleic bases in immobilized ssDNA inside the pores[44–47]. Because the nanopore small dimension, only single-stranded DNA or RNA molecules can be translocated through these pores; dsDNA (2.2 nm B form)[48,49] is too large to cross the inner pore constriction (1.2 and 1.4 nm respectively for MspA PDB code: 1UUN and αHL PDB code: 3ANZ, Figure 1-4).

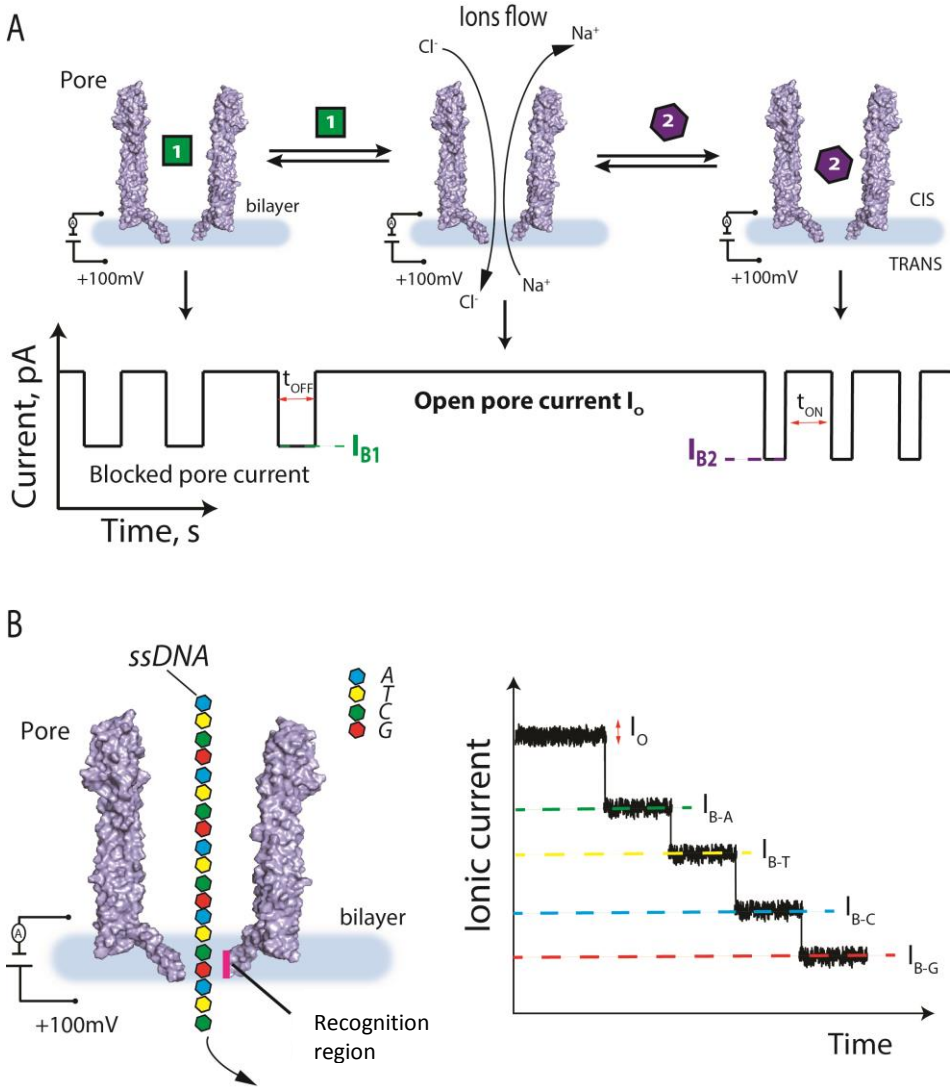

Figure 1-5 Nanopore sensing.
A Nanopore sensing analysis. Under applied potential ions from the electrolyte solution flow through the nanopore generating an ionic current (open pore current I_O). Analytes (1 and 2) can enter the pore and provide a characteristic current signature (blocked pore currents I_{B1} and I_{B2}), which can be used for their identification. We refer to the translocation time as t_{OFF} (dwell time) and to the time between two consecutive translocation events as t_{ON} (inter-event time interval). **B** Nanopore sequencing. Ideally during the translocation of ssDNA inside a nanopore, the open pore current (I_O) is reduced to a lower level (I_B), corresponding to one specific nucleo-base (I_{B-A}, I_{B-T}, I_{B-C} or I_{B-G}), which is passing a recognition region within the biological nanopore constriction. Nanopore representations A and B are generated from ClyA crystal structure deposited in the protein data bank (PDB code: 2WCD).

The bacteriophage connector φ29 has more recently emerged for the ability to translocate dsDNA molecules due to its larger inner pore diameter [50–52]. (φ29 connector 3.6 nm, PDB code: 1IJG, Figure 1-4). The importance of direct dsDNA translocation through biological nanopores is fundamental for the future development of direct analyses of genomic DNA samples, as mapping or genome profiling and furthermore allowing the investigation of DNA-protein interactions or the detection of drugs, that can specifically bind to dsDNA[20,53–55].

1.2.2 Nanopore sensing of nucleic acids

When a biological nanopore is reconstituted in an artificial lipid membrane, in aqueous solution and under an electrical applied potential, ions are conducted through the nanopore generating a net ionic current[37,56]. A DNA molecule can enter the pore and provide a characteristic current blockade event, which amplitude and duration time can be used to identify the molecule, while the frequency of events can be used to determine its concentration in solution[29,30]. The electrophoretic translocation of DNA molecules through biological nanopores is under intense investigation in the effort to develop a low-cost and high-speed new-generation DNA sequencing technology[42,43]. When a single-stranded DNA molecule is electrophoretically driven through a nanopore, ideally each DNA base is read out during translocation by measuring the modulation of the ionic current (*e.g.* Na^+ and Cl^-) as the DNA base passes a specific recognition site inside the pore[57] (Figure 1-5B, Figure 1-6).

The staphylococcal toxin alpha haemolysin (αHL) was the first biological nanopore that emerged as potential nanopore-based sequencer tool[30]. DNA analysis with αHL pores are limited to ssDNA molecules only due to the small pore inner constriction (1.4 nm, αHL PDB code: 3ANZ)[33], though dsDNA (2.2 nm B form)[49] is too large to directly cross the pore inner lumen[58]. When ssDNA molecules translocate through αHL pores, because of the high translocation speed, it is not possible to measure prompt changes in the ionic current corresponding to the molecule sequence[16]. DNA immobilization, giving longer time for the electrical read-out measurement, was used to test if the nanopore could effectively detect between different oligo sequences when immobilized inside the nanopore. Nucleo-base detection in ssDNA molecules with αHL nanopores, was observed by using a DNA-hairpin (dsDNA formation) or streptavidin (through biotin linkage) to immobilized under applied potential a ssDNA molecule inside the pore lumen[45,59]. Under applied potential the bulky DNA-hairpin or streptavidin prevent the full

translocation of the complexed ssDNA molecule, which upon capture occupies the full length of the pore[57,58,60].

Stoddart et al.[43] showed that when biotinylated ssDNA homopolymers poly (dC) and poly (dA) complexed with streptavidin are captured through αHL nanopores, it is possible to observe two current levels (block-pore current I_B or residual current $I_{RES\%} = I_B/I_O*100$) corresponding respectively to each homopolymer (Figure 1-6A). Furthermore, they investigated which region of the inner lumen is responsible for the homopolymer current blockades discrimination. They tested a set of ssDNA homopolymers (polydC) containing each a single adenine base substitution, exchanged at different positions corresponding from the top to the bottom of the αHL inner lumen pore. In this way, it was found that the αHL β-barrel contains three recognition regions, of which one in particular below the pore constriction could be further exploited to discriminate among the four nucleo-bases[45,61]. Indeed, four current levels were observed when ssDNA strands (poly-dC) that differed with a single base (A, T, G or C) at fixed position, corresponding to the recognition region in the middle pore β-barrel, were immobilized through a streptavidin biotin-linkage into the pore[61].

More recently, the biological nanopore porin A (MspA) from *Mycobacterium smegmatis* was used in nucleo-base discrimination, showing higher separation between the current levels corresponding to the four DNA bases immobilized inside the pore (> 10 times)[46,47] over αHL pores during experiments[57]. The MspA pore structure discloses a narrower and subtler constriction (1.2 nm wide and 0.6 nm height, MspA PDB code: 1UUN) at the trans-membrane entrance[32], which is the used recognition region inside the pore allowing precise nucleo-base detection (Figure 1-6B). Also MspA pore, as for α-haemolysin, can only allow the translocation of ssDNA molecules through the pore narrowest constriction and free translocation of ssDNA molecules is too fast for accurate sequence analyses[46,47]. Derrington et al.[44] showed that it is possible to employ MspA nanopores for continuous nucleo-base reading by using a duplex interrupted (DI) nanopore

sequencing approach (Figure 1-6B). They constructed a hybrid DNA polymer to reduce the DNA translocation speed through the MspA pore. This hybrid DNA contained alternate short dsDNA and ssDNA regions (duplex interrupted). Each ssDNA sequence contains three consecutive nucleotides AAA, TTT, CCC or GGG, which are read at the pore constriction during translocation. Under high-applied potential (+120 mV) the polymer is captured into the MspA lumen, but the short dsDNA regions delayed the full translocation through the pore. Subsequently to the polymer capture, because of the high-applied potential the dsDNA regions are one by one unzipped and the polymer can stepwise move forward for 14 nucleotides step at time (each dsDNA region) through the pore constriction. In this way, every dsDNA region temporary stops the polymer further threading through the pore. The time necessary to unzip the 14bp dsDNA is sufficient for the pore to provide a specific current read for the three nucleotides sequence (ssDNA region), which occupies the recognition site at the MspA narrow constriction during the polymer translocation[46,47].

This innovative work was designed to show a starting approach for slowing down free DNA translocation, allowing sequencing without DNA immobilization. Effectively, single base detection within the αHL and MspA pores, was only observed when the thread ssDNA molecule was immobilized inside the nanopore. Besides, one of the most crucial obstacles to overcome in the effort to develop a new nanopore technology for DNA sequencing is the high translocation speed of DNA molecules through the nanopores. DNA translocates through αHL pores at 1-3 μs/ base rate, which is prohibitively fast for accurate base reads from background noise[44]. Various approaches have been adopted to slow down the translocation speed, including using DNA hairpins or other duplex formation[45,59], rotaxanes[62], introducing positive charges inside the nanopore as molecular brakes[63] and furthermore alteration of experimental physical conditions such as increasing viscosity or salt concentration or decreasing the applied voltage[30,40,64,65]. Promising results were more recently shown by combining nanopores with DNA-processive enzymes, which can slow down the DNA translocation speed by controlling the

threading through the nanopore, base by base of the processed polymer. DNA polymerase and exonuclease enzymes have been employed with the biological nanopore alpha haemolysin and porin A from *Mycobacterium smegmatis* showing encouraging progress towards continuous DNA sequencing analyses.

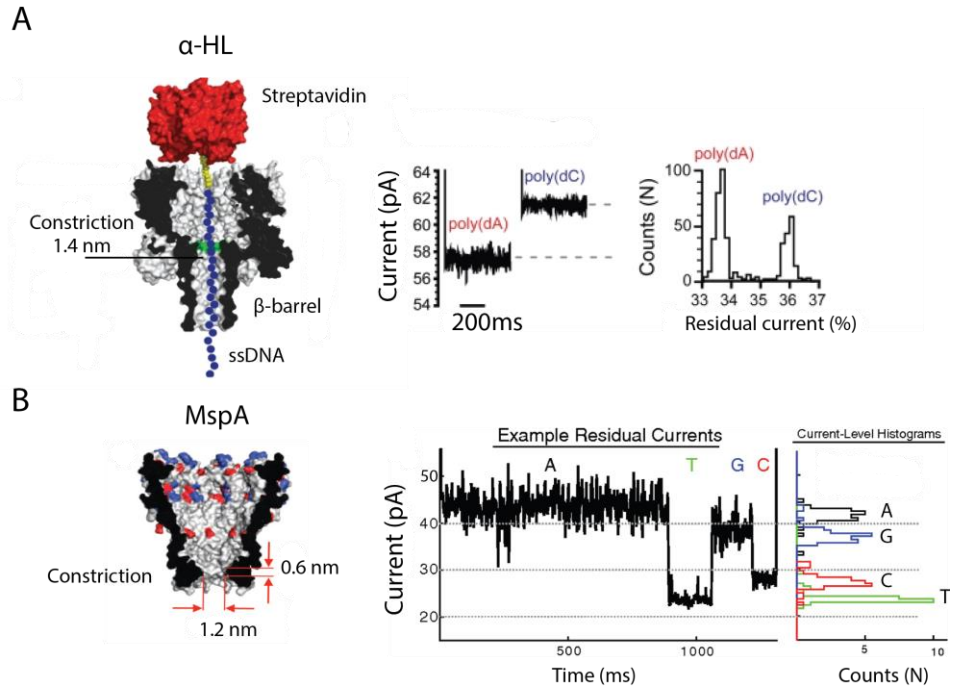

Figure 1-6 Biological nanopores for DNA sensing.
A Homopolymeric (60mer) DNA oligonucleotide (blue circles) is immobilized inside αHL pore (gray, cross-section) by using a biotin (yellow)–streptavidin (red) complex. Different current levels (right panel) showed when poly (dA) and poly (dC) polymers are respectively immobilized inside the pore. Event histogram represents the blockages number over the residual current level for the two oligonucleotides. **B** Cross-section for MspA nanopore (PDB code: 1UUN). Nearby the pore *trans* entrance a narrow constriction (1.2 nm width and 0.6 nm height.) originates the pore recognition region. Right panel, current trace for duplex interrupted (DI) nanopore sequencing. The sequencing information is carried between two consecutive dsDNA regions, which must be sequentially unzipped as the DNA is pulled through the pore, enabling the residual current to determine the sequence. Each step in the residual current is representative of three nucleotides within MspA constriction held by a 14 bp DNA duplex. Event histograms are generating for each of these steps. Figures A and B are adapted from references 45 and 46.

1.2.3 Nanopore-based sequencer systems

Due to noise in the measurement, the translocation speed of free nucleic acids through biological pores is too fast for accurate data acquisition included base identification during sequencing analysis[44]. The control of the DNA translocation speed is therefore fundamental not only for enabling sequencing but also for other applications for nanopores with nucleic acids, such as mapping, oligo length and concentration measurements[65]. Enzymes are used to control DNA translocation through the pore to allow the continuous and accurate identification of translocating molecules. In particular, two main nanopore-based approaches were designed for sequencing analyses with DNA-processive enzymes. One is based on sequencing of cleaved single nucleotides from a ssDNA molecule template by exonuclease enzymes[66] and the second method employs direct strand sequencing with a DNA polymerase enzyme (DNAP)[67].

Clarke et al.[68] showed one of the first strategies to combine a nanopore sequencer with a DNA processive enzyme. They used the *Escherichia coli* exonuclease I (EcoExoI) to process ssDNA molecules, which cleaved nucleotides are identified by the αHL pore (Figure 1-7A). The exonuclease EcoExoI binds to a ssDNA molecule in solution and upon activation starts cleaving individual nucleotides from the strand. Under an applied electrical potential the released nucleotides are translocated through an engineered αHL pore with a covalently attached adapter molecule (aminocyclodextrin) [68]. Different current levels, corresponding to each nucleoside 5' monophosphate molecule translocating through the pore, were detected with accuracies of 99.4, 90.3, 90.9 and 99.9% respectively for dGMP, dTMP, dAMP and dCMP under optimal enzyme operating conditions (200/ 500 mM KCl, 25 mM Tris-HCl, pH 7.5, +180 mV and room temperature)[68]. In order to integrate this base-detecting nanopore into an exonuclease sequencing system, the released dNMP flow into the pore has to reflect the template ssDNA molecule sequence. A possible solution could be the attachment of the enzyme to the nanopore. In this way the formed 5'-monophosphate nucleotide is promptly

released and read through the pore and the translocation order and time match the one from the template ssDNA sequence.

More recently DNA polymerases (DNAP) have been studied with biological nanopores alpha haemolysin[67,69] and porin A[70,71]. The *E. coli* DNA polymerase I Klenow fragment (the enzyme large fragment with the polymerase domain), the bacteriophages T7 and phi29 DNA polymerases[72–74] were proposed as molecular motors to control the movement of DNA in single-nucleotide steps through an αHL pore. In particular the phi29 DNA polymerase is remarkably processive[75,76], able to synthesize long DNA molecules (> 70 kb) and against high loading forces (37 pN)[77] necessary to drive the molecules inside the nanopore. During this approach the DNAP binds to a DNA molecule substrate, however the polymerase activity is inhibited by the absence of magnesium salt in solution. Under constant applied potential the formed complex (DNA strand plus enzyme) is captured through the nanopore. The DNAP prevents the full translocation of the binding DNA molecule, which occupies the pore inner lumen (Figure 1-7B). Upon enzyme activation (by adding magnesium salt and dNTP) the polymerase reaction can start: the enzyme moves the ssDNA strand base by base against the applied potential to originate the double-stranded DNA. Each DNA base is read out by measuring the modulation of the ionic current as the DNA bases slowly pass a specific recognition site inside the pore. After polymerization the new synthetized dsDNA is released and a new complex can be captured through the pore.

Manrao et al.[70] used the MspA pore combined with the phi29 DNAP (Figure 1-7B). They showed the current patterns associated with two consecutive different processes, the translocation and subsequently phi29 DNAP synthesis of a hybrid ss/dsDNA oligo[46], enabling sequence reading of known DNA molecules[70]. The phi29 DNAP binds to a hybrid ss/dsDNA oligo (blocking oligomer) and under applied potential the complex (DNA-oligo/ DNAP) is captured through the MspA pore. The translocation time is delayed from the unzipping of short dsDNA regions in the polymer sequence as previously described from Derrington et al[46]. Steady

current levels are measured during translocation corresponding to three consecutive nucleotides included in the polymer ssDNA sequences (AAA, TTT, GGG and CCC, Figure 1-7B). Also, two consecutive abasic residues (bulky chemically-modified nucleo-base indicated as X) were introduced in the polymer sequence, generating a distinct high current peak when passing through the pore constriction. As the characteristic current enhancement was measured, the phi29 DNAP was activated starting the polymerase reaction. Consequently to the enzyme activation, the phi29 DNAP pulls the DNA strand backwards through the pore against the applied potential. Same current levels, previously observed during translocation, are shown as the bases are moved backwards through the pore constriction during the polymerization process (Figure 1-7B). Moreover, the abasic residues (XX) current enhancement was observed in the current trace during translocation and afterwards during synthesis, helping to easily address the execution of both processes in the experiment (Figure 1-7B).

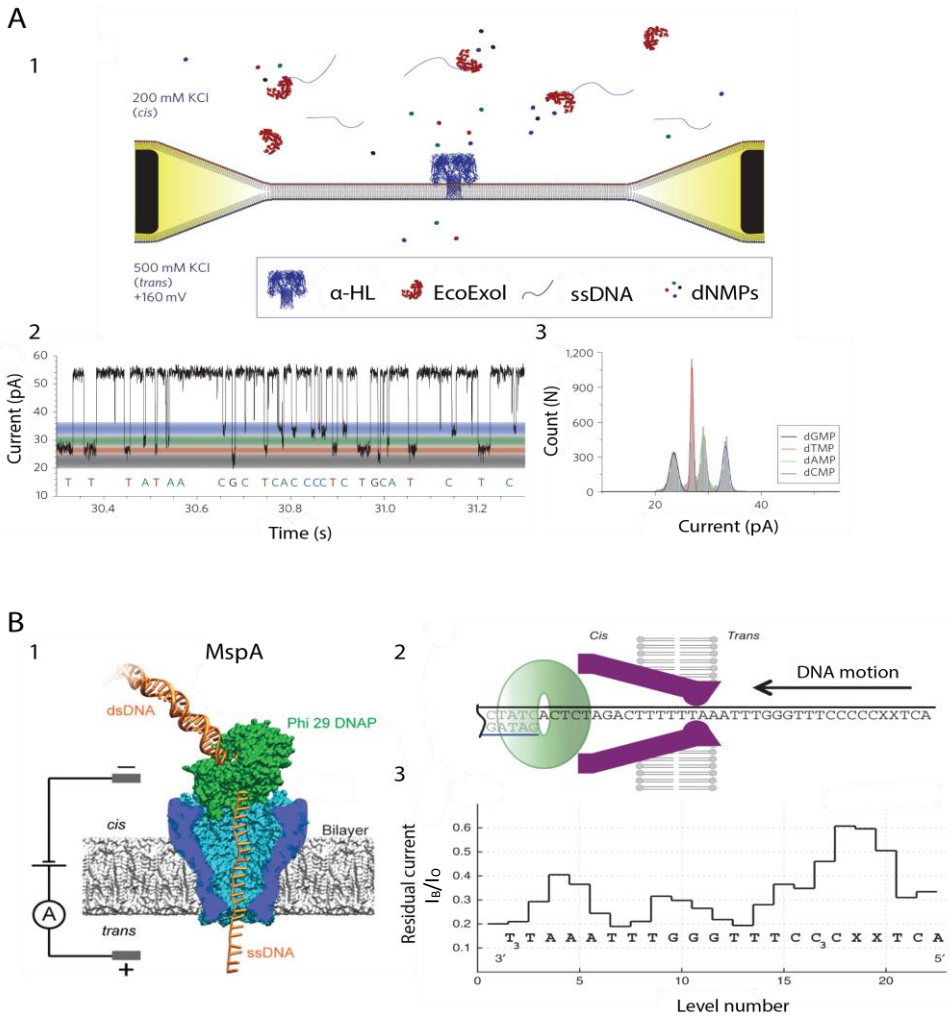

Figure 1-7 Nanopore-based sequencer systems.
A 1. Single nucleotides are cleaved from ssDNA strands by exonuclease EcoExoI. Nucleotides are released and translocated through an engineered αHL. **2.** Current trace for dGMP, dTMP, dAMP and dCMP translocation. Each current level (colored bands) corresponds to one specific translocated nucleotide. **3.** Histogram peaks representation for nucleotide translocation events, showing Gaussian fits. **B 1.** MspA nanopore (blue) embedded in a phospholipid bilayer (grey) and coupled with the DNA polymerase phi29 (green) processing a DNA strand (orange). **2-3.** Cartoon representation and related mean currents of levels extracted from typical current traces during DNA polymerization with phi29**.** The current plot, associate with the DNA sequence, shows the produced current level during synthesis by phi29 DNAP for multiple thymines (dT4) at the beginning of the read (Ib /Io ~ 0.20), dA3 (Ib /Io ~ 0.40), dG3 (Ib /Io ~ 0.30) and for two abasic residues (X) at the end of the read (Ib /Io ~ 0.61). Figures A and B are reproduced from references 68 and 70.

1.2.4 DNA translocation and nanopore engineering

Nucleic acids analysis with membrane nanopores is an advantageous process that has received strong interest for the many possible applications that can be exploited[38]. In particular, the biological nanopores alpha haemolysin (αHL) and porin A (MspA) have been extensively used for single-stranded DNA analyses, trying to develop a cheap and fast sequencing technology, where a stretch of a few nucleotides in a ssDNA is quickly read out as it translocates through a nanopore[44]. However, direct dsDNA analyses with the αHL or the MspA pore are not possible, because of their narrow inner pore constriction[32,33] (αHL PDB code: 3ANZ and MspA PDB code: 1UUN, Figure 1-4), which allows only the translocation of ssDNA molecules[58]. Enabling the translocation of double-stranded DNA molecules is advantageous because it could be exploited for the development of dsDNA applications such as DNA mapping analysis[54] with biological nanopores. More recently, the bacteriophage connector φ29 has emerged for the ability to translocate dsDNA molecules (2.2 nm B form)[49] due to its larger inner pore size[50–52] (φ29 connector 3.6 nm inner pore constriction, PDB code: 1IJG, Figure 1-4). The φ29 nanopore is not found in nature as membrane pore, but originated from the DNA-packing motor connector from the φ29 bacteriophage that it is used to transfer dsDNA phage-plasmid into host cells[50]. Wendell et al.[50] showed that φ29 nanopores reconstituted into lipid bilayers allow the translocation of dsDNA molecules from one side to the other of the connectors[50,51]. Under applied potential, dsDNA molecules electrophoretically translocate through the φ29 connector reducing transiently the measured open pore current[51]. Interestingly, dsDNA could only pass through the connector channel in one direction when initiated from the trans-membrane side. No translocation events were observed when DNA molecules were added to the connector top wide entrance (Figure 1-8A). The many negatively charged residues at the top side and in the inner lumen of the connector, as shown from the pore crystal structure[20] (φ29 connector PDB code: 1IJG), might prevent DNA translocation through φ29 when initiated from the top entry (charge repulsions: the electrostatic effect). Nanopore engineering

can be exploited to favor DNA translocation by reducing the pore inner negative charge density. Several studies showed the dependency of DNA translocation on the inner pore charge distribution[47,78]. The MspA wild type (WT) inner pore lumen contains many negatively charged residues, which hamper the translocation of DNA through the pore[47]. Butler et al.[47] engineered the MspA-WT nanopore to be able to translocate DNA molecules. They replaced aspartate residues with asparagines at three different positions in the pore constriction region (3 sets of negative charges knocked out). The resulting MspA pore showed characteristic DNA translocation events (transient deep current reductions of the open pore current, ~5 blockades/ s), when under high-applied voltage ssDNA (poly- $(dT)_{50}$, 8 μM) was electrophoretically driven into the nanopore (Figure 1-8B). In another implementation, to improve the frequency of translocation events, additional negatively charged residues were replaced with positively charged residues (arginine and lysine residues) at three other positions inside the pore vestibule and top entrance (Figure 1-8B). The resulting MspA mutant showed 5 times fold higher frequency rate (~25 blockades/ s, 8 μM poly-$(dT)_{50}$) for DNA capture events[47]. In a more extensive study, Maglia et al.[78] tested the effect of multiple charged side-chain mutagenesis on the frequency of DNA translocation through αHL pores. They observed enhanced translocation of ssDNA molecules when glutamate residues at the WT pore constriction were replaced with asparagines (E111N-WT, 1 set of negative charges knocked out) or arginines were introduced to the top entrance of the αHL pore (M113R-WT, 1 set of positive charges added, Figure 1-8C). In addition, they showed that DNA current blockades presented different amplitude and duration time values. DNA events were classified in five different groups showing three conductance levels: open, mid and low-amplitude state (Figure 1-8C). On the basis of these results, they proposed a model for the interaction of DNA with the αHL pore. In order to translocate through the nanopore, DNA must first collide with the pore top entrance and enter the vestibule to further cross the whole inner lumen and exit from the opposite entrance. A DNA molecule can also be captured temporary inside the pore vestibule and eventually

exit from the same top entrance[78]. In this case it is indicated as DNA capture event and not translocation. However, the characteristic ionic current modulation associated with DNA interactions shows similar patterns for translocation or transient capture events. The effective translocation of a DNA molecule through a nanopore could be probed by PCR amplification of the translocated DNA molecules[30] or formation of a rotaxane[62]. Notably, rotaxanes are interlocked systems in which a linear molecule (DNA) is locked at each end by two bulky stoppers (streptavidin or DNA-hairpin) through a macrocyclic ring (nanopore). The rotaxane can be assembled only after translocation of the DNA molecule from one compartment to the other through the nanopore (see 3.3.2 Formation of a nanopore:DNA rotaxane, page 73). DNA capture and further translocation through the pore is not limited only from the negatively charged residues in the pore inner lumen (electrostatic repulsion effect[79,80]), other forces acting on DNA molecules during interaction with the nanopore have been described in different studies: 1) the electrophoretic force[30], 2) the electro-osmotic force[81] and 3) the entropic effect[82].

1) The DNA driven electrophoretic force depends on the electrical applied potential and its intensity: $F=zeV/a$, where z is the effective charge per base, e is the elementary unit charge, V is the electrostatic potential drop through the pore and a is the base-to-base distance along the DNA polymer[83]. Therefore, DNA translocation is a voltage dependent process, where the higher the applied voltage the higher the number of observed translocation events[30,65,78,83]. However, single channel recording from planar lipid bilayer never exceeds 300 mV applied-voltage, due to the bilayer and nanopore stability (see 2.3 Planar lipid bilayers). Biological nanopores can be sensitive to high-applied voltages during DNA detection measurements, generating a background high-noise level and spontaneous current blockade events (pore-gating) that invalidates the accurate electrical signal reading. The MspA-WT pore showed many pore gating events, spontaneous transient and long-lasting current blockades of the free pore ionic current, which

above +100 mV-applied voltage were so frequent that DNA detection experiments were not practical with this pore[47]. Butler et al.[47] substituted three aspartate residues at the pore trans-membrane entrance by single-point mutation. The nanopore engineering improved the pore voltage-stability and the resulting MspA mutant showed dramatically reduced frequency of gating events, making it possible to conduct DNA detection experiments at voltages even above 180 mV[47].

2) Another factor, that possibly affects DNA translocation, is the electro-osmotic effect[81,84]. The pore electro-osmosis is the solvent flow through the nanopore. Ions from the electrolyte solution (cations P^+ and anions P^-) translocate through the nanopore carrying water molecules, which generate the osmotic flow[35]. Nanopores can be cationic ($P^+ / P^- > 1$) or anionic ($P^+ / P^- < 1$) selective, therefore depending on the pore ionic permeability there will be a net flow of water going from one side to the other of the nanopore. The net osmotic flow might facilitate or hamper the entry of molecules inside the pore[78,81,85]. Gu et al.[86] engineered the αHL pore with charged cyclodextrins as molecular adapters to study the effect of charge modifications on the pore ionic permeability[86]. They showed that the electro-osmotic flow can be tuned by changing the inner pore charge density in the αHL pore and this might be exploited to promote DNA or other molecule translocation.

3) Ultimately there is an entropic effect that applies to entropic contributions such as the structural conformation of DNA molecules during interaction with the pore[82,84]. In particular ssDNA molecules can assume a coiled conformation at high ionic strenghts[87], which might limit the molecule capture frequency and further translocation by preventing one of the polymer end to thread through the pore[88]. Further, a coiled DNA confirmation might be too bulky to enter a nanopore inner lumen (Figure 1-4 Biological nanopores). However, DNA uncoiling can be facilitated by working at high-voltage applied and at low ionic strengths[89,90]. Applying high-voltage might help to pull one end of the coiled DNA molecule inside the nanopore favoring translocation[91]. While at low ionic strengths

the DNA phosphate-backbone charges are unscreened by the low counterion concentration in solution, therefore DNA molecules undergo a more linear conformation due to the intra-molecular charges repulsions[65,87,90]. However, if lowering the ionic strength solution promotes to linearize DNA molecules favoring threading through the nanopore, on the other hand increases the electrostatic repulsions between the DNA and the negatively charged residues inside the pore. Extensive nanopore engineering could be required to remove the inner pore negative charges to be able to translocate DNA molecules at low ionic strengths. In conclusion, nanopore engineering is a resourceful process, in which the precise modification of single residues in a biological nanopore might allow to reduce electrostatic repulsions with DNA molecules[78], tune the electro-osmotic flow[86] and improve the pore voltage-stability[47], making it possible to favor DNA translocation through a biological nanopore.

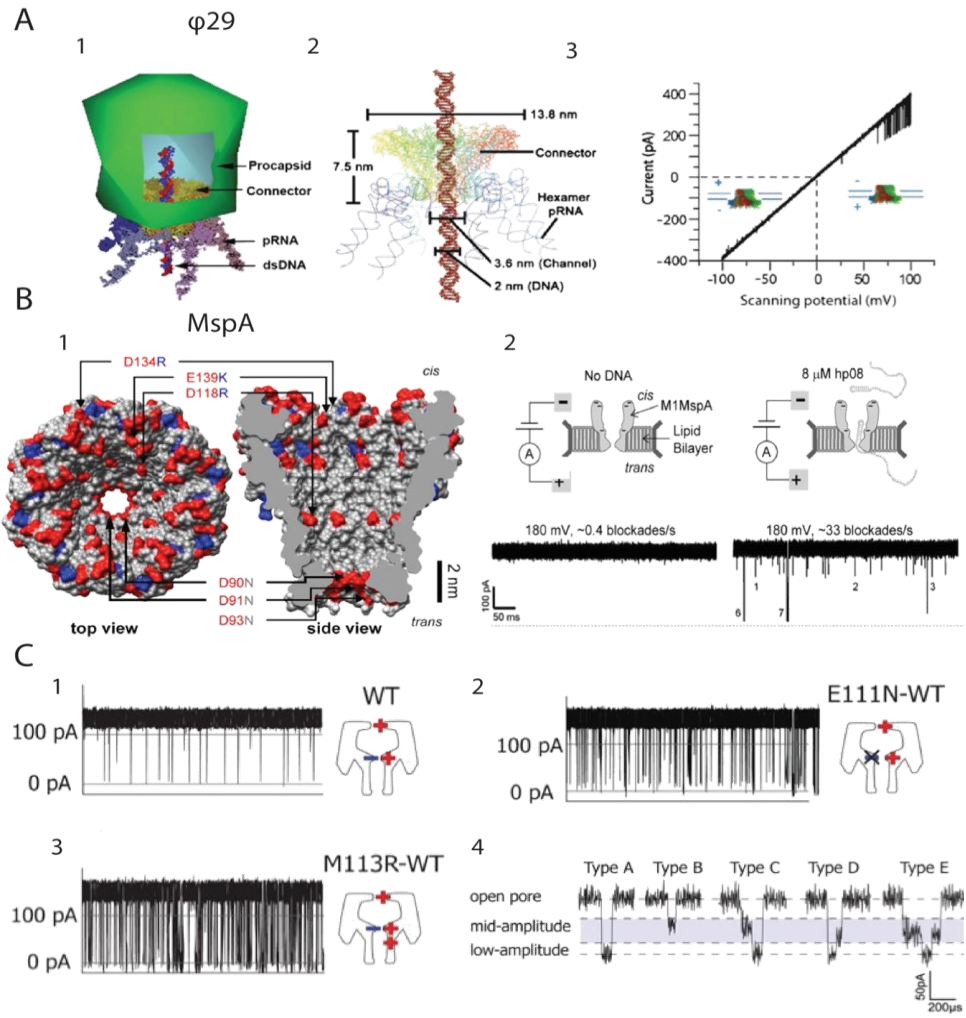

Figure 1-8 DNA translocation and nanopore engineering.
A 1-2. φ29 bacteriophage illustration and its DNA packaging motor showing DNA translocation through the connector. **3.** Unidirectional DNA translocation through φ29 connector. Voltage ramping from -100 mV to +100 mV with dsDNA added in both compartments with a single connector. Transient current blockades are shown during DNA translocation. **B 1.** MspA. The position number and identities for each tested mutation is indicated in the pore crystal structure. **2.** Experimental diagram for DNA detection experiments. Ionic current traces observed for MspA before and after adding 8 **μ**M DNA at 180 mV. **C** The effect of charged side-chain substitutions on DNA translocation with αHL pores. **1** αHL-WT (0.53 μM ssDNA). **2** E111N-WT (0.47 μM ssDNA). **3** M113R-WT (0.46 μM ssDNA). **4** Magnified current blockades from reported traces. Five representative events (Type A-E) are shown, each with a different amplitude level and variable dwelling time. Figure A, B and C are reproduced from references 47, 51 and 78.

1.2.5 Hybrid biological-solid-state nanopores

Biological nanopores have been employed in combination with solid-state nanopores (SSN) for the development of new experimental platforms to provide enduring and high-throughput DNA analyses[92,93]. Solid-state nanopores have been developed alongside with biological nanopores for single molecule analysis, including DNA sensing[94,95]. SSN are artificial nano–scale openings generated in a synthetic material by using different methods of fabrications. The most common materials used comprise from silicon nitride (Si_3N_4) as precursor[94], silicon dioxide (SiO_2)[96], aluminum oxide (Al_2O_3)[95], boron nitride (BN)[97] and more recently graphene[98]. The formation of an array of nanopores is generally achieved by direct irradiation of perforating particles (electrons or ions) on the surface of the selected material. Many techniques, such as: focused ion beam (FIB), electron-beam lithography and ion milling track-etch method, provide successful generation of multiple pores of desire size and shape with nanometer precision[95,96]. Among the main advantages offered by SSN such as robustness and endurance compared with lipid-based systems[95], the ability to tune size and shape of the pore[96] and the possibility to integrating with optical readout techniques[99], SSN have shown a lack in resolution for the discrimination of molecules of similar size[64,100]. Therefore hybrid nanopore systems were developed to overcome this limitation and improve the SSN detection performance (Figure 1-9). Hybrid biological-solid-state nanopore systems refer to two mainly arrays: a) surface functionalization of solid-state nanopores with biological compounds and b) joint together biological and solid-state nanopores. In the first case, there is a modification of the surface chemistry of SSN, which was used to help the precise detection and discrimination of DNA oligos and proteins[92,95]. Iqbal et al.[92] developed solid-state nanopore channels with DNA selectivity. A SiO_2 nanopore functionalized with hairpin DNA, showed to be able to distinguish ssDNA oligos completely complementary to the hairpin sequence from ssDNA oligos that differ even by a single nucleotide in the sequence, based on the translocation time (Figure 1-9A). In the second case, protein channels are inserted into a SSN array. Hall et al.[93] proposed a hybrid pore

formation by directed insertion of alpha haemolysin into SiN solid-state nanopores[93]. Alpha haemolysin pores were engineered with a dsDNA tail, which is captured through the SiN pore and under constant applied potential can pull the αHL pore atop the SiN pore (Figure 1-9B). Although DNA translocation results showed reduced ionic resolution for the current reads and enhanced electrical background noise compared to the planar lipid bilayer recordings with the α-HL pore, this ingenious setup can be further developed for high-throughput single molecule analysis.

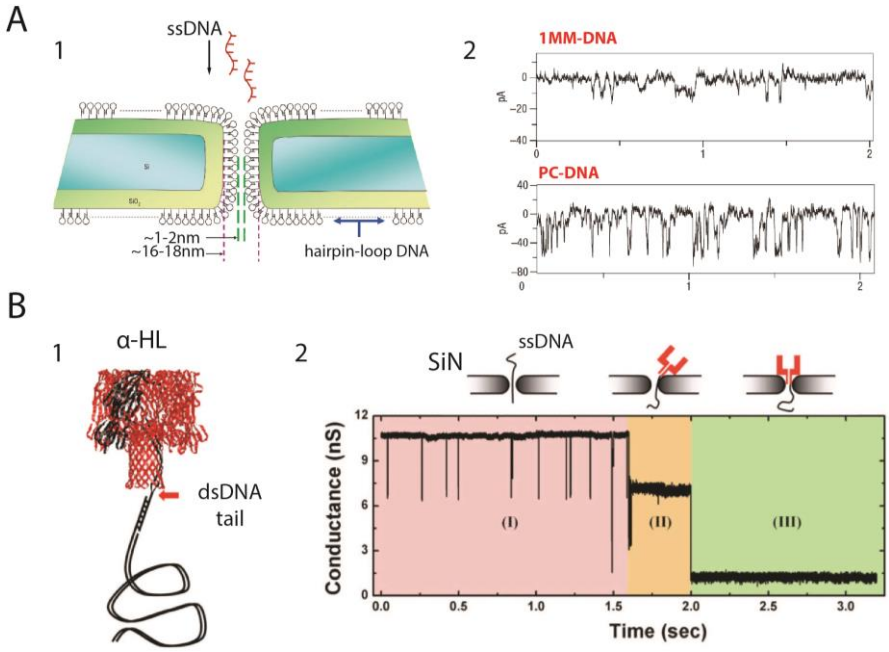

Figure 1-9 Hybrid biological-solid-state nanopores.
A 1. Schematic representation of a SiO_2 solid-state nanopore functionalized with hairpin DNA. **2.** Current traces show different translocation events through the hybrid nanopore for ssDNA oligos with a single base mismatch (1MM-DNA) or fully complementary (PC-DNA) to the hairpin sequence. **B 1.** Engineered αHL pore, showing an attached dsDNA tail, is pulled inside a SiN solid-sate nanopore by electrophoresis **2.** A current trace shows typical events for ssDNA translocation through SiN nanopore (I) and the formation of the hybrid nanopore in stages (II) and (III). Figures A and B are reproduced from references 92 and 93.

1.2.6 Nanopore applications and future challenges

Nanopores have been employed for the identification and quantification of a wide variety of analytes including both biological and chemical compounds such as nucleic acids[30], peptides and proteins[20,101], organic molecules[31,102] and enantiomers[103]. Nanopore-based sequencers have the potential to be developed as next-generation sequencing technique, which might accomplish the 1000$ human genome goal set by the National Institutes of Health of the United States of America[44]. The visionary prospective to sequence the human genome in less than one hour and at low cost, would bring radical progress in medicine and disease diagnosis[104]. At these conditions, fast and cheap, most of the people could afford to have their genome sequenced. Enabling easily reading of nucleic acids would not only drive towards personalized medicine[104,105], many more applications that are too expensive or unachievable with the actual techniques at the moment would also be possible. Nanopores can detect epigenetic markers or other base modifications[106], which can potentially be directly identified and their rule into genetic disorders or to cancer activation and promotion could be better understood[107,108]. The direct sequencing also of RNAs, which can lead to applications such the direct detection of non-coding RNA, has very promising applications[109]. Furthermore, beyond the classic DNA analysis such as sequencing and mapping, nanopores might be used to size, separate, identify and quantify nucleic acid molecules[40]. Among the many applications that can be envisaged, nanopores can be used not only to analyze but also to selectively transport nucleic acids[52]. Nanopores could mediate nucleic acids transportation through biological membranes and this could have important implications in drug delivery or gene therapy[110]. Among the many advantages, including fast readings, label-free, minimal sample requirements and preparation, promising long read lengths, portable hardware and low cost DNA sequencing[44]; nanopores have still important challenges to overcome for the future. A key limitation is the ultra-fast speed during free DNA translocation, which prevents the precise reading of DNA molecule sequences. The DNA translocation speed through nanopores is beyond

the resolution of existing optical or electrical technologies used in combination with the nanopores[44]. Therefore, slowing down DNA translocation will be still the main focus for the near future. Oxford Nanopore Technologies (ONT) has launched on the market two sequencing products: the GridION in 2012 and the MinION in 2013. The GridION is a bulky laboratory sequencing system containing changeable cartridges, each of which contains arrays of biological nanopores. The MinION is small, portable and single-use DNA sequencing device with the size a bit larger than a USB memory stick[111]. Though the preliminary reported analyses, for the genomic sequencing of *E. coli* K-12 generated with MinION devices, showed high error rates (90%)[49,114], more recent results demonstrated a considerable improvement on the analysis accuracy. Ashton et al.[113] in 2015 used MinION devices to investigate the chromosomal insertion site for the antibiotic resistance in *Salmonella enterica* serovar Typhi, haplotype H58. MinION sequencers could perform with a flow cells with more than 400 active nanopores each device, producing a maximum yield of 90 Mbp in 48 hours with considerably lowered error rates (30%)[113]. These latest results showed the real potential of the MinION device in clinical laboratories to study bacterial pathogens. Further improvements are still needed in MinION data quality and yield, although these results are very promising and encouraging for the future application of nanopore-based analysis tools on the human genome.

1.3 Aims and objectives of the research

The aim of this research project is to develop the biological nanopore Cytolysin A as a biosensor for single molecule detection of both ssDNA and dsDNA molecules. At present the biological nanopores alpha haemolysin and porin A have been extensively employed for ssDNA analyses showing in particular enormous progress towards DNA sequencing[110-114]. However, their small inner lumen (<1.5 nm) allows the translocation of ssDNA molecules only, limiting direct dsDNA molecule reading[4-6]. The ClyA inner pore constriction (3.3 nm) is large enough for the translocation of both single and double-stranded DNA molecules[6]. Enabling dsDNA translocation is of particular importance for the future development of genomic applications such as DNA mapping analyses with biological nanopores[54]. The drawing of genomic maps could be exploited for the identification of specific genomic sequences and their association with physiological disorders might be useful for biomedical applications[104]. In addition, ClyA inner pore cavity is large enough to allow the capture of small drugs or biological markers, which can specifically bind to DNA molecules during translocation and be subsequently identified through the nanopore[20,53]. However, DNA binding with biological or chemical compounds is often hampered by the high-ionic strength of the solution[20], which is required for precise current measurements with small nanopores[1,12,32]. ClyA large inner pore lumen allows a consistent ionic flow, which is still preserved at low ionic strengths providing a precise ionic current reading[20]. Moreover, ClyA pores could be ideal candidates for high-throughput DNA analyses integrated into single-molecule sequencing devices as the GridION or MinION (Oxford Nanopore Technologies), where DNA samples during analysis are processed and managed by DNA-processive enzymes at near physiological salt concentration[110-114]. On this direction, ClyA pores could be also used at physiological salt concentration for example to study the mechanism of action of enzymes that process nucleic acids in real-time and required low-ionic strength for their activity[67,69,73]. Therefore, performing DNA analyses at low-ionic strength would be particularly advantageous for ClyA

nanopores, enabling the development of the many applications only possible at near physiological salt concentrations.

Research objectives

Objective 1: DNA translocation through ClyA nanopore. In the first part of this research our goal was to demonstrate that DNA detection experiments with ClyA pores were practical. DNA detection analysis with a membrane nanopore is based on the electrophoretic entry and further translocation of a single DNA molecule inside the nanopore lumen in order to provide a characteristic ionic current blockade, which contains the information for the molecule identification[1,2]. The numerous negatively charged residues coating the inner pore lumen limit the DNA entry and further passage through the ClyA pores. Inspired from our previous work with the αHL pore[115], we sought to neutralize the overall negative inner pore charge by working at high ionic strength (2.5M NaCl). The electrostatic repulsions, between the pore inner negative charges and the negatively charged DNA molecules, were reduced by the screening effect of counterions from the concentrated electrolyte buffer solution. At this condition, DNA translocation was probed by the formation of a DNA/ protein rotaxane.

Objective 2: Specific recognition of DNA molecules with ClyA nanopore. Many nucleic acid applications, such as high-throughput analyses for nucleic acids detection, purification and concentration, require the specific recognition of one oligo in a DNA sample solution. We modified ClyA nanopore with ssDNA molecules chemically attached atop the pore to develop a nanopore machine able to detect and selectively transport a DNA oligo across a lipid membrane.

Objective 3: Engineering ClyA nanopore to translocate DNA at low ionic strengths. At physiological salt concentrations, ClyA pores could be used together with enzymes to assist DNA translocation during analyses[73]. Therefore, ClyA inner pore negative charge density was reduced to translocate DNA molecules through the pore at low ionic strengths. One of the most advantageous properties of

biological nanopores is that their structure can be controllably modified by precise residue replacements. Encouraged from previous works with the αHL and MspA pore[47,78], we engineered the ClyA pore by removing negatively charged residues or / and introducing positively charged residues at specific positions in the inner lumen.

Objective 4: Engineering ClyA nanopore to translocate DNA from the trans-membrane side of the pore. In another implementation, we engineered the ClyA pore transmembrane region to translocate DNA from the *trans* to the *cis* side of the pore. The numerous negatively charged residues at the pore *trans* entry hampered DNA translocation when initiated from this side of the pore at low ionic strengths. The introduction of positively charged residues, as observed for the *cis* side, might favor DNA translocation, allowing DNA analysis at both side of the ClyA pore.

1.4 References

1. Del Castillo, F.J., Leal, S.C., Moreno, F., Del Castillo, I., The Escherichia coli K-12 sheA gene encodes a 34-kDa secreted haemolysin. *Mol. Microbiol.* 25(1): 107–115 (1997).

2. Oscarsson, J., Mizunoe, Y., Li, L., Lai, X.H., Wieslander, A., Uhlin, B.E., Molecular analysis of the cytolytic protein ClyA (SheA) from Escherichia coli. *Mol. Microbiol.* 32(6): 1226–1238 (1999).

3. Wyborn, N.R., Stapleton, M.R., Norte, V.A., Roberts, R.E., Grafton, J., Green, J., Regulation of Escherichia coli hemolysin E expression by H-NS and Salmonella SlyA. *Microbiology* 186(6): 1620–1628 (2004).

4. Oscarsson, J., Westermark, M., Löfdahl, S., Olsen, B., Palmgren, H., Mizunoe, Y., Wai, S.N., Uhlin, B.E., Characterization of a pore-forming cytotoxin expressed by Salmonella enterica serovars Typhi and Paratyphi A. *Infect. Immun.* 70(10): 5759–5769 (2002).

5. Lai, X.H., Arencibia, I., Johansson, A., Wai, S.N., Oscarsson, J., Kalfas, S., Sundqvist, K.G., Mizunoe, Y., Sjöstedt, A., Uhlin, B.E., Cytocidal and apoptotic effects of the ClyA protein from Escherichia coli on primary and cultured monocytes and macrophages. *Infect. Immun.* 68(7): 4363–4367 (2000).

6. Wallace, A.J., Stillman, T.J., Atkins, A., Jamieson, S.J., Bullough, P.A., Green, J., Artymiuk, P.J., E.coli hemolysin E (HlyE, ClyA, SheA): X-ray crystal structure of the toxin and observation of membrane pores by electron microscopy. *Cell* 100(2): 265–276 (2000).

7. Faucher, S.P., Forest, C., Béland, M., Daigle, F., A novel PhoP-regulated locus encoding the cytolysin ClyA and the secreted invasin TaiA of Salmonella enterica serovar Typhi is involved in virulence. *Microbiology* 155(2): 477–488 (2009).

8. Green, J., Baldwin, M.L., The molecular basis for the differential regulation of the hlyE-encoded haemolysin of Escherichia coli by FNR and HlyX lies in the improved activating region 1 contact of HlyX. *Microbiology* 143(12): 3785–3793 (1997).

9. Hunt, S., Green, J., Artymiuk, P.J., Hemolysin E (HlyE, ClyA, SheA) and related toxins. *Adv Exp Med Biol.* 677: 116-26 (2010).

10. Westermark, M., Oscarsson, J., Mizunoe, Y., Urbonaviciene, J., Uhlin, B.E., Silencing and activation of ClyA cytotoxin expression in Escherichia coli. *J. Bacteriol.* 182(22): 6347–6357 (2000).

11. Ludwig, A., Bauer, S., Benz, R., Bergmann, B., Goebel, W., Analysis of the SlyA-controlled expression, subcellular localization and pore-forming activity of a 34 kDa haemolysin (ClyA) from Escherichia coli K-12. *Mol Microbiol.* 31(2): 557-567 (1999).

12. Prost, L.R., Miller, S.I., The Salmonellae PhoQ sensor: mechanisms of detection of phagosome signals. *Cell. Microbiol.* 10(3): 576–582 (2008).

13. Eifler, N., Vetsch, M., Gregorini, M., Ringler, P., Chami, M., Philippsen, A., Fritz, A., Müller, S.A., Glockshuber, R., Engel, A., Grauschopf, U., Cytotoxin ClyA from Escherichia coli assembles to a 13-meric pore independent of its redox-state. *EMBO J.* 25(11): 2652–2661 (2006).

14. Tzokov, S.B., Wyborn, N.R., Stillman, T.J., Jamieson, S., Czudnochowski, N., Artymiuk, P.J., Green, J., Bullough, P.A., Structure of the hemolysin E (HlyE, ClyA, and SheA) channel in its membrane-bound form. *J. Biol. Chem.* 281(32): 23042–23049 (2006).

15. Benke, S., Roderer, D., Wunderlich, B., Nettels, D., Glockshuber, R., Schuler, B., The assembly dynamics of the cytolytic pore toxin ClyA. *Nat. Commun.* 6(6198): 1–13 (2015).

16. Atkins, A., Wyborn, N.R., Wallace, A.J., Stillman, T.J., Black, L.K., Fielding, A.B., Hisakado, M., Artymiuk, P.J., Green, J., Structure-function relationships of a novel bacterial toxin, hemolysin E: The role of α G. *J. Biol. Chem.* 275(52): 41150–41155 (2000).

17. Ludwig, A., Völkerink, G., Von Rhein, C., Bauer, S., Maier, E., Bergmann, B., Goebel, W., Benz, R., Mutations affecting export and activity of cytolysin A from Escherichia coli. *J. Bacteriol.* 192(15): 4001–4011 (2010).

18. Mueller, M., Grauschopf, U., Maier, T., Glockshuber, R., Ban, N., The structure of a cytolytic alpha-helical toxin pore reveals its assembly mechanism. *Nature* 459(7247): 726–730 (2009).

19. Roderer, D., Benke, S., Müller, M., Fäh-Rechsteiner, H., Ban, N., Schuler, B., Glockshuber, R., Characterization of variants of the pore-forming toxin ClyA from Escherichia coli controlled by a redox switch. *Biochemistry* 53(40): 6357-6369 (2014).

20. Soskine, M., Biesemans, A., Maglia, G., Single-molecule analyte recognition with ClyA nanopores equipped with internal protein adaptors. *J. Am. Chem. Soc.* 137(17): 5793–5797 (2015).

21. Soskine, M., Biesemans, A., Moeyaert, B., Cheley, S., Bayley, H., Maglia, G., An engineered ClyA nanopore detects folded target proteins by selective external association and pore entry. *Nano Lett.* 12(9): 4895–4900 (2012).

22. Soskine, M., Biesemans, A., De Maeyer, M., Maglia, G., Tuning the size and properties of ClyA nanopores assisted by directed evolution. *J. Am. Chem. Soc.* 135(36): 13456–13463 (2013).

23. Hunt, S., Moir, A.J., Tzokov, S., Bullough, P.A., Artymiuk, P.J., Green, J., The formation and structure of Escherichia coli K-12 haemolysin E pores. *Microbiology* 154(2): 633–642 (2008).

24. Ptitsyn, O.B., Molten globule and protein folding. *Adv. Protein Chem.* 47: 83–229 (1995).

25. Ohgushi, M., Wada, A., 'Molten-globule state': a compact form of globular proteins with mobile side-chains. *FEBS Lett.* 164(1): 21–24 (1983).

26. Kuzmenkina, E.V, Heyes, C.D., Nienhaus, G.U., Single-molecule Forster resonance energy transfer study of protein dynamics under denaturing conditions. *Proc. Natl. Acad. Sci. USA.* 102(43): 15471–15476 (2005).

27. Fancy, D.A., Kodadek, T., Chemistry for the analysis of protein-protein interactions: rapid and efficient cross-linking triggered by long wavelength light. *Proc. Natl. Acad. Sci. USA.* 96(11): 6020–6024 (1999).

28. Dertinger, T., Pacheco, V., Von der Hocht, I., Hartmann, R., Gregor, I., Enderlein, J., Two-focus fluorescence correlation spectroscopy: a new tool for accurate and absolute diffusion measurements. *ChemPhysChem* 8(3): 433–443 (2007).

29. Deamer, D.W., Branton, D., Characterization of nucleic acids by nanopore analysis. *Acc. Chem. Res.* 35(10): 817–825 (2002).

30. Kasianowicz, J.J., Brandin, E., Branton, D., Deamer, D.W., Characterization of individual polynucleotide molecules using a membrane channel. *Proc. Natl. Acad. Sci. USA.* 93(24): 13770–13773 (1996).

31. Gu, L.Q., Braha, O., Conlan, S., Cheley, S., Bayley, H., Stochastic sensing of organic analytes by a pore-forming protein containing a molecular adapter. *Nature* 398(6729): 686–690 (1999).

32. Faller, M., Niederweis, M., Schulz, G.E., The structure of a mycobacterial outer-membrane channel. *Science* 303(5661): 1189–1192 (2004).

33. Gouaux, E., alpha-Hemolysin from Staphylococcus aureus: an archetype of beta-barrel, channel-forming toxins. *J. Struct. Biol.* 121(2): 110–122 (1998).

34. Simpson, A.A., Leiman, P.G., Tao, Y., He, Y., Badasso, M.O., Jardine, P.J., Anderson, D.L., Rossmann, M.G., Structure determination of the head-tail connector of bacteriophage phi9. *Acta Crystallogr D Biol Crystallogr.* 57(Pt 9): 1260–1269 (2001).

35. Aguilella, V.M., Alcaraz, A., The ionic selectivity of large protein ion channels. *Contrib. to Sci.* 4(1): 11–19 (2008).

36. Coulter, W.H., Means for Counting particles suspended in a fluid. US Patent No.2656508 (1953).

37. Maglia, G., Heron, A.J., Stoddart, D., Japrung, D., Bayley, H., Analysis of single nucleic acid molecules with protein nanopores. *Methods Enzymol.* 475: 591–623 (2010).

38. Bayley, H., Cremer, P.S., Stochastic sensors inspired by biology. *Nature* 413(6852): 226–230 (2001).

39. Howorka, S., Cheley, S., Bayley, H., Sequence-specific detection of individual DNA strands using engineered nanopores. *Nat. Biotechnol.* 19(7): 636–639 (2001).

40. Meller, A., Nivon, L., Brandin, E., Golovchenko, J., Branton, D., Rapid nanopore discrimination between single polynucleotide molecules. *Proc. Natl. Acad. Sci. USA.* 97(3): 1079–1084 (2000).

41. Meller, A., Branton, D., Single molecule measurements of DNA transport through a nanopore. *Electrophoresis* 23(16): 2583–2591 (2002).

42. Bayley, H., Sequencing single molecules of DNA. *Curr. Opin. Chem. Biol.* 10(6): 628–637 (2006).

43. Branton, D., Deamer, D.W., Marziali, A., Bayley, H., Benner, S.A., Butler, T., Di Ventra, M., Garaj, S., Hibbs, A., Huang, X., Jovanovich, S.B., Krstic, P.S., Lindsay, S., Ling, X.S.,Mastrangelo, C.H., Meller, A., Oliver, J.S., Pershin, Y.V., Ramsey, J.M., Riehn, R., Soni, G.V., Tabard-Cossa, V., Wanunu, M., Wiggin, M., Schloss, J.A., The potential and challenges of nanopore sequencing. *Nat. Biotechnol.* 26(10): 1146–1153 (2008).

44. Ashkenasy, N., Sánchez-Quesada, J., Ghadiri, M.R., Bayley, H., Recognizing a single base in an individual DNA strand: a step toward nanopore DNA sequencing. *Angew. Chem. Int. Ed. Engl.* 44(9): 1401–1404 (2005).

45. Stoddart, D., Heron, A. J., Mikhailova, E., Maglia, G., Bayley, H., Single-nucleotide discrimination in immobilized DNA oligonucleotides with a biological nanopore. *Proc. Natl. Acad. Sci. USA*. 106(19): 7702–7707 (2009).

46. Derrington, I.M., Butler, T.Z., Collins, M.D., Manrao, E., Pavlenok, M., Niederweis, M., Gundlach, J.H., Nanopore DNA sequencing with MspA. *Proc. Natl. Acad. Sci. USA*. 107(37): 16060–16065 (2010).

47. Butler, T.Z., Pavlenok, M., Derrington, I.M., Niederweis, M., Gundlach, J. H., Single-molecule DNA detection with an engineered MspA protein nanopore. *Proc. Natl. Acad. Sci. USA*. 105(52): 20647–20652 (2008).

48. Watson, J.D., Crick, F.H., Molecular structure of nucleic acids: a structure for deoxyribose nucleic acid. *Nature* 171(4356): 737-738 (1953).

49. Mandelkern, M., Elias, J.G., Eden, D., Crothers, D.M., The dimensions of DNA in solution. *J. Mol. Biol.* 152(1): 153–161 (1981).

50. Wendell, D., Jing, P., Geng, J., Subramaniam, V., Lee, T.J., Montemagno, C., Guo, P., Translocation of double-stranded DNA through membrane-adapted phi29 motor protein nanopores. *Nat. Nanotechnol.* 4(11): 765–772 (2009).

51. Jing, P., Haque, F., Shu, D., Montemagno, C., Guo, P., One-way traffic of a viral motor channel for double-stranded DNA translocation. *Nano Lett.* 10(9): 3620–3627 (2010).

52. Franceschini, L., Soskine, M., Biesemans, A., Maglia, G., A nanopore machine promotes the vectorial transport of DNA across membranes. *Nat. Commun.* 4: 2415 (2013).

53. Spiering, A., Getfert, S., Sischka, A., Reimann, P., Anselmetti, D., Nanopore translocation dynamics of a single DNA-bound protein. *Nano Lett.* 11(7): 2978–2982 (2011).

54. Neely, R.K., Deen, J., Hofkens, J., Optical mapping of DNA: single-molecule-based methods for mapping genomes. *Biopolymers* 95(5): 298–311 (2011).

55. Grada, A., Weinbrecht, K., Next-generation sequencing: methodology and application. *J. Invest. Dermatol.* 133(8): e11 (2013).

56. Sakmann, B., Neher, E. E., The patch clamp technique. *Sci Am.* 266(3): 44-51 (1992).

57. Stoddart, D., Heron, A.J., Klingelhoefer, J., Mikhailova, E., Maglia, G, Bayley, H., Nucleobase recognition in ssDNA at the central constriction of the αhemolysin pore. *Nano Lett.* 10(9), 3633–3637 (2010).

58. Akeson, M., Branton, D., Kasianowicz, J.J., Brandin, E., Deamer, D.W., Microsecond time-scale discrimination among polycytidylic acid, polyadenylic acid, and polyuridylic acid as homopolymers or as segments within single RNA molecules. *Biophys. J.* 77(6): 3227–3233 (1999).

59. Mathé, J., Visram, H., Viasnoff, V., Rabin, Y., Meller, A., Nanopore unzipping of individual DNA hairpin molecules. *Biophys. J.* 87(5): 3205–3212 (2004).

60. Vercoutere, W.A., Winters-Hilt, S., DeGuzman, V.S., Deamer, D., Ridino, S.E., Rodgers, J.T., Olsen, H.E., Marziali, A., Akeson, M., Discrimination among individual Watson–Crick base pairs at the termini of single DNA hairpin molecules. *Nucleic Acids Res.* 31(4): 1311–1318 (2003).

61. Stoddart, D., Maglia, G., Mikhailova, E., Heron, A.J., Bayley, H., Multiple base-recognition sites in a biological nanopore – two heads are better than one. *Angew. Chem. Int. Ed. Engl.* 49(3): 556–559 (2010).

62. Sánchez-Quesada, J., Saghatelian, A., Cheley, S., Bayley, H., Ghadiri, M.R., Single DNA Rotaxanes of a transmembrane pore protein. *Angew. Chem. Int. Ed. Engl.* 43(23): 3063–3067 (2004).

63. Restrepo, M.R., Mikhailova, E., Bayley, H., Maglia, G., Controlled translocation of individual DNA molecules through protein nanopores with engineered molecular brakes. *Nano Lett.* 11(2): 746–750 (2011).

64. Merchant, C.A., Healy, K., Wanunu, M., Ray, V., Peterman, N., Bartel, J., Fischbein, M.D., Venta, K., Luo, Z., Johnson, A.T., Drndić, M., DNA translocation through graphene nanopores. *Nano Lett.* 10(8): 2915–2921 (2010).

65. Meller, A., Nivon, L., Branton, D., Voltage-driven DNA translocations through a nanopore. *Phys. Rev. Lett.* 86(15): 3435–3438 (2001).

66. Astier, Y., Braha, O., Bayley, H., Toward single molecule DNA sequencing: Direct identification of ribonucleoside and deoxyribonucleoside 5'-monophosphates by using an engineered protein nanopore equipped with a molecular adapter. *J. Am. Chem. Soc.* 128(5): 1705–1710 (2006).

67. Cockroft, S.L., Chu, J., Amorin, M., Bayley, H., Ghadiri, M.R., A single-molecule nanopore device detects DNA polymerase activity with single-nucleotide resolution. *J. Am. Chem. Soc.* 130(3): 818–820 (2008).

68. Clarke, J., Wu, H.C., Jayasinghe, L., Patel, A., Reid, S., Bayley, H., Continuous base identification for single-molecule nanopore DNA sequencing. *Nat. Nanotechnol.* 4(4): 265–270 (2009).

69. Benner, S., Chen, R.J., Wilson, N.A., Abu-Shumays, R., Hurt, N., Lieberman, K.R., Deamer, D.W., Dunbar, W.B., Akeson, M., Sequence-specific detection of individual DNA polymerase complexes in real time using a nanopore. *Nat. Nanotechnol.* 2(11): 718–724 (2007).

70. Manrao, E.A., Derrington, I.M., Laszlo, A.H., Langford, K.W., Hopper, M.K., Gillgren, N., Pavlenok, M., Niederweis, M., Gundlach, J.H., Reading DNA at single-nucleotide resolution with a mutant MspA nanopore and phi29 DNA polymerase. *Nat. Biotechnol.* 30(4): 349–353 (2012).

71. Deamer, D., Nanopore analysis of nucleic acids bound to exonucleases and polymerases. *Annu. Rev. Biophys.* **39:** 79–90 (2010).

72. Berman, A.J., Kamtekar, S., Goodman, J.L., Lázaro, J.M., De Vega, M., Blanco, L., Salas, M., Steitz, T.A., Structures of phi29 DNA polymerase complexed with substrate: the mechanism of translocation in B-family polymerases. *EMBO J.* 26(14): 3494–3505 (2007).

73. Lieberman, K.R., Cherf, G.M., Doody, M.J., Olasagasti, F., Kolodji, Y., Akeson, M., Processive replication of single DNA molecules in a nanopore catalyzed by phi29 DNA polymerase. *J. Am. Chem. Soc.* 132(50): 17961–17972 (2010).

74. Kamtekar, S., Berman, A.J., Wang, J., Lázaro, J.M., De Vega, M., Blanco, L., Salas, M., Steitz, T.A., The φ29 DNA polymerase:protein-primer structure suggests a model for the initiation to elongation transition. *EMBO J.* 25(6): 1335–1343 (2006).

75. Kamtekar, S., Berman, A.J., Wang, J., Lázaro, J.M., De Vega, M., Blanco, L., Salas, M., Steitz, T.A., Insights into strand displacement and processivity from the crystal structure of the protein-primed DNA polymerase of bacteriophage phi29. *Mol. Cell* 16(4): 609–18 (2004).

76. Blanco, L., Bernad, A., Lázaro, J.M., Martín, G., Garmendia, C., Salas, M., Highly efficient DNA synthesis by the phage phi29 DNA polymerase. Symmetrical mode of DNA replication. *J. Biol. Chem.* 264(15): 8935–8940 (1989).

77. Ibarra, B., Chemla, Y.R., Plyasunov, S., Smith, S.B., Lázaro, J.M., Salas, M., Bustamante, C., Proofreading dynamics of a processive DNA polymerase. *EMBO J.* 28(18): 2794–2802 (2009).

78. Maglia, G., Restrepo, M.R., Mikhailova, E., Bayley, H., Enhanced translocation of single DNA molecules through alpha-hemolysin nanopores by manipulation of internal charge. *Proc. Natl. Acad. Sci. USA.* 105(50): 19720–19725 (2008).

79. Ghosal, S., The effect of salt concentration on the electrophoretic speed of a polyelectrolyte through a nanopore. *Phys. Rev. Lett.* 98(23): 238104 (2007).

80. Manning, G., The molecular theory of polyelectrolyte solutions with applications to the electrostatic properties of polynucleotides. *Q. Rev. Biophys.* 11(2): 179–246 (1978).

81. Wong, C.T., Muthukumar, M., Polymer capture by electro-osmotic flow of oppositely charged nanopores. *J. Chem. Phys.* 126(16): 1–6 (2007).

82. Muthukumar, M., Baumgaertner, A., Effects of entropic barriers on polymer dynamics. *Macromolecules* 22(4): 1937–1941 (1989).

83. Lubensky, D.K., Nelson, D.R., Driven polymer translocation through a narrow pore. *Biophys. J.* 77(4): 1824–1838 (1999).

84. Chen, L., Conlisk, A.T., Forces affecting double-stranded DNA translocation through synthetic nanopores. *Biomed. Microdevices* 13(2): 403–414 (2011).

85. Gershow, M., Golovchenko, J.A., Recapturing and trapping single molecules with a solid-state nanopore. *Nature nanotechnology* 2(12): 775–779 (2007).

86. Gu, L.Q., Dalla Serra, M., Vincent, J.B., Vigh, G., Cheley, S., Braha, O., Bayley, H., Reversal of charge selectivity in transmembrane protein pores by using noncovalent molecular adapters. *Proc. Natl. Acad. Sci. USA.* 97(8): 3959–3964 (2000).

87. Tinland, B., Pluen, A., Sturm, J., Weill, G., Persistence length of single-stranded DNA. *Macromolecules* 9297(97): 5763–5765 (1997).

88. Baumann, C.G., Smith, S.B., Bloomfield, V.A., Bustamante, C., Ionic effects on the elasticity of single DNA molecules. *Proc. Natl. Acad. Sci. USA.* 94(12): 6185–6190 (1997).

89. Sung, W., Park, P.J., Polymer translocation through a pore in a membrane. *Phys Rev Lett.* 77(4): 783-786 (1996).

90. He, Y., Tsutsui, M., Scheicher, R.H., Fan, C., Taniguchi, M., Kawai, T., Mechanism of how salt-gradient-induced charges affect the translocation of DNA molecules through a nanopore. *Biophys. J.* 105(3): 776–782 (2013).

91. Levy, S., Mannion, J., Cheng, J., Reccius, C., Craighead, H., Entropic unfolding of DNA molecules in nanofluidic channels. *Nano Lett.* 8(11): 3839–3844 (2008).

92. Iqbal, S.M., Akin, D., Bashir, R., Solid-state nanopore channels with DNA selectivity. *Nat. Nanotechnol.* 2(4)**:** 243–248 (2007).

93. Hall, A.R., Scott, A., Rotem, D., Mehta, K.K., Bayley, H., Dekker, C., Hybrid pore formation by directed insertion of alpha hemolysin into solid-state nanopores. *Nat. Nanotechnol.* 5(12): 874–877 (2010).

94. Li, J., Stein, D., McMullan, C., Branton, D., Aziz, M.J., Golovchenko, J.A., Ion-beam sculpting at nanometre length scales. *Nature* 412(6843): 166–169 (2001).

95. Venkatesan, B.M., Dorvel, B., Yemenicioglu, S., Watkins, N., Petrov, I., Bashir, R., Highly sensitive, mechanically stable nanopore sensors for DNA analysis. *Adv. Mater.* 21(27): 2771–2776 (2009).

96. Storm, A.J., Chen, J.H., Ling, X.S., Zandbergen, H.W., Dekker, C., Fabrication of solid-state nanopores with single-nanometre precision. *Nat. Mater.* 2(8): 537–540 (2003).

97. Zhou, Z., Hu, Y., Wang, H., Xu, Z., Wang, W., Bai, X., Shan, X., Lu, X., DNA Translocation through hydrophilic nanopore in hexagonal boron nitride. *Sci. Rep.* 3: 3287 (2013).

98. Sommer, B., Sonntag, J., Ganczarczyk, A., Braam, D., Prinz, G., Lorke, A., Geller, M., Electron-beam induced nano-etching of suspended graphene. *Sci. Rep.* 5: 7781 (2015).

99. McNally, B., Singer, A., Yu, Z., Sun, Y., Weng, Z., Meller, A.. Optical recognition of converted DNA nucleotides for single-molecule DNA sequencing using nanopore arrays. *Nano Lett.* 10(6): 2237–2244 (2010).

100. Storm, A.J., Storm, C., Chen, J., Zandbergen, H., Joanny, J.F., Dekker, C., Fast DNA translocation through a solid-state nanopore. *Nano Lett.* 5(7): 1193-1197 (2005).

101. Wolfe, A.J., Mohammad, M.M., Cheley, S., Bayley, H., Movileanu, L., Catalyzing the translocation of polypeptides through attractive interactions. *J. Am. Chem. Soc.* 129(45): 14034–14041 (2007).

102. Cheley, S., Gu, L.Q., Bayley, H., Stochastic sensing of nanomolar inositol 1,4,5-trisphosphate with an engineered pore. *Chem. Biol.* 9(7): 829–838 (2002).

103. Kang, X.F., Cheley, S., Guan, X., Bayley, H., Stochastic detection of enantiomers. *J. Am. Chem. Soc.* 128(33): 10684–10685 (2006).

104. Balasubramanian, S., Sequencing nucleic acids: from chemistry to medicine. *Chem. Commun. (Camb).* 47(26): 7281–7286 (2011).

105. Pasche, B., Absher, D., Whole-genome sequencing: a step closer to personalized medicine. *JAMA* 305(15): 1596–1597 (2011).

106. Wallace, E.V., Stoddart, D., Heron, A.J., Mikhailova, E., Maglia, G., Donohoe, T.J., Bayley, H., Identification of epigenetic DNA modifications with a protein nanopore. *Chem. Commun. (Camb).* 46(43): 8195–8197 (2010).

107. Shuen, A., Foulkes, W.D., Clinical implications of next-generation sequencing for cancer medicine. *Curr. Oncol.* 17(5): 39–42 (2010).

108. Subramanian, G., Adams, M.D., Venter, J.C., Broder, S., Implications of the human genome for understanding human biology and medicine. *JAMA* 286(18): 2296–2307 (2001).

109. Nakane, J.J., Akeson, M., Marziali, A., Nanopore sensors for nucleic acid analysis. *J. Phys. Condens. Matter* 15(32): R1365–R1393 (2003).

110. Gurnev, P., Nestorovich, E., Channel-forming bacterial toxins in biosensing and macromolecule delivery. *Toxins* 6(8): 2483-2540 (2014).

111. Eisenstein, M., Oxford Nanopore announcement sets sequencing sector abuzz. *Nat Biotech* 30(4): 295–296 (2012).

112. Quick, J., Quinlan, A., Loman, N., A reference bacterial genome dataset generated on the MinION portable single-molecule nanopore sequencer. *Gigascience* 3(1): 22 (2014).

113. Ashton, P.M., Nair, S., Dallman, T., Rubino, S., Rabsch, W., Mwaigwisya, S., Wain, J., O'Grady, J., MinION nanopore sequencing identifies the position and structure of a bacterial antibiotic resistance island. *Nat. Biotechnol.* 33(3): 296–300 (2015).

114. Mikheyev, A.S., Tin, M.M., A first look at the Oxford Nanopore MinION sequencer. *Mol. Ecol. Resour.* 14(6): 1097–1102 (2014).

115. Franceschini, L., Mikhailova, E., Bayley, H., Maglia, G., Nucleobase recognition at alkaline pH and apparent pKa of single DNA bases immobilised within a biological nanopore. *Chem. Commun. (Camb)* 48(10): 1520-1522 (2012).

Chapter 2

Single channel recording from planar lipid bilayers

2.1 Nanopore engineering and purification

ClyA monomeric proteins used in our lab for single channel recording experiments are expressed in *E. coli* competent cells, previously transformed with ClyA gene from *Salmonella enterica* serovar Typhi inserted into pET system vector (Novagen). The ClyA protein sequence was integrated with polyhistidine-tag (six histidine residues) at the protein C-terminal end for purification purpose. The plasmid provides ampicillin resistance to the host cells after transformation, so that it possible to select transformed colonies plated in Petri dishes (LB, agar 1-2%, ampicillin 100 μg/mL).

2.1.1 Nanopore engineering

Single point mutations to the *Salmonella enterica* serovar Typhi ClyA-WT gene are introduced by PCR mutagenesis, following the "mega-primer" method[1]. In this procedure, two PCR are performed to prepare each new ClyA template construct. A mutagenic mega-primer is synthetized in the first PCR and used as primer in a second PCR. In the first PCR we use T7 promoter or terminator as first forward or reverse primer respectively, in combination with a mutagenic primer (25mer synthetic oligo, IDT) carrying the residue substitution. For mutations nearby the protein N or C-terminal end, we use a primer sequence complementary to the middle protein sequence instead of T7 primers. Therefore, the amplification product (mega-primer) needs to be 200 − 500 bp for optimal gel separation. The first PCR product, containing the mega-primer, is loaded into an electrophoresis gel for a preliminary purification (2% agarose-TAE and crystal violet). After run, the sample is cut out the gel and purified in a spin silica-membrane-based column (PCR quick purification kit, QIAGEN). 5 μL of purified mega-primers are checked on 2% agarose-TAE gel and 5-10 μL are employed as primers (forward and reverse primer) for a second PCR. In the second PCR the mega-primers will amplify the whole plasmid DNA, generating a new DNA template carrying the introduced mutation. The PCR template (used for the PCR) is eliminated by digestion with

fast digest DpnI (Fermenthas) incubated for 1 hour at 37 °C. 0.1- 1 μL are used for transformation with *E. coli* electro-competent cells (E. cloni 10 G Lucigen). Transformed competent cells are plated into Petri dishes (LB, agar 1-2%, ampicillin 100 μg/ mL) and incubated at 37 °C overnight. Single colonies are picked and further grown for DNA amplification and extraction. Each selected colony is incubated in 10-15 mL medium (2xYT or LB, ampicillin 100 μg/ mL) at 37 °C overnight. Mini-prep DNA extraction kit (QIAGEN), is performed to extract the DNA needed for sequencing (LGC Genomics). If DNA sequencing results confirm the introduced mutation in the protein sequence, the DNA sample can be classified and further used for protein expression.

2.1.2 **Nanopore purification**

We start from a single colony obtained from bacterial transformation of ClyA gene into *E. coli* competent cells (E. Cloni, BL21 DE3 chem.comp cells Lucigen). The colony is incubated in 0.25 L medium (2xYT or LB and ampicillin 100 μg/ mL) at 37 °C for 5-8 hours. When the medium optical density (OD) is increased (0.5−0.8 spectrophotometer reading at 595 nm), protein expression is induced with isopropyl β−D−1−thiogalactopyranoside (IPTG), final concentration 0.5 mM at 21 °C overnight[2]. Bacterial pellet, obtained by centrifugation (20-30 min, 6−7K rpm), is lysed through several freeze and thaw cycles (3 to 5 times, between 21°C and -80 °C) and resuspended in 20 mL lyse-buffer (150 mM NaCl, 15 mM TRIS-HCl, pH 7, 1 U / mL DNase I Fermenthas and 0.1 – 0.2 mg of lysozyme Sigma-Aldrich) incubated at 37 °C for 30 min. Low power sonication (20-50 kHz, pulse-mode) is performed on the lysate for short time intervals (15−20 s) for 3 to 5 times on ice. This allows the monomeric soluble fraction to completely resuspend in solution. Expressed monomeric proteins contain a polyhistidine-tag at the C- terminal end. It is possible to purify a large amount of monomers from the harvested lysate by using Ni-NTA beads (nickel-charged, resin QIAGEN). Monomers concentration after purification is typically between 7−10 mg/ mL.

Polyacrylamide gel electrophoresis in sodium dodecyl sulfate (SDS−PAGE) is run to check protein expression and purification, showing a large band at position approximately 35 kDa for the monomeric protein (Figure 2-1A). Oligomerization is induced by incubating purified monomers in 0.2% N-Dodecyl-β-D-maltoside (DDM) at 37 °C for 20 min. The formed oligomers are run on blue native (BN) PAGE under native conditions[3,4] (Figure 2-1B). The separation process is based on binding of Coomassie blue G250, which provides a uniform negative charge to the protein. Monomeric and oligomeric proteins are separated during migration according to the molecular mass and size. High separation performance is due the polyacrylamide gel gradient (decreasing gel matrix of 4−15%). Bands are cut out from the gel and protein resuspended by simple diffusion in extraction buffer (150 mM NaCl, 15 mM TRIS-HCl, pH 7, 0.02% DDM and 1 mM EDTA). Excised gel bands can be stored directly at 4 °C or at −80 °C for long term storage (Figure 2-1C).

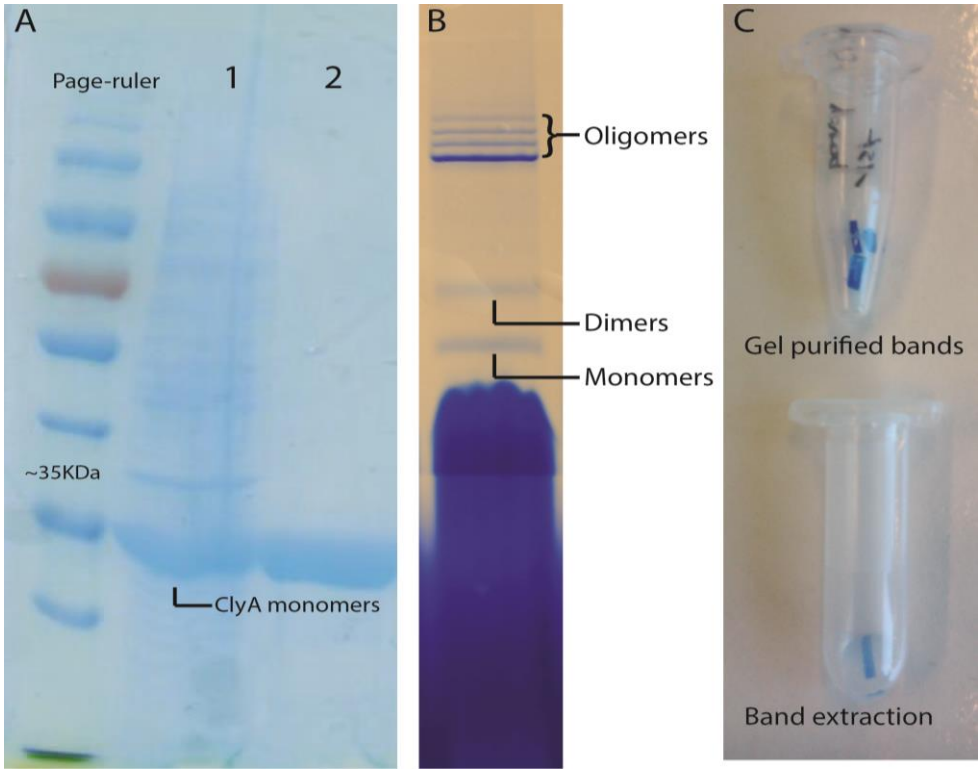

Figure 2-1 ClyA monomers and oligomers purification.
A SDS−PAGE, 34 kDa band for monomeric protein; before (1) and after (2) purification by affinity tag (NiNTA). **B** ClyA oligomers are prepared from monomers by the addition of 0.2% DDM. The formed oligomers are run into a blue native gel electrophoresis in 4−15 % polyacrylamide gel (BN−PAGE). **C** Gel purified bands are stored in Eppendorf tube at 4 °C for short term storage and each band can be extracted by diffusion in buffered solution (0.15 M NaCl, 15 mM TRIS-HCl, 0.02 % DDM and 1 mM EDTA) for 10-15 min.

2.2 Electrophysiological measurements

In our lab we perform bioelectrical measurements from biological nanopores inserted into planar lipid bilayers. We use the same electrophysiological equipment and techniques as described in the Axon guide. (A guide to Electrophysiology and Biophysics Laboratory Techniques, Molecular Devices).

Electrophysiological equipment (Figure 2-2) is used to measure the current, which is the flow of ions (Na^+ and Cl^-) conducted through the biological nanopore ClyA per unit of time (Figure 1-5). Current (I) is measured in amperes (A), usually Pico or Nano amperes (nA) in single channel experiments. According to the Ohm's law, the current (I) generated across a permeable membrane through an external resistance (R), produces a potential difference (ΔV) $\rightarrow \Delta V = I\,R$. The electrical potential, also termed as voltage, is indicated as V and measured in millivolt (mV), changes in V are indicated as ΔV (V differences)[5]. There is a linear relation between ΔV and I (current) in aqueous ionic solution. Therefore, we can quantify the current generated through a pore by measuring the changes in the membrane voltage (ΔV) during the experiment at constant applied voltage (controlled)[5–7].

Chamber. Nanopores insert into artificial planar lipid bilayers reconstituted in a custom-made device termed chamber (Figure 2-2A). Each chamber shows two top-opened compartments, of variable volume (0.5-2 mL) indicated as *cis* and *trans*, which are separated by a 20 μm thick Teflon film (PTFE, Goodfellow UK). An aperture of ~100 μm in diameter, is formed in the middle of the PTFE film with a voltage spark generator[8]. This aperture is the only connection between the *cis* and *trans* compartment in the chamber. 1-2 μL of oil solution (10% v/v Hexadecane in Pentane) is applied to the Teflon film and consequently both chamber compartments are filled with buffered electrolyte solution. Planar lipid bilayers are generated across the oiled opening by pipetting multiple times the buffered solution containing 1-5 μL of 10% w/v lipid solution (1,2-diphytanoyl-sn-glycero-3-phosphocholine, DPhPC 10 mg mL^{-1} in pentane). The oil works as a joint

connection, forming an interface between the plastic film (opening) and the lipid bilayer. Well-formed lipid bilayers cover the whole aperture, sealing the connection between the *cis* and *trans* compartment[9].

Electrodes. The electrical potential (V) is applied to the electrolyte solution in the chamber compartments via Ag/AgCl electrodes (Figure 2-2B). At the electrodes, the ionic current in solution is transformed into electron current inside the copper wire. Electrodes are constituted of a material (Ag/AgCl) that can reversible react with one of the ions in solution (Cl^-). The redox can lead to electron formation (anode) or electron consumption (cathode):

$$Ag_{(S)} + Cl^- \leftrightharpoons AgCl_{(s)} + e^-$$

$$AgCl_{(s)} \leftrightharpoons Ag^+ + Cl^- \overset{e^-}{\longleftrightarrow} Ag_{(s)} + Cl^-$$

The silver/silver chloride electrode redox reaction can be presented in two different ways as shown above. The reaction is between silver (metal) and its salt (*AgCl*). Silver ($Ag_{(s)}$) can be oxidized to form salt ($AgCl_{(s)}$) with the chloride (Cl^-) in solution, or the silver from the salt (Ag^+) can be reduced to form metal silver ($Ag_{(s)}$).

The dependency of the electrical potential (*E*) at each electrode on the activity or effective concentration of chloride-ions in solution is given by the Nernst equation:

$$E = E^0_{Ag/AgCl} - \frac{RT}{F} \ln a_{Cl^-}$$

Where *E* is the electrical potential at one of the two electrodes (*cis* and *trans*), E^0 is the Ag/AgCl standard electrochemical potential, *T* is the absolute temperature on the kelvin scale (+ 273.15 °C), *R* is the universal gas constant: 8.314 472 $J\,K^{-1}\,mol^{-1}$, *F* is the Faraday constant, the number of coulombs per mole of electrons: $9.64853399\times10^4\ C\,mol^{-1}$, *a* is the activity of Cl^- ions near the electrode solution interface[5].

A 10-15 cm copper wire is welded to a silver and a golden pin respectively to each end. The silver pin is coated in AgCl film, after overnight incubation in diluted

bleach solution (sodium hypochlorite NaClO 1-5%). The formed Ag/AgCl electrode is inserted into a 200 μL plastic tip, filled with agar salt solution (agar salt bridge, 3 - 5 % w/v low melt agarose in 3 M NaCl). For each electrode the golden pin is connected to the amplifier and the plastic tip (containing the Ag/AgCl pin) to one chamber compartment (agar-bridge electrodes Figure 2-2). The potential difference between the two electrodes must be zero, if they are immersed in connected compartments with equimolar chloride concentrations. Changes in the concentration (*e.g.* by solution evaporation during long-time experiments) can cause an offset voltage (The Axon Guide). Agar salt bridge electrodes are preferably used over Ag/AgCl electrodes due to their longer working lifetime and mainly to prevent the offset voltage. The plastic tip recreates an environment, where the [Cl^-] remains constant during measurements. In addition, agar salt bridge electrodes are usually filled with a highly concentrated electrolyte solution (2- 4 M salt), which reduces the electrode resistance, improving the voltage noise and provides a wider recording bandwidth (The Axon Guide). Ag/AgCl electrodes are exhaustible, showing white spots after long time use. Therefore, the AgCl coated surface is removed by gentle metallic brushing and the silver pin is bleached once again overnight.

Electrical setup and Faraday cage. Both electrodes are connected to the chamber and to the amplifier headstage (HS-9A voltage gain of Axopatch 200B patch-clamp amplifier, Molecular Devices, Figure 2-2A), which is connected to the digitizer (1440A 16-bit, Molecular Devices). The applied potential refers to the potential of the working electrode connected to the *trans* compartment of the chamber. Electrical measurements are operated in a voltage clamp mode, in which the applied voltage is kept fixed. The operator can set a specific applied voltage (*e.g.* +50 mV) and the system can accurately measure the ionic current, generated through the pore, by the required work to keep the set voltage constant. Therefore, the ionic current is proportional to the applied voltage and to the number and conductance of each operating channel[5–7]. Single channel experiments are performed in an isolating steel or aluminum case, the Faraday enclosure

(Figure 2-2C), preventing external electrical signals and environmental noises to interfere with the analysis (The Axon Guide).

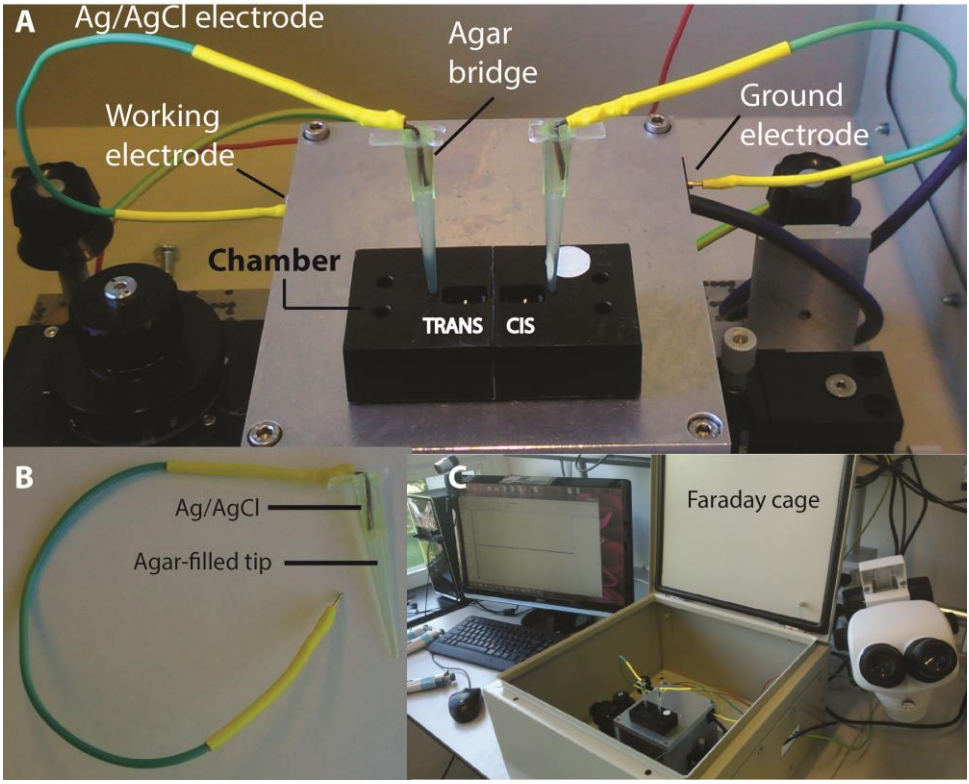

Figure 2-2 Electrophysiological equipment: experimental setup.
A Planar lipid bilayers are reconstituted into a custom-made device (chamber), which shows two top-open compartments (*cis* and *trans*) filled with electrolyte solution. By convention the *cis* and *trans* compartments are connected respectively to the ground electro and to the working electrode. **B** Ag/AgCl electrodes are inserted into a plastic tip, filled with (3-5% w/v low melt agarose in 3M NaCl, agar-bridge electrodes), to prevent electrode exhaustion and silver leakage during measurements. **C** Single channel experiments are performed in an isolating steel case, the Faraday cage.

2.3 Planar lipid bilayers

Planar lipid bilayers seal the microscopic aperture in the Teflon film, preventing the passage of ions and water molecules from one compartment to the other of the chamber (Figure 2-2A). Bilayers are formed following Montal-Muller approach[9]; where the buffered solution, in one of the two chamber compartments, is constantly mixed by gently pipetting of half of the solution volume (250 μL). This mixing moves first the buffer level beneath the aperture and then it raises back through it, allowing the lipids added to the solution (5 μL 10% w/ v DPhPC in pentane) to form a lamellar phase across the oiled Teflon aperture[9,10]. If the bilayer is properly formed, under constant applied voltage no current is generated in the system (Figure 2-3C), since ions cannot cross the lipid barrier (the read current output is set zero pA). As a measure of well-formed bilayers we check the bilayer capacitance (The Axon Guide). Under pulsed applied voltage the formed bilayer works as a capacitor generating current (Figure 2-3A). Charges are stored in a capacitor only when there is a change in the voltage across the capacitor. Therefore the resulting current (I) is proportional to the applied voltage (ΔV) change with time (Δt): $I = C \frac{\Delta V}{\Delta t}$. We use a commercial analog waveform generator, providing a triangular wave input of (20 Hz). The input is checked and calibrated by using a bilayer model cell (MCB-1U, Molecular Devices)[8]. The capacitance is shown as square wave outputs of 80- 150 pA for 100-150 μm apertures reconstituted bilayers[8,11]. The measured capacitance gives a direct indication on the size of the bilayer and furthermore for the presence of eventual leaking sites formed in the bilayer. Leaks deviate square waves into a triangular shaped wave output (Figure 2-3A). In addition, leaks generate a current background under constant applied voltage, increasing the zero pA current output (Figure 2-3B). DPhPC lipids have shown optimal performing properties in our lab, bilayers have long lifetime (>5 hours) and are resistant to constant applied voltage (up to 200 mV). Though lipids are resistant to a wide range of temperatures[12–14], experiments are performed in a controlled temperature room never below 21 °C, due to the freezing point of

hexadecane oil (fusion point 18 °C). Working at < 21 °C might prevent bilayers formation. One of the most common problems is excess oil in the Teflon aperture, which prevents bilayer formation. A thoroughly cleaning routine, using first hot tap water, distilled deionized-water (ddH_2O) and diluted ethanol, is necessary to remove excess oil and carry out new experiments.

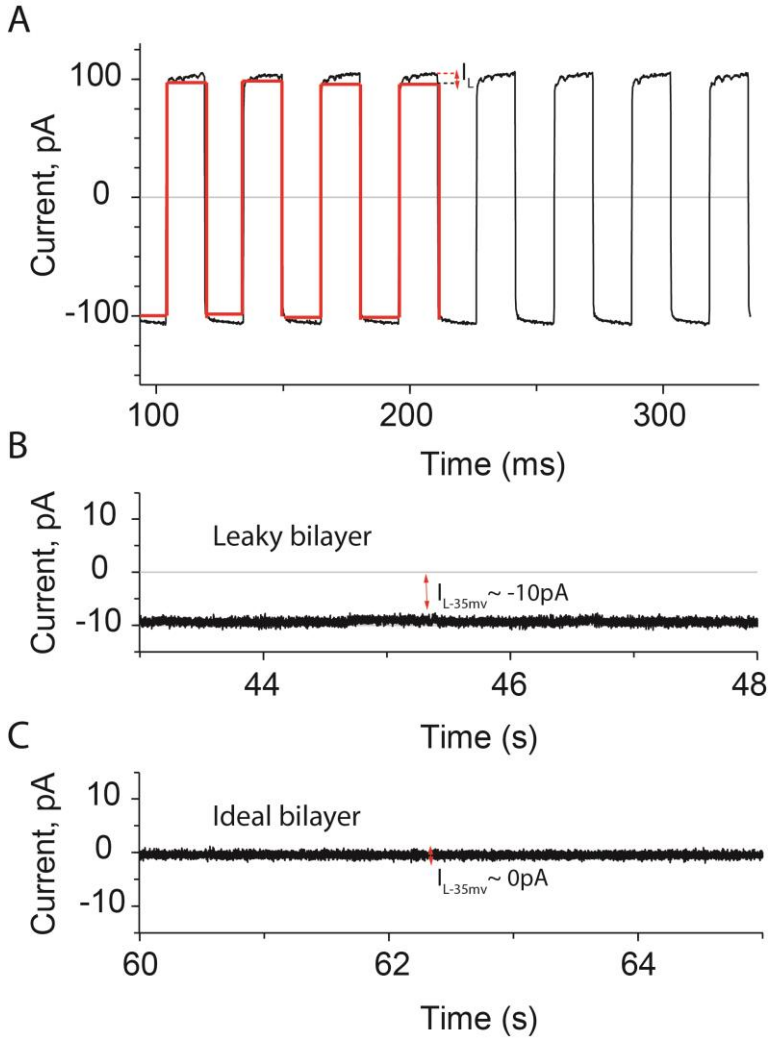

Figure 2-3 Lipid bilayer capacitance and current leakage.
A Visual measurement of the bilayer capacitance. An ideal square trend (red) is lined on the measured bilayer capacitance, which shows a triangular shaped outline. The detachment at the top peak from the red and black lines indicates a leaky bilayer (I_L). **B** Under constant voltage applied (-50 mv) the leakage in the lipid bilayer generates a background current ~10 pA. **C** Properly formed bilayers show no current leakage (~ 0 pA) under constant applied voltage (-50 mv).

2.4 Single channel experiment

ClyA nanopore solution (0.01–0.1 ng ml^{-1}) is added to the chamber *cis* compartment (connected to the ground electrode) under applied voltage (±35 mV) through the working electrode in *trans*. The current output generated in absence of channels in the planer lipid bilayer is equal to zero pA (Figure 2-4A). Upon a single pore insertion, ions following the applied potential can flow from one compartment to the other through the pore inner lumen, generating ionic current. Therefore the measured ionic current is dependent on the number of inserted pores and the adopted experimental conditions such as the salt concentration, pH and temperature. Multiple pore insertions show stepwise increment of the current level (Figure 2-4B). After insertion of a single pore, excess protein in the *cis* compartment can be removed by perfusion. 10-20% of the buffered solution in *cis* is replaced with new solution lowering protein concentration and thus the probability of a new channel insertion[8]. The open pore conductance (I_O, pA) is referred to the ionic current conducted from a single channel, where no analytes occupy the inner pore vestibule. Charged analytes added in solution such as ssDNA or dsDNA, follow the electrical gradient and translocate through the pore, changing the pore conductance. It is possible to measure the translocation time (t_{OFF}, ms), the time between two consecutive translocation events (t_{ON}, ms, inter-event time interval), which is the inverse of the frequency of translocation events (f), the block current (I_B, pA) and residual current (I_B / I_O = I_{RES}) for each translocation event[8]. Changes in the open pore conductance can also occur where no analytes are translocating through the pore, we refer to this events as gating of the pore (Figure 2-4C). Two main gating events are observed during SCR experiments: fast and slow gating, which are respectively transient and long lasting blockages of the open pore current. Consequently to a long lasting blockage (slow gating), the pore conductance I_O can be restored by manual reversal of the applied potential. It is compulsory to start each new experiment with a preliminary “control” recording, where no analytes are added to the electrolyte solution. During control the pore

gating is tested at different applied voltages (35-100 mV) for several minutes. This is a fundamental step to characterize the pore gating and understand the modulation of the ionic current by subsequently analytes added to the solution. Normally, we prefer to work at applied voltage where no pore gating events are observed within a timespan of at least 30 seconds. In this way it is possible to avoid analyses errors of the observed events.

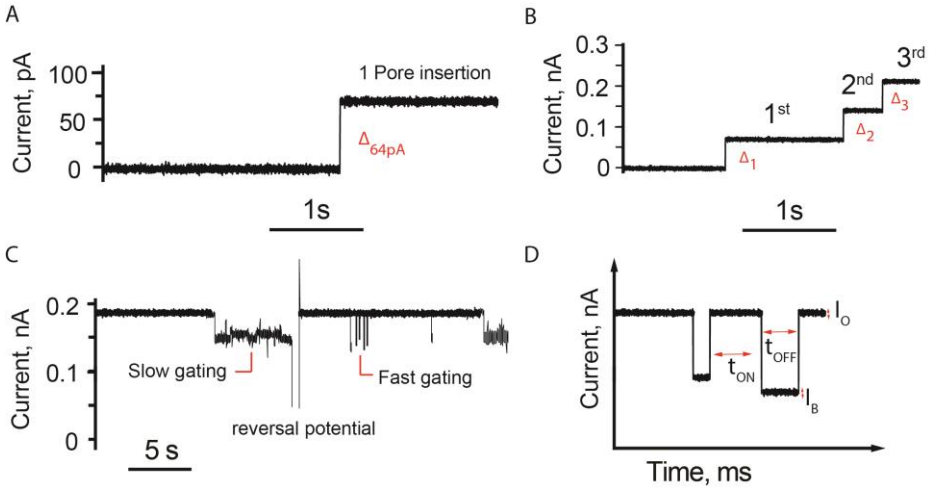

Figure 2-4 Electrical recording from planar bilayers.
A ClyA single channel insertion under +35mV applied potential. The recorded current (0pA) jumps to 64 pA (Δ64 pA) after a single pore insertion (0.15 M NaCl, 15 mM TRIS-HCl, pH 7.5). **B** Multiple channels insertion show stepwise current enhancement. Each pore insertion gives a Δ_x current increment ($\Delta_1 = \Delta_2 = \Delta_3 = 64$ pA). The overall current (I_O) is equal to $\sum_x^1 \Delta$ and the number of inserted pores (x) is equal to I_O / Δ_1. **C)** Slow and fast gating events under +100 mV applied voltage for ClyA nanopores. The open pore conductance is reduced to temporary lower levels and can be restored by the reversal of the applied potential (±100 mV). **D** The current trace shows the translocation time (t_{OFF}, ms), the inter-event time (t_{ON}, ms), the block current (I_B, pA) and open pore current (I_O, pA) during a typical DNA translocation experiment.

2.5 Measurements: Data acquisition

During electrical recording experiments, it is possible to monitor the ionic current conducted through the pore by using a computer connected to the electrophysiological equipment. The Axopatch 200B patch-clamp amplifier (Molecular Devices) operated in voltage clamp mode gives direct reading of the continuous analog current signal by the modulation of the needed voltage (ΔV) to keep the set applied voltage constant (The Axon Guide). The provided analog voltage signal, which is generated to compensate the analog current signal, is transmitted to the digitizer (1440A 16-bit, Molecular Devices) where it is converted into a binary numbers code with finite resolution. The amplifier dynamic input range is ± 10 V, which divides the signal into 2^{16} (65536) values (bins), providing a resolution of 0.305 mV per bin (20 V/ 2^{16}). The output gain has a dynamic range of ±10 nA and a resolution of 0.305 pA per bin. It can be changed between 0.5-500 times to increase the resolution (decreased binwidth), at the expense of dynamic range. We set the output gain at 10 times for DNA experiments (at 0.15 M NaCl), which corresponds to a dynamic range of 1 nA and a resolution of 0.0305 pA per bin[8]. A computer running Clampex software (Molecular Devices) can handle the continuous flow of information and displays the current signal in a user-friendly interface. Clampex software is used to collect and display the current signal, however the software can be employed also to apply an electric potential through the amplifier (The Axon Guide). Clampex software has five data acquisition modes; we use Gap free and Episodic Stimulation modes for DNA translocation experiments. In the Gap Free protocol, the current signal is continuously digitized, displayed and can be recorded. The applied voltage can be promptly changed through the software (sequencing keys) or manually directly from the amplifier voltage knob. The Episodic Stimulation protocol is instead used to apply consecutive voltage steps of established lifetime such as for I-V curves and voltage ramps. The Axopatch 200B amplifier has a recording bandwidth of 100 kHz, and the digitizer has a maximum sampling rate of 250 kHz (4 μs) per

channel, which determines the maximum temporal resolution. Current resolution is primarily limited by the noise in the system, which can be removed by filtering. Low-pass filtering limits the bandwidth of the data by cutting signals above the corner frequency (or cut-off frequency) of the filter. The applied filter cut-off should be greater than five times the inverse of the mean event time[5,8,15]. It is also important to work with the correct sampling rate. The Axon guide. (A guide to Electrophysiology and Biophysics Laboratory Techniques, Molecular Devices) indicates that the sampling rate should be twice at least of the cut-off frequency of the applied filter. However, it is preferable to oversample avoiding inaccurate current estimates, sampling ten or five times the cut-off frequency[8]. We record free DNA translocation experiments by applying a 10 kHz low-pass Bessel filter and using a 20 μs (50 kHz) sampling rate.

2.6 **Data Analysis**

Current traces recorded during single channel experiments can be subsequently analyzed by Clampfit Software (Molecular Devices) [5,8]. The main software feature offers a single channel search analyzing option, where each current trace is organized in levels and analyzed. Levels are set for the current trace (*e.g.* level 0 = open pore current and level 1 = blocked current level). During the reading, if the ionic current amplitude in the trace matches any of the set levels, the software saves the data automatically, collecting all the event features such as the amplitude value, dwell time and the inter-event time in a result window. It is possible to extract all the saved values for a specific level and calculating basic statistics (*e.g.* mean, average, standard deviation). The data are displayed as histogram representations and Gaussian or exponential fits can be generated. The open pore current (I_O) and the block current (I_B) can be calculated by Gaussian fittings, where the main peak represents the mean current amplitude (I_O level 0, I_B level 1). The DNA translocation dwell time is calculated by fitting the dwell time

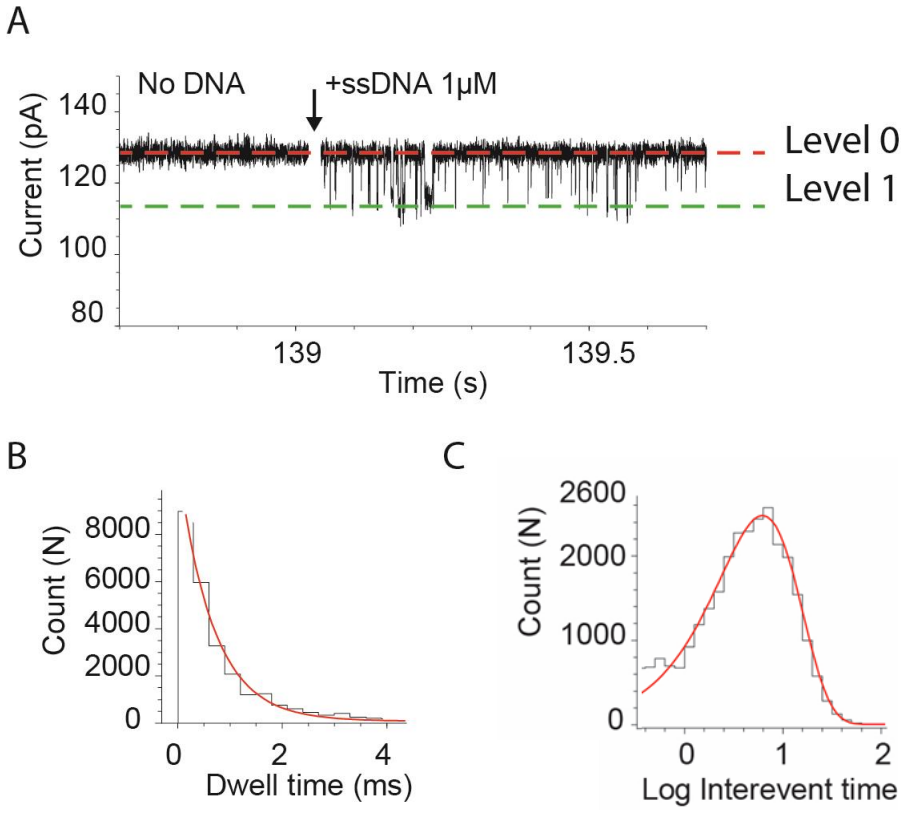

Figure 2-5 DNA translocation data analysis
A Typical current trace for ssDNA translocation at +70 mV in 0.15 M NaCl. The open pore current (red line, Level 0) is transiently reduced to a lower level (green line, Level l) after adding 1 μM ssDNA to the pore *cis* solution. The current signal is acquired at 100 μs (10kHz) sampling rate and filtered at 2 kHz (low-pass Bessel filter), each collected data point is automatically assigned to the corresponding level on the base of its amplitude. **B** Conventional histogram of the DNA translocation dwell time from the block pore current level 1. The fitting for a single exponential distribution is calculated by Clampfit software. **C** Histogram of the DNA translocation inter-event time in logarithmic scale from the block pore current level 1. The fitting (shown in red) for an exponential distribution in logarithmic scale is calculated by Clampfit software.

of the blocked pore current (I_B, level 1) to a single exponential standard from a cumulative histogram, thus the inter-event time is calculated by fitting the inter-event time of the blocked pore current (I_B, level 1) to a single exponential (logarithmic binning, 10 bin per decade, Figure 2-5). Free DNA translocation events are recorded at 20 μs (50 kHz) sampling rate and filtered at 10 kHz low-pass Bessel filter (at 100 μs (10kHz) sampling rate and filtered at 2 kHz low-pass Bessel filter in 0.15 M NaCl). During data analysis traces can be further filtered to improve events detection and selection from background noise[15]. At high salt concentrations DNA translocation events are well solved and distinguished from the open pore current base line, therefore no additional filtering is required. While at low salt concentrations it is necessary to apply a further filter, between 2-6 kHz depending on the background level noise of the trace. Extensive filtering might invalidate data analysis removing some of the important recorded events[15]. Checking the number of events and their dwell time resolution at different applied filter for the same trace might help to choose the optimal filter setting for each condition.

2.7 **Materials: DNA preparation**

Testing the translocation of nucleic acids through nanopores requires large quantity of nucleic acids (μM concentrations). In our experiments we used short synthetic ss/dsDNA or long custom-made dsDNA samples. Integrated DNA Technologies (IDT) offers a large assortment of synthetic nucleic acids. ssDNA or dsDNA can be synthesized in different lengths (2-200 nucleotides) and at different molar scale (25 nmole up to 10 μmole DNA oligo). In addition, oligos can be chemically modified at their 5' or 3' end, providing a broad list of possible tags such as biotin, cholesterol, etc. Pure oligonucleotides can be needed for specific experimental investigations, therefore HPLC or PAGE purified oligos can be requested. Furthermore, dsDNA can be prepared by mixing two synthetic complementary ssDNA oligos: one oligo must be 5' or 3' biotinylated and the second one added in

excess (20% higher molar concentration). In a temperature-controlled device (PCR or heating block) the temperature is increased first up to 95 °C for one minute and then gradually decreased to room temperature to facilitate the annealing process. At the annealing stage the temperature is stepwise decreased (*e.g.* 1-2 °C, each held for one minute). The formed dsDNA is then purified from the excess of ssDNA with affinity chromatography using a biotin-binding column containing monomeric avidin immobilized on agarose beads (Thermo Scientific Pierce). Pure dsDNA is eluted in biotin blocking/ elution buffer according to the protocol and stored at -20 ºC. Typically, a DNA concentration of 200 ng ml^{-1} is obtained. A 2% agarose gel in TAE buffer can be run to check the size of the dsDNA. Purified dsDNA samples are divided into aliquots (50-100 µL) and stored at -20 ºC in the presence of 1 mM EDTA. Long DNA molecules (>200 bp) are prepared *in vitro* by using PCR multiple cycle amplification. It is possible to obtain dsDNA of the desired length and high concentration by using a dsDNA template of known sequence and two synthetic primers (forward and reverse). If either forward or reverse synthetic primer contains a specific chemical tag (*e.g.* biotin tag at the 5' end), the resulting amplified dsDNA product will exhibit the introduced tag group, at one end of the strand. We use Taq DNA Polymerase from REDTaq ReadyMix (Sigma) for each PCR Reaction Mix. After a maximum number of 35 cycles, the PCR product of 20 or more reaction tubes (50 µl each tube) is first digested with DpnI (to eliminate the template DNA) and further purified by PCR quick purification kit (QIAGEN). A 2% agarose gel (TAE buffer) is run to check the size of the amplified oligo. Typical product concentration achieved following this approach, is 200 ng ml^{-1}.

2.8 References

1. Ke, S.H., Madison, E.L., Rapid and efficient site-directed mutagenesis by single-tube 'megaprimer' PCR method. *Nucleic Acids Res.* 25(16): 3371–3372 (1997).

2. Eifler, N., Vetsch, M., Gregorini, M., Ringler, P., Chami, M., Philippsen, A., Fritz, A., Müller, S.A., Glockshuber, R., Engel, A., Grauschopf, U., Cytotoxin ClyA from Escherichia coli assembles to a 13-meric pore independent of its redox-state. *EMBO J.* 25(11): 2652–2661 (2006).

3. Schagger, H., Von Jagow, G., Blue native electrophoresis for isolation of membrane protein complexes in enzymatically active form. *Anal. Biochem.* 199(2): 223–231 (1991).

4. Schagger, H., Cramer, W.A., Von Jagow, G., Analysis of molecular masses and oligomeric states of protein complexes by blue native electrophoresis and isolation of membrane protein complexes by two-dimensional native electrophoresis. *Anal. Biochem.* 217(2): 220–230 (1994).

5. Archer, M.D., "Genesis of the Nernst equation" in Electrochemistry, past and present, Stock, J.T., Orna, M.V., Eds. American Chemical Society, Washington DC, 115-126 (1989).

6. Alvarez, O., "How to set up a bilayer system" in Ion channel reconstitution, Miller, C., Ed. Plenum Press, New York, 115-130 (1986).

7. Sakmann, B., Neher, E. E., The patch clamp technique. *Sci Am.* 266(3): 44-51 (1992).

8. Maglia, G., Heron, A.J., Stoddart, D., Japrung, D., Bayley, H., Analysis of single nucleic acid molecules with protein nanopores. *Methods Enzymol.* 475: 591–623 (2010).

9. Montal, M., Mueller, P., Formation of bimolecular membranes from lipid monolayers and a study of their electrical properties. *Proc. Natl. Acad. Sci. USA.* 69(12): 3561–3566 (1972).

10. White, S.H., Petersen, D.C., Simon, S., Yafuso, M., Formation of planar bilayer membranes from lipid monolayers. A critique. *Biophys. J.* 16(5): 481–489 (1976).

11. Peterman, M.C., Ziebarth, J.M., Braha, O., Bayley, H., Fishman, H.A., Bloom, D.M., Ion channels and lipid bilayer membranes under high potentials using microfabricated apertures. *Biomed. Microdevices* 4(3): 231-236 (2002).

12. Lindsey, H., Petersen, N.O., Chan, S.I., Physicochemical characterization of 1,2-diphytanoyl-sn-glycero-3-phosphocholine in model membrane systems. *Biochim. Biophys. Acta* 555(1): 147–167 (1979).

13. Kang, X.F., Gu, L.Q., Cheley, S., Bayley, H., Single protein pores containing molecular adapters at high temperatures. *Angew. Chem. Int. Ed. Engl.* 44(10): 1495–1499 (2005).

14. Hung, W.C., Chen, F.Y., Huang, H.W., Order-disorder transition in bilayers of diphytanoyl phosphatidylcholine. *Biochim. Biophys. Acta* 1467(1): 198–206 (2000).

15. Silberberg, S.D., Magleby, K.L., Preventing errors when estimating single channel properties from the analysis of current fluctuations. *Biophys. J.* 65(4): 1570–1584 (1993).

Chapter 3

A nanopore machine promotes the vectorial transport of DNA across membranes

This chapter was published as:
Franceschini, L., Soskine, M., Biesemans, A. and Maglia, G.
Nature Communication. 4:2415 (2013).

L. F., M. S. and G. M. designed the research,
L. F. performed the experiments for the research,
M. S. and A. B. provided the ClyA pores used in this work,
G. M. and L. F. wrote the paper.

3.1 Abstract

The transport of nucleic acids through membrane pores is a fundamental biological process that occurs in all-living organisms. It occurs, for example, during the import of viral DNA into the host cell or during the nuclear pore complex-mediated transport of mRNA in and out the cell nucleus and has implications in nucleic acid drug delivery and gene therapy. Here we describe an engineered DNA transporter that is able to recognize and chaperone a specific DNA molecule across a biological membrane under a fixed transmembrane potential. The transported DNA strand is then released by a simple mechanism based on DNA strand displacement. This nanopore machine might be used to separate or concentrate nucleic acids or to transport genetic information across biological membranes.

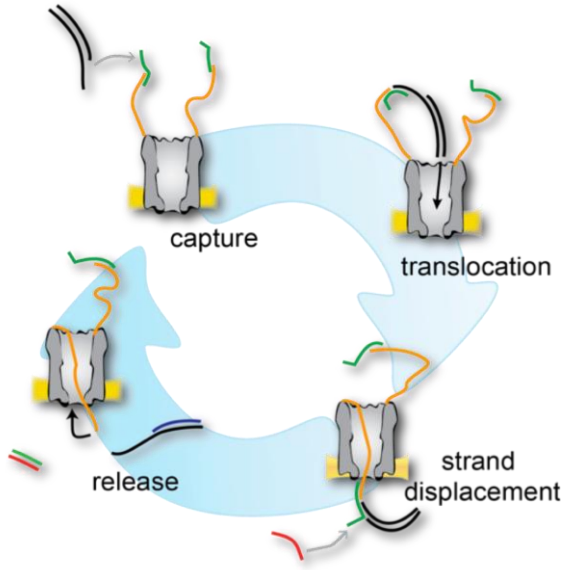

Figure 3-1 Transport of DNA across lipid membranes.
Cartoon representation for a ClyA nanopore (grey) engineered with ssDNA molecules (orange-green) attached atop of the pore. The nanopore is imbedded into a lipid bilayer (yellow). A specific DNA molecule (black) is driven by the applied potential nearby the nanopore, hybridizes to the ssDNA molecules attached atop of the pore and is transported through the pore, where a ssDNA molecule (red) starts a strand displacement reaction to release the DNA cargo.

3.2 Introduction

The use of natural components as building blocks in nanotechnology is advantageous because artificial biological devices are intrinsically able to interface with biological systems. However, adding new functions to proteins is not trivial because, despite important recent advances[1–3], the folding of proteins cannot be easily predicted from the sequence; moreover, to date the use of artificial protein systems in nanotechnology has been mainly limited to self-assembled protein arrays[4,5]. Recently, DNA has emerged as a preferred element to build and confer functionality to biologically based devices[6]. Self-assembled DNA nanostructures now range from compact 3D objects with a well-defined shape[7–9] to complex functional assemblies such as nanopores[10,11] that are capable of spanning artificial membranes[12,13]. The thermodynamics of DNA duplex formation have also been exploited to build systems that utilize strand hybridization, branch migration, and dissociation for dynamic state reconfiguration[6,14]. Such DNA devices can switch configuration multiple times as detected by high and low FRET emission states[15], act as computing elements for example to build molecular logic circuits that perform mathematical operations[16] or to reconfigure self-assembled DNA structures[17] and therefore have potential for imbedding control within molecular systems. Strand-displacement reactions have also been used to control mechanical actuation, as shown for DNA ‘walkers’ that can move along DNA tracks after the external addition of DNA reagents[18–24]. In the present work, we incorporate a DNA unit on the top of a protein nanopore to form a membrane-bound molecular machine that transports selected DNA molecules through the nanopore. The transported DNA is released by a strand displacement reaction. Similarly to biological transporters, our device is capable of carrying a specific substrate across a biological membrane.

3.3 Results

3.3.1 dsDNA translocation through ClyA nanopores

We used an engineered version of Cytolysin A (ClyA) from *Salmonella enterica* serovar Typhi that was selected for its enhanced activity (ClyA-CS), solubility and favorable behavior in planar lipid bilayers when compared with wild-type ClyA (ClyA-WT nanopores)[25]. In lipid bilayers, ClyA nanopores assembled with a preferred orientation (Figure 3-2A) that could be easily assessed by the slightly asymmetrical current– voltage relationship of the pore[25]. The internal diameter of the ClyA dodecamer (3.3 nm at its narrower entrance [26], Figure 3-2A) is larger than the diameter of dsDNA (2.2 nm for the B form), indicating that dsDNA should readily translocate through the pore when driven by an electrical potential. However, most likely because of the negatively charged residues lining the lumen of ClyA (the net lumen charge is -120), at physiological salt concentrations, DNA does not enter the nanopore[25]. Inspired by our previous work with alpha haemolysin (αHL) nanopores at high alkaline pH[27,28], we tested the ability of DNA to translocate through ClyA- CS nanopores at high ionic strength, where the internal charges are screened. In 2.5 M NaCl, 15 mM Tris-HCl, pH 7.5 and under +100 mV applied potential, the addition of 0.12 mM of biotinylated dsDNA 1 (290 bp, Table 3-S1) to the *cis* compartment produced transient current blockades (I_B) to the open pore current (I_O) showing a residual current ($I_{RES} = I_B / I_O$) of 0.63 ± 0.01 (mean ± s.d., I_B level 1^*_{+100} = 1.10 ± 0.03 nA, mean ± s.d., n = 3 experiments), with a dwell time of 2.0 ± 0.6 ms (mean ± s.d.) because of the entry of the DNA into the lumen of the pore (Figure 3-2B). The subsequent addition to the *cis* compartment of 0.3 mM of neutravidin, which forms a tight complex with biotin, converted the transient blockades into long lasting current blockades (level 1_{+100} = 1.19 ± 0.01 nA, mean ± s.d., n = 4) with a higher residual current value ($I_{RES+100}$ = 0.68 ± 0.01, mean ± s.d., n = 4). The open pore current could be restored by reversal of the applied potential to -100 mV (Figure 3-2B).

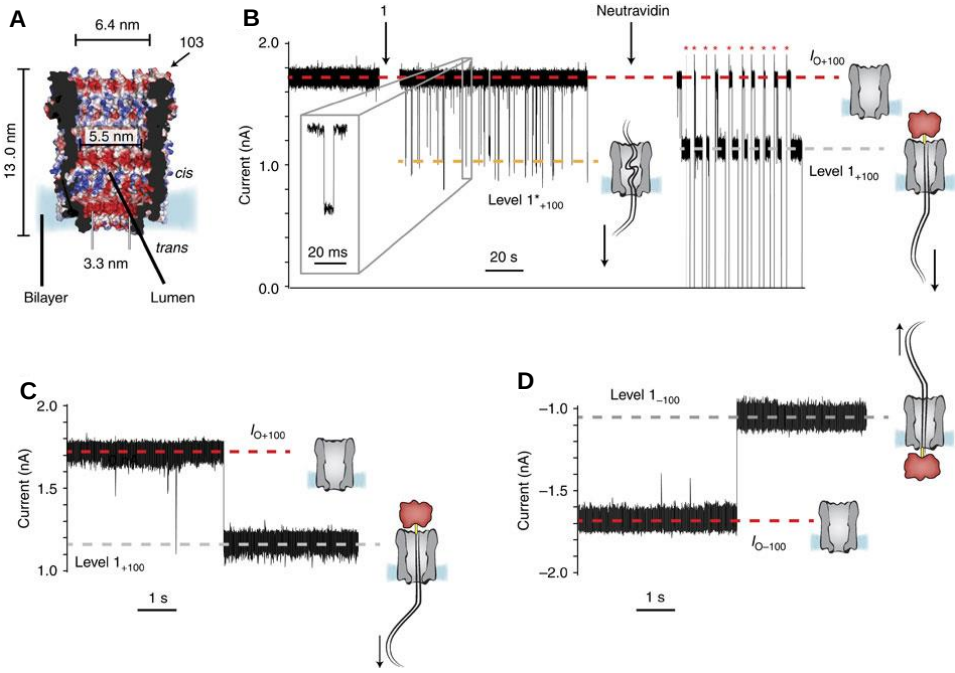

Figure 3-2 dsDNA translocation through ClyA nanopores.
On the right of the current traces, ClyA and neutravidin are depicted as grey and red cartoons, respectively, and the dsDNA is shown as a black double line. **A** A section through ClyA from *S.* Typhi constructed by homology modelling from the *E. coli* ClyA structure (PDB: 2WCD, 90% sequence identity)[25]. ClyA is shown as surface representation and colored according to the 'in vacuo' electrostatics (red for negative regions, and blue for positive regions, Pymol). The arrow shows the location of residue serine 103 (WT sequence) further engineered in this work. The pore dimensions are given considering the van der Waals radii of the atoms. **B** At +100 mV, the addition of 0.12 mM of 290 bp dsDNA **1** to the *cis* side of a ClyA nanopore provoked short current blockades of I_{RES} = 0.63 ± 0.01 (mean ± s.d., level I_{O+100} = 1.74 ± 0.05 nA, mean ± s.d. and level 1^*_{+100} = 1.10 ± 0.03 nA, mean ± s.d., n = 3) that were because of the translocation of dsDNA through the pore. The addition of neutravidin to the *cis* chamber converted the short current blockades to higher conductance and long-lasting current blockades with $I_{RES+100}$ = 0.68 ± 0.01 (mean ± s.d., level 1_{+100} = 1.19 ± 0.01 nA, mean ± s.d., n = 4) due to the threading of DNA through the pore. The open pore current was restored by reversing the potential to −100 mV (red asterisks) and the stepping back to +100 mV. The inset shows a typical transient current blockade. **C** Details of a current blockade because of the formation of a *cis* pseudo rotaxane at +100 mV. **D** Formation of a trans pseudo rotaxane at −100 mV by threading the dsDNA:neutravidin complex (see above) from the *trans* side (level 1_{-100} = − 1.02 ± 0.03 nA, mean ± s.d., $I_{RES-100}$ = 0.62 ± 0.01, mean ± s.d., n = 4). The electrical recordings were carried out in 2.5 M NaCl, 15 mM Tris-HCl, pH 7.5 at 22 °C. Data were recorded by applying a 10-kHz low-pass Bessel filter and using a 20 µs (50 kHz) sampling rate.

These results suggest that at positive applied potentials, dsDNA added to the *cis* compartment is transported through the pore to the *trans* chamber and that neutravidin prevents the full translocation of DNA through ClyA nanopores by forming a *cis* protein:DNA complex where the DNA occupies the full length of the pore (Figure 3-2C). Trans complexes could also be formed at -100 mV (level 1_{-100} = 1.02 ± 0.03 nA, mean ± s.d., $I_{RES-100}$ = 0.62 ± 0.01, mean ± s.d., n = 4) when the threading of the dsDNA:neutravidin complex is initiated from the *trans* side (Figure 3-2D).

3.3.2 Formation of a nanopore:DNA rotaxane

To prove that dsDNA translocates through ClyA nanopores, we sought to build a DNA:nanopore rotaxane, in which a dsDNA molecule added to the *trans* side of a ClyA nanopore hybridizes with a second DNA strand on the *cis* side after threading through the lumen. Rotaxanes are supramolecular interlocked systems in which a linear unit (thread) passes through a macrocyclic ring and is tapped by two bulky substituents (stoppers) at each end. Such mechanically joined molecules have applications, for example, as switches in molecular electronics[29] or as components in molecular machines[30]. Rotaxanes have been made non-covalently from a variety of molecules including dsDNA[31] or by locking biotinylated ssDNA molecules threaded through an αHL nanopore with streptavidin on one side and a DNA hairpin on the other side (dsDNA cannot translocate through αHL)[32]. Here we used a ClyA nanopore, ClyA-2, that contained 12 ssDNA molecules 2 (51 nucleotides, Table 3-S1,Figure 3-3A and Figure 3-4A,C-D) covalently attached at their 5'-ends to cysteine residues introduced at the *cis* entrance of the pore (at position 103, Figure 3-2A) via disulphide linkages. 2 was designed to act as a rotaxane stopper. The thread 3 was a dsDNA molecule (59 bp, Figure 3-3A and Table 3-S1) with an additional 31 nucleotides of ssDNA at the 5'-end that was designed to hybridize indirectly with the stopper at the *cis* side.

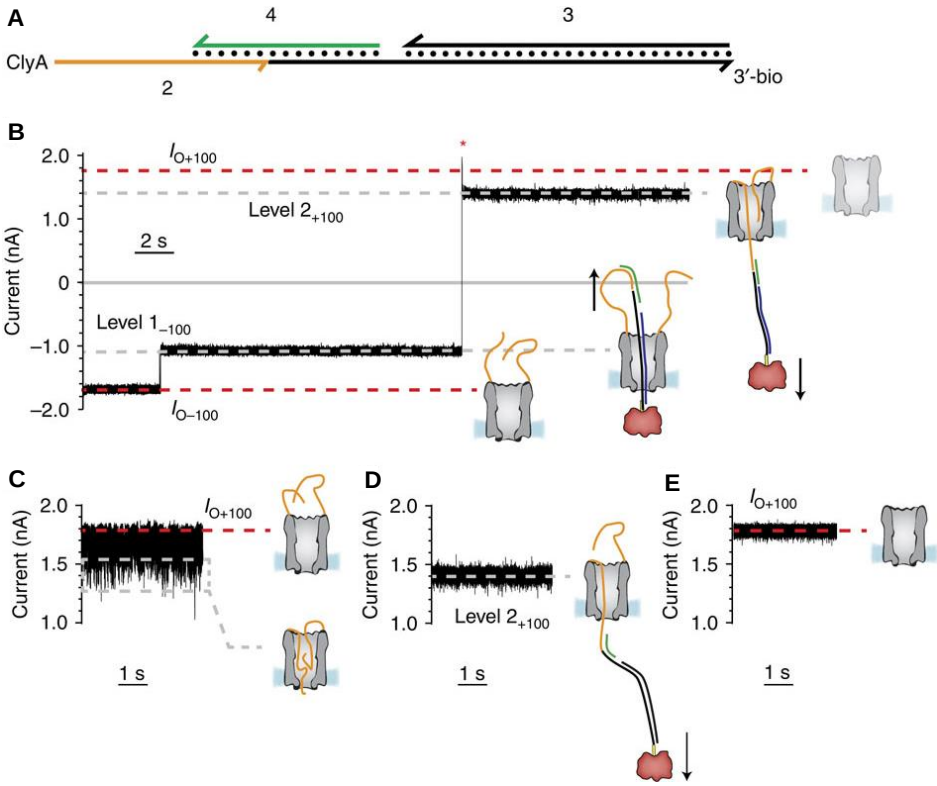

Figure 3-3 Formation of a nanopore–DNA rotaxane.
A Representation of the hybridization of the DNA molecules used to form the rotaxane. Arrowheads mark the 3'-ends of strands. The suffix bio indicates a biotin moiety. **B** Rotaxane formation. At −100 mV following the addition of the DNA hybrid 3 (1.0 μM) complexed with neutravidin (0.3 μM, tetramer) and oligo 4 (1.0 μM) to the *trans* compartment, the open pore current of ClyA-2 (I_{O-100} = −1.71 ± 0.07 nA, mean ± s.d., n = 4) was reduced to level 1_{-100} = −1.1 ± 0.04 nA (mean ± s.d., $I_{RES-100}$ value of 0.64 ± 0.02, mean ± s.d., n = 4), indicating that dsDNA threaded the pore from the *trans* side. Stepping to +100 mV (red asterisk) produced a current block with $I_{RES+100}$ = 0.77 ± 0.04 (mean ± s.d., level 2_{+100} = 1.31 ± 0.09 nA, mean ± s.d., n = 4), indicating that the DNA was still occupying the pore at positive applied potentials. Level 2 most likely corresponded to ssDNA 2 occupying the vestibule of the pore. Successive switching to positive and negative applied potentials did not restore the open pore current, confirming that a rotaxane was permanently formed. (C–E) Rotaxane removal. **C** At +100 mV, the ionic current through ClyA-2 nanopores showed a multitude of fast current blockades (Figure 3-3), suggesting that the ssDNA molecules attached to the *cis* entrance transiently entered the lumen of the pore. **D** After the rotaxane was formed (b), at +100 mV the nanopore showed a steady ionic current (level 2_{+100}), suggesting that a single DNA molecule was occupying the pore. **E** Twenty minutes after the addition of 20 mM DTT to the *cis* compartment, the DNA molecules atop the ClyA pore were removed by disulphide bond exchange and the open pore current at +100 mV was restored (I_{O+100} = 1.78 ± 0.07 nA, mean ± s.d., n = 4). The electrical recordings were carried out in 2.5 M NaCl, 15 mM Tris-HCl, pH 7.5, at 22 °C. Data were recorded by applying a 10-kHz low-pass Bessel filter and using a 20 μs (50 kHz) sampling rate.

3 also contained a 3'-biotinylated linker that was used for complexation with neutravidin at the *trans* side. The linkage between the thread and stopper on the *cis* side was mediated by a bridging ssDNA molecule 4 (Table 3-S1, Figure 3-3A) that was complementary to the last 16 nucleobases of 2 and to the first 25 nucleobases of 3. Each time 3 and 4 were added to the *trans* compartment, at -100 mV the DNA thread was captured by the pore and not released upon reversal of the potential to +100 mV (level 2_{+100}, $I_{RES+100}$ = 0.77 ± 0.04, mean ± s.d., n = 4, Figure 3-3B), indicating that a DNA rotaxane was formed (Figure 3-3B). Interestingly, at +100 mV the residual current of the rotaxane ($I_{RES+100}$ = 0.77 ± 0.04, mean ± s.d.) was higher than the I_{RES} values of the *cis* or *trans* protein:DNA complexes (pseudorotaxane) threads (0.68 ± 0.01, mean ± s.d., and 0.62 ± 0.01, mean ± s.d., respectively), suggesting that an unhybridized ssDNA stretch of 2 spanned the pore at positive potentials (Figure 3-3B-D). The rotaxane could be disassembled by the addition of 20 mM dithiothreitol (DTT) to the *cis* chamber, which reduced the disulphide bond between 2 and ClyA and restored the open pore current at +100 mV (Figure 3-3C–E). Control experiments showed that when 3 was added to the *trans* side and captured at -100 mV in the absence of the bridging sequence 4, the pore open current could be restored upon reversal of the potential to +100 mV (Figure 3-4B). 3 was readily expelled from the pore at +100 mV as it could not hybridized to ClyA-2 without 4. Furthermore, the capture of 3•4 at - 100 mV after the removal of 2 from the pore top (after cleavage with DTT) did not allow the permanent capture of 3•4 upon reversing the potential to +100 mV, restoring the open pore current (Figure 3-4B).

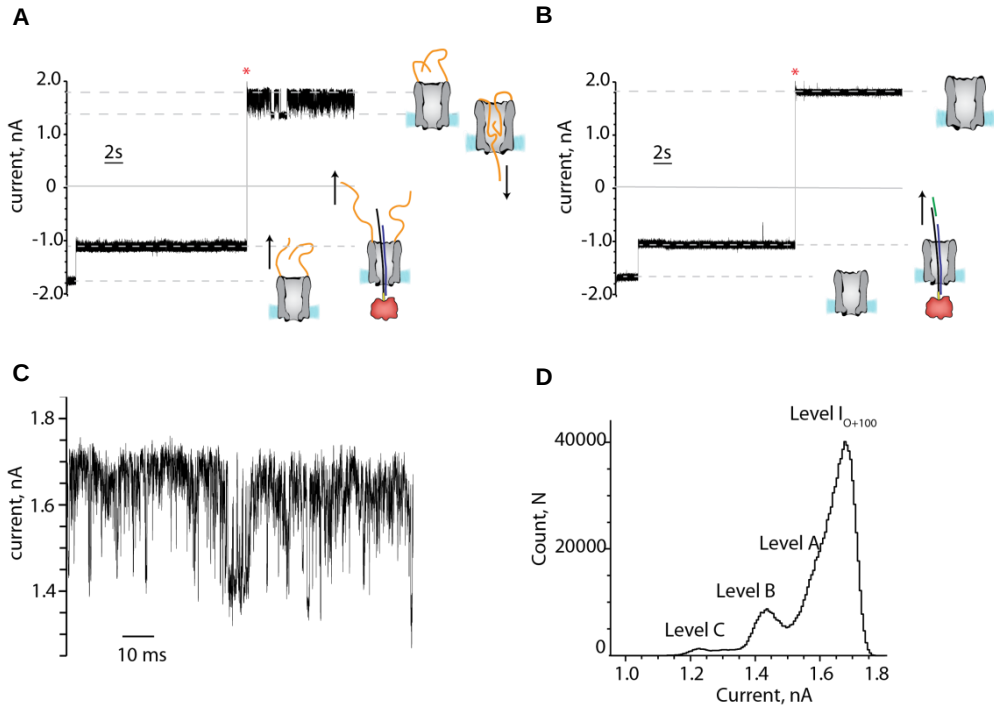

Figure 3-4 Control experiments showing that all components of Fig. 3-3 are necessary to form a DNA rotaxane.

A The absence of the bridging sequence 4 does not allow a linkage to form between ClyA- 2 and 3. After the complex is captured at -100 mV it is readily expelled from the pore at +100 mV (red asterisk) as shown by the typical current signature of an open pore current for ClyA- **2** at +100 mV. **B** The removal of **2** from the pore top (for example after cleavage with DTT) does not allow the 3•4 DNA hybrid to bind to the pore when captured at - 100 mV. Upon reversing the potential to +100 mV (red asterisk) the open pore current is restored. **C** Typical current recording for a ClyA-2 nanopore at +100 mV. **D** All points histogram (5 pA bin size) for 20 seconds of ClyA-2 open pore currents. Level I_{O+100} = 1.71 ± 0.07 nA, level A = 1.62 ± 0.12 nA, level B = 1.43 ± 0.05 nA and level C = 1.28 ± 0.06 nA. These values, determined from 12 experiments, presumably represent different arrangements of the DNA strands lodged within the lumen of the ClyA pore. The electrical recordings were carried out in 2.5 M NaCl, 15 mM Tris-HCl, pH 7.5, at 22 °C. Data were recorded by applying a 10 kHz low-pass Bessel filter and using a 20 µs (50 kHz) sampling rate.

3.3.3 ssDNA and dsDNA blockades of ClyA pores

At high-positive applied potentials, the ionic current of ClyA-2 nanopores fluctuated between the open pore level and several blocked pore levels (Figure 3- 4C-D). Presumably the different blocked current levels observed, at constant positive applied potentials, represent different arrangements of the 12 DNA strands entering contemporarily and temporarily the lumen of the ClyA pore. The ssDNA molecules tethered to the top of the pore entered the lumen of ClyA but did not permanently thread to the *trans* side. Further supporting this interpretation, at +100 mV, the addition of a 90mer ssDNA with irrelevant sequence 5a (Table 3-S1) complexed with neutravidin to the *cis* side of ClyA-CS provoked transient current blockades (Figure 3-5), which were converted into long-lasting DNA threading events upon the subsequent addition to the *cis* compartment of equimolar concentrations of the complementary ssDNA 5b (Table 3-S1, Figure 3-5). To further investigate the capability of ssDNA to span the pore, we tested the ability of the DNA hybrid 3, which is formed by a 3'-biotinylated dsDNA section of 59 nucleobase pairs preceded by a 31-nucleotides 5'-overhang, to translocate through ClyA-CS pores. At +100 mV, the addition of 3 in complex with neutravidin to the *cis* side of a ClyA-CS pore provoked long-lasting current blockades with $I_{RES+100} = 0.69 \pm 0.01$ (mean ± s.d., Figure 3-S5), the same $I_{RES+100}$ value as observed for a *cis* pseudo rotaxane ($I_{RES+100} = 0.68$), suggesting that at this potential the DNA hybrid threads through ClyA and dsDNA spans the lumen of the pore. As the translocation of 3 can only be initiated from the ssDNA section of the DNA duplex, these results suggest that at +100 mV the ssDNA leading sequence of 3 is capable of translocating the lumen of ClyA. Interestingly, at +50 and +70 mV the current blockades were mostly transient (Figure 3-S5), suggesting that at this voltages ssDNA might not pass through the ClyA pore. The addition of strand 6, which is complementary to the first 12 nucleobases of 3, also produced transient current blockades at +50 mV but the current blockades were permanent at +70mV (Figure 3-S5), indicating that the additional dsDNA segment facilitated DNA translocation. The threading of ssDNA or dsDNA into biological nanopores

is often observed above a threshold potential[33–38] (Figure 3-S2) that can be tuned by altering the charge distribution of the lumen of the pore or by changing the ionic strength of the solution[27,39]. Therefore, our findings indicate that ssDNA has a higher threshold for threading through the pore than dsDNA. In solution, a generic ssDNA sequence has a relatively flexible (the persistence length of poly $(dT)_{40}$ is ~1.5 nm in 1 M KCl[40]) but compact structure, which is formed by intrastrand base pairing and base-pair stacking interactions[41–43], that needs to be disrupted to allow the entry of the ssDNA into the pore. By contrast, in dsDNA, intermolecular base pairing mediates duplex formation and short (150 bp) dsDNA molecules behave as rigid rods (the persistence length of dsDNA in 1 M NaCl is ~50 nm[44]) that do not need unfolding to thread through the ClyA pore. Therefore, the higher threshold for ssDNA threading through ClyA is most likely the result of a large entropic barrier because of the confinement of a flexible ssDNA molecule within the pore and to the uncoiling of the polymer before entering the nanopore.

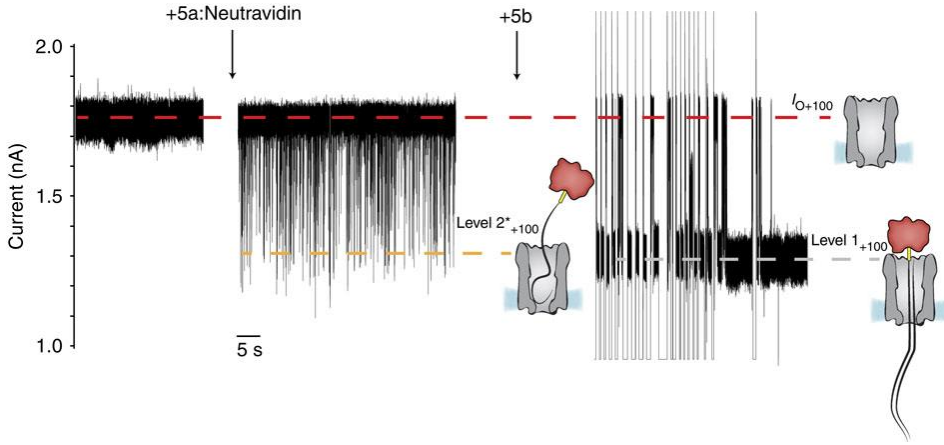

Figure 3-5 ssDNA and dsDNA blockades of ClyA-CS.
At +100 mV, the addition of 2.0 μM of a biotinylated ssDNA (5a) to the *cis* side of ClyA-CS nanopores in the presence of 0.6 μM neutravidin (tetramer) provoked transient current blockades (level 2^*_{+100} = 1.24 ± 0.02 nA, mean ± s.d., $I_{RES+100}$ = 0.69 ± 0.04, mean ± s.d., n = 3), indicating that ssDNA entered the lumen of the pore but only transiently. The subsequent addition of 2.0 μM of the complementary ssDNA strand (5b) to the *cis* compartment converted the current blockades into permanent level 1_{+100} blocks (1.22 ± 0.13 nA, mean ± s.d., $I_{RES+100}$ = 0.67 ± 0.01, mean ± s.d., n = 3), indicating that the dsDNA so formed spanned the entire length of the pore. After each DNA capture, the open pore was regenerated by manual reversal of the potential to +100 mV. Spikes above and below the open pore current level represent capacitive transients. The electrical recordings were carried out in 2.5 M NaCl, 15 mM Tris-HCl, pH 7.5, at 22 °C. Data were recorded by applying a 10-kHz low-pass Bessel filter and using a 20 μs (50 kHz) sampling rate.

3.3.4 Sequence-specific DNA transport through a nanopore machine

As at positive applied potentials ssDNA threads the ClyA pore only transiently, ssDNA molecules attached to the *cis* entrance of ClyA will probe the *cis* solution. On the other hand, as at positive applied potentials dsDNA threads the ClyA pore, when the ssDNA molecule becomes double-stranded (for example, by strand hybridization) the dsDNA strand will translocate through the pore and sample the *trans* solution. Therefore, we designed a nanopore:DNA device, in which the hybridization of a specific ssDNA molecule to the *cis* side of the ClyA-2 nanopore

promoted the translocation of the DNA duplex through the pore. The DNA duplex was then disassembled by a strand-displacement reaction (Figure 3-6A), which resulted in the transport of the DNA cargo across the bilayer and the return of 2 to the *cis* chamber by movement against the applied potential. Conveniently, we found that at both +50 and +100 mV, the addition of a generic dsDNA molecule or a non-specific ssDNA molecule to the *cis* side of ClyA-2 did not produce current blockades (Figure 3-6B and Figure 3-S3), indicating that the tethered ssDNA molecules produced a steric and/or electrostatic impediment that prevented or drastically reduced the entry of free dsDNA and also non-specific ssDNA from solution. Therefore, without the complication of dsDNA transport from solution, the ssDNA covalently attached atop the nanopore conferred specificity to the system by promoting the transport of selected ssDNA molecules while creating a barrier for the translocation of non-specific DNAs. At +50 mV (Figure 3-6B) or +100 mV (not shown), the addition of 3 to the *cis* side of ClyA-2 did not produce current blockades, further confirming that the ssDNA molecules attached to ClyA-2 prevent the entry of non-specific DNA in solution (3 cannot hybridize directly to 2). Nonetheless, after the addition to the *cis* chamber of 6, which is complementary to the last 15 nucleotides of 2 and to the first 12 nucleobases of 3 (Table 3-S1), the dsDNA hybrid nanopore showed permanent current blockades with I_{RES+50} = 0.70 ± 0.02 (mean ± s.d., level 2_{+50} = 0.59 ± 0.02 nA, mean ± s.d., n = 5, Figure 3-6C) the hallmark of DNA capture. The translocation of 3 to the *trans* side was confirmed by the formation of a rotaxane upon addition of neutravidin (0.3 μM, tetramer) to the *trans* chamber (Figure 3-6C-D, Figure 3-SE-F). Crucially, 6 was designed to include a 10-nucleotide 5'-single-stranded extension to serve as toehold for dissociation of the DNA thread (Figure 3-6A). Gratifying, the addition to the *trans* chamber of 7, a ssDNA molecule complementary to 6 (Table 3-S1), released 3 from the nanopore by first hybridizing to the toehold and then promoting strand displacement (Figure 3-6A). This was observed by the restoration of the open pore current because the ssDNA molecules tethered to ClyA returned to the *cis* side after 3 and 6−7 duplex were released from the pore

(Figure 3-6D). Remarkably, the nanopore showed several successions of open and blocked current levels, reflecting cycles of capture, translocation and release, as the DNA cargos were captured from the *cis* chamber, transported through the pore and released to the *trans* chamber (Figure 3-6D). The restoring of the open pore current was not due to the spontaneous retraction of the dsDNA duplex to the *cis* compartment because at +50 mV dsDNA molecules could not exit the pore against the applied potential (Figure 3-S2). In addition, a previous study found that the binding to streptavidin of single biotinylated PEG molecules tethered to the *cis* side of a αHL pore has an on-rate of $3.8 \times 10^{6} M^{-1} s^{-1}$ (ref.[45]), indicating that the DNA−neutravidin complex formed in about 200 ms, which is faster than the observed DNA release time (1.7 ± 0.4 s, mean ± s.d., n = 4).

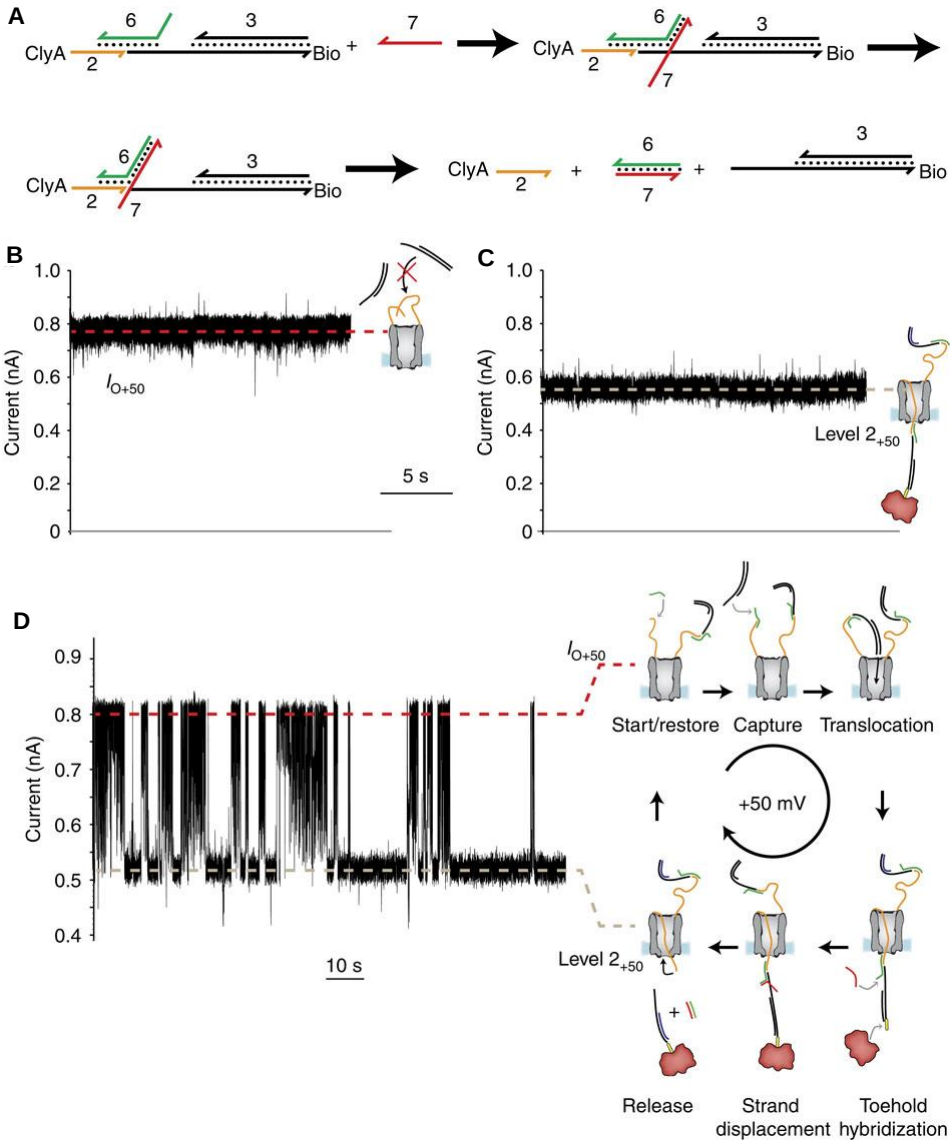

Figure 3-6 Transport of DNA through ClyA nanopores.
A Schematic representation of the strand-displacement reaction that promoted the release of DNA from the pore. The suffix bio indicates a biotin moiety. **B** At +50 mV and in the presence of 3 (0.3 μM), ClyA-2 showed a steady open pore current (I_{O+50} = 0.85 ± 0.01 nA, mean ± s.d., n = 3), showing that the ssDNA strands attached to the pore did not thread through the lumen of the pore and prevented the translocation of dsDNA form solution. **C**) The addition of the ssDNA strand 6 (40 nM) to the *cis* chamber in the presence of the strand 3 and 0.3 μM neutravidin (tetramer) in the *trans* compartment produced long-lasting current blockades with I_{RES+50} = 0.70 ± 0.02 (mean ± s.d., level 2_{+50} = 0.59 ± 0.02 nA, mean ± s.d., n = 5), indicating that the dsDNA hybrid

threaded the pore. **D** The subsequent addition of 1 μM of 7 to the *trans* chamber (+50 mV) promoted the release of the DNA thread by a strand displacement reaction. 2 returned to the *cis* compartment against the applied potential and the open pore current was restored. Specific dsDNA molecules were then sequentially captured and released as shown by successive blocked and open pore currents. In this experiment, the applied potential was set to +50 mV and not to +100 mV as in the rest of this work. This is because at +100 mV ClyA-2 occasionally produced long current blockades that were similar to typical events provoked by the capture of non-specific DNA (Figure 3-S4). Such current blockades were not observed at lower applied potentials; hence, we performed this experiment at +50 mV. In addition, at +50 mV the rate of DNA capture was lower than at +100 mV, and therefore the cycles of capture and release were more easily observed. The electrical recordings were carried out in 2.5 M NaCl, 15 mM Tris HCl, pH 7.5 at 22 °C. Data were recorded by applying a 2-kHz low-pass Bessel filter and using a 100 μs (10 kHz) sampling rate.

3.3.5 **Releasing kinetics and cycling**

Through the analysis of event lifetimes (τ_{OFF}) of the blocked pore current (level 2), we measured a kinetic constant of 0.59 ± 0.14 $\mu M^{-1}s^{-1}$ for the strand-displacement reaction at the *trans* chamber. This value corresponded reasonably well with the ~1 $\mu M^{-1}s^{-1}$ rate constants measured for equivalent strand-displacement reactions in ensemble experiments[46], further confirming that the dsDNA segment of the DNA thread is largely exposed to the *trans* solution (that is, it is not confined within the pore lumen). We observed an average of 41 ± 22 (mean ± s.d., n = 7) cycles before the DNA thread could no longer be released or captured. Occasionally, the cycling spontaneously started again after a few tens of minutes. As we observed more cycles while the bridging oligo 6 and release oligo 7 were high-performance liquid chromatography-purified, it is likely that the DNA strands contained contaminants of DNA molecules of defected synthesis (for example, with shorter toeholds or imperfect complementary sequences), which slowed down or stopped the strand-displacement reaction operated by 7 or failed to capture the DNA thread operated by 6.

3.3.6 Energy landscape of DNA transport

At positive applied potential, the transport of DNA from the *cis* compartment to the *trans* compartment is energetically favorable because the DNA molecules diffuse down a concentration and an electrical potential gradient. However, the threading of ssDNA was not observed experimentally, revealing a large and mainly entropic energy barrier for ssDNA transport through the pore. By contrast, the threading of tethered dsDNA was observed mainly because duplex hybridization atop of the pore reduced the entropic energy barrier for DNA translocation. Once the tethered dsDNA was on the *trans* side of a ClyA-2 pore, the cargo dsDNA would eventually be slowly and spontaneously released to the *trans* chamber. In this work, this process is catalyzed by the strand-displacement reaction operated by the fuel strand in the *trans* chamber. Finally, the translocated tethered ssDNA 2 retracted against the applied potential to the *cis* compartment. Presumably, the return to the *cis* compartment against the potential and the formation of a compact ssDNA structure in the *cis* compartment was favored over the confinement of a ssDNA strand in the pore under +50 mV and the formation of a smaller compact ssDNA structure in the *trans* compartment.

3.4 Discussion

In this work, we have built a membrane-imbedded DNA transporter that is able to selectively shuttle DNA molecules across a phospholipid membrane. Notably, this molecular machine does not allow the translocation of either ssDNA or non-tethered dsDNA; at constant transmembrane potential, it works without external intervention and is modulated by two single-stranded DNA molecules: one attached to the pore that promotes the capture of DNA and the other in the *trans* solution that behaves as ‘fuel’ and promotes the release of a transported DNA cargo.

3.5 Summary

In the present work we demonstrated double-stranded DNA (dsDNA) translocation for the first time through the biological nanopore Cytolysin A (ClyA) from *Salmonella enterica* serovar Typhi. The translocation of dsDNA molecules through biological nanopores is of fundamental importance for the development of direct genomic analyses with biological nanopores. Furthermore, we engineered the nanopore to selectively transport nucleic acids across lipid membranes. The resulting nanopore-device is able to recognize and chaperone a specific DNA molecule across a biological membrane under a fixed trans-membrane potential. Several applications with this DNA transporter could be further develop in the future, such as high-throughput analyses for nucleic acids detection, purification, concentration or the transportation of genetic information across biological membranes. The internal diameter of the ClyA is larger than the diameter of dsDNA, indicating that dsDNA should readily translocate through the nanopore when driven by an electrical potential. Due to the abundance of negatively charged residues lining the lumen of ClyA, DNA does not enter the nanopore at low ionic strength conditions. We observed that DNA could only translocate at high ionic strength, where the internal charges were screened. We formed a complex with biotinylated dsDNA attached to a neutravidin protein, which was permanently immobilized inside the nanopore under constant applied potential. A DNA:nanopore rotaxane was formed to prove that DNA molecules could fully translocate through the ClyA nanopore. The only possible way for the rotaxane to be assembled lies in the ability for a DNA molecule to enter the pore at one entrance, tread the inner lumen and hybridize with another DNA molecule at the opposite entrance of the nanopore. Furthermore, we found that at high ionic strength the threading of ssDNA or dsDNA into the ClyA pore showed a different result. While dsDNA could be permanently immobilized inside the pore, ssDNA molecules could enter the pore but only transiently, it was entropically constrained to promptly exit the inner pore lumen. We sought to use this inbred property as an advantage to develop a nanopore machine. ClyA nanopores were engineered to

present ssDNA molecules chemically attached atop the pore. As observed the ssDNA molecules did not enter the pore permanently under fixed applied potential, but when the ssDNA molecule hybridizes with a ssDNA molecule added in solution, the DNA duplex formation promoted the DNA translocation through the pore. The DNA duplex was then disassembled in the opposite compartment by a strand-displacement reaction, which resulted in the transport of the DNA cargo across the bilayer. The ssDNA covalently attached atop the nanopore produced a steric and / or electrostatic impediment that prevented or drastically reduced the translocation of any unspecific dsDNA or ssDNA added in solution.

3.6 Methods and Materials

3.6.1 DNA oligos and reagents

DNA was purchased from Integrated DNA Technologies (IDT). 6 and 7 were high-performance liquid chromatography-purified by the maker. Neutravidin was acquired from Thermo Fisher and 1,2-diphytanoyl-sn-glycero-3phosphocholine from Avanti Polar Lipids. β-Dodecyl maltoside (DDM) was purchased from GLYCON Biochemicals GmbH. Enzymes were bought from Fermentas and all other materials from Sigma, unless otherwise specified.

3.6.2 Protein preparation

ClyA-CS was made from ClyA-SS, a *S.* Typhi ClyA gene where the cysteine residues at position 87 and 285 of the wild type sequence (ClyA-WT) were replaced with serines. ClyA-CS contains five mutations relative to the ClyA-SS sequence: S87C, L99Q, E103G, F166Y and K294R. Monomers containing a C- terminal oligo-histidine tag were expressed in *E. coli* BL 21 cells and the soluble fraction purified using Ni-NTA affinity chromatography. ClyA dodecamers were formed by the addition of 0.2% DDM and were separated from monomers using blue native polyacrylamide gel electrophoresis. The lowest band of oligomeric

ClyA-CS was extracted and stored at 4 ºC. ClyA-2 nanopores were prepared by covalently attaching 2 to a ClyA protein, in which the two WT cysteine residues (positions 87 and 285) were substituted with serine (ClyA-SS), and a cysteine was introduced at position 103 (aspartate in the WT gene; ClyA-SSC_{103}). ClyA-SSC_{103} was constructed from ClyA-SS, which also encoded a Gly-Ser-Ser linker followed by a C-terminal hexahistidine tag by using the megaprimer method[47] using Phire Hot Start DNA Polymerase (Finnzymes). The lyophilized DNA 2 (5'−TTTTTTTTTATCTACGAATTCATCAGGGCTAAAGAGTGCAGAGTTA CTTAG−3'), containing a protected thiol group attached to the 5' hydroxyl of the DNA strand via a C6 linker (5ThioMC6-D, IDT), was dissolved in TAE buffer (40 mM Tris.HCl, 20 mM acetic acid, 1 mM EDTA, pH 8.5) and reduced with 10 mM DTT for 1 h at 21ºC. DTT in excess was then extracted by phase separation with ethyl acetate added to the reduced aptamer solution. The thiolated aptamers in the aqueous phase were activated with 10 mM 4,4'-dithiopyridine for 1 h at 21ºC. Also 4, 4'-dithiopyridine excess was removed by phase separation with diethyl ether. The activated thiolated aptamers were stored at -20 ºC. ClyA-SSC_{103} monomers were purified in presence of β-mercaptoethanol, which was added to the protein purification buffer (15 mM β-mercaptoethanol) until the final step in which the protein monomers were washed on a Ni-NTA resin with 17 column volumes of buffer containing β- mercaptoethanol and then three volumes of thiol-free buffer. ClyA- SSC_{103} monomers were incubated with activated thiolated aptamer for 2 h at 21 ºC. ClyA-SSC_{103} monomers conjugated with aptamers (ClyA-2 monomers) were purified from excess of unmodified ClyA-SSC_{103} monomers by blue native polyacrylamide gel electrophoresis (BN-PAGE) containing 0.1 % SDS (w/v) in the loading buffer. Conjugated ClyA-SSC_{103} (ClyA-2) monomers were oligomerized in DDM and purified by BN-PAGE. Purified ClyA-2 pores were stored at -80 ºC in 10 mM EDTA and 20 % glycerol[25].

3.6.3 DNA preparation

1 was made using PCR amplification of a pT7 ClyA-WT DNA template using a 5' biotinylated forward primer (bio-5'−TAATACGACTCACTATAGGG−3') and a non−biotinylated reverse primer (5'−CATCAGCAGCACTTTGATATCGCC CACC−3') using Taq DNA Polymerase from REDTaq ReadyMix PCR Reaction Mix (Sigma). After a maximum number of 35 cycles, the PCR products of 24 reaction tubes (50 µl each tube) were purified by using a PCR quick purification kit (QIAGEN), and the size of the construct was checked by using a 2% agarose gel (TAE buffer). The typical product concentration was ~200 ng ml^{-1}. 3 was formed by incubating a 3'-biotinylated ssDNA molecule (5'−GGATGACCTGATCCAGATATTTATTATACAGGTCCAGCGCACCGT CAGCCCAATCGCACTTTTCACAAAAAGAGAGAGAGATCGATTACC−3' bio, 3a), with a 20% excess of a partially complementary ssDNA (5'−GGTAATCGATCTCTCTCTCTTTTTGTGAAAAGTGCGATTGGGCTG ACGGTGCGCTGGAC−3', 3b, Table 3-S1). The temperature was brought to 95 ºC for 1min and then decreased stepwise to room temperature. At around the estimated annealing temperature, the temperature was decreased in 2 ºC steps, each held for 1 minute. The hybrid DNA was then purified from the excess of ssDNA with affinity chromatography using a biotin-binding column containing monomeric avidin immobilized on agarose beads (Thermo Scientific Pierce). 3 was eluted in Biotin Blocking/Elution Buffer according to the protocol and stored at - 20 ºC without further purification. Typically, a DNA concentration of ~400 ng ml^{-1} was obtained. The size of the dsDNA was checked by using a 2 % agarose gel in TAE buffer. The purified dsDNA was stored at -20 ºC in the presence of 1 mM EDTA.

3.6.4 Electrical recordings and data analysis

Artificial planar lipid bilayers were prepared as described[48]. If not otherwise specified, the signal was collected at a sampling rate of 50 kHz after processing with a 10-kHz Bessel filter. The lipid bilayer was formed by the addition of 1–2 µl

of a 10 % v/ v solution of 1,2-diphytanoylsn-glycero-3-phosphocholine in pentane. The electrical potential was applied by using Ag/AgCl electrodes submerged in agar bridges (3 % w/ v low melt agarose in 2.5 M NaCl buffer). The applied potential refers to the potential of the working electrode connected to the *trans* compartment of the apparatus. ClyA nanopore solutions (0.01–0.1 ng ml^{-1}) were added to the *cis* compartment, which was connected to the ground electrode. After the insertion of a single pore, excess protein was removed by several cycles of perfusion. Electrical recordings were carried out in 2.5 M NaCl, 15 mM Tris-HCl, pH 8.0, at 22 ºC. The errors indicate the standard deviation from the average for at least three independent repeats, the number of which is indicated by 'n'. The duration of the DNA release cycle was measured by fitting the dwell time of the blocked pore current (level 2_{+50}) to a single exponential (logarithmic binning, 10 bin per decade). I_O and I_B values were calculated from Gaussian fitting to all-point histograms of the open pore and blocked pore currents, respectively. Each I_{RES} value was calculated as average from the ratio I_B/ I_O for at least three experiments.

3.7 Acknowledgements

We thank Hagan Bayley for useful comments on the manuscript and the European Research Council (European Commission's Seventh Framework Programme, project no. 260884) for funding. Franceschini L. and Biesemans A. are funded by a PhD grant from the Agency for Innovation by Science and Technology (IWT) Flanders.

3.8 References

1. Fletcher, J.M., Harniman, R.L., Barnes, F.R., Boyle, A.L., Collins, A., Mantell, J., Sharp, T.H., Antognozzi, M., Booth, P.J., Linden, N., Miles, M.J., Sessions, R. B.,Verkade, P., Woolfson, D.N., Self-assembling cages from coiled-coil peptide modules. *Science* 340(6132): 595–599 (2013).

2. Gradišar, H., Božič S., Doles, T., Vengust, D, Hafner-Bratkovič, I., Mertelj, A., Webb, B., Šali, A., Klavžar, S., Jerala, R., Design of a single-chain polypeptide tetrahedron assembled from coiled-coil segments. *Nat. Chem. Biol.* 9(6): 362–366 (2013).

3. King, N.P., Sheffler, W., Sawaya, M.R., Vollmar, B.S., Sumida, J.P., André, I., Gonen, T., Yeates, T.O., Baker, D., Computational design of self-assembling protein nanomaterials with atomic level accuracy. *Science* 336(6085): 1171–1174 (2012).

4. Sinclair, J.C., Davies, K.M., Venien-Bryan, C., Noble, M.E., Generation of protein lattices by fusing proteins with matching rotational symmetry. *Nat. Nanotech.* 6(9): 558–562 (2011).

5. Ramachandran, N., Hainsworth, E., Bhullar, B., Eisenstein, S., Rosen, B., Lau A.Y., Walter, J.C., LaBaer, J., Self-assembling protein microarrays. *Science* 305(5680), 86–90 (2004).

6. Simmel, F.C., DNA-based assembly lines and nanofactories. *Curr. Opin. Biotechnol.* 23(4): 516–521 (2012).

7. Ke, Y., Ong, L.L., Shih, W.M., Yin, P., Three-dimensional structures selfassembled from DNA bricks. *Science* 338(6111): 1177–1183 (2012).

8. Chen, J.H., Seeman, N.C., Synthesis from DNA of a molecule with the connectivity of a cube. *Nature* 350(6319): 631–633 (1991).

9. Douglas, S.M., Dietz, H., Liedl, T., Högberg, B., Graf, F., Shih, W. M., Self-assembly of DNA into nanoscale three-dimensional shapes. *Nature* 459(7245): 414–418 (2009).

10. Wei, R., Martin, T.G., Rant, U., Dietz, H., DNA origami gatekeepers for solidstate nanopores. *Angew. Chem. Int. Ed. Engl.* 51(20): 4864–4867 (2012).

11. Bell, N.A., Engst, C.R., Ablay, M., Divitini, G., Ducati, C., Liedl, T., Keyser, U.F., DNA origami nanopores. *Nano Lett.* 12(1): 512–517 (2012).

12. Burns, J.R., Stulz, E., Howorka, S., Self-assembled DNA nanopores that span lipid bilayers. *Nano Lett*. 13(6): 2351–2356 (2013).

13. Langecker, M., Arnaut, V., Martin, T.G., List, J., Renner, S., Mayer, M., Dietz, H., Simmel, F.C., Synthetic lipid membrane channels formed by designed DNA nanostructures. *Science* 338(6109): 932–936 (2012).

14. Zhang, D.Y., Seelig, G., Dynamic DNA nanotechnology using stranddisplacement reactions. *Nat. Chem.* 3(2): 103–113 (2011).

15. Graugnard, E., Kellis, D.L., Bui, H., Barnes, S., Kuang, W., Lee, J., Hughes, W.L., Knowlton, W.B., Yurke, B., DNA-controlled excitonic switches. *Nano. Lett.* 12(4): 2117–2122 (2012).

16. Qian, L., Winfree, E., Scaling up digital circuit computation with DNA strand displacement cascades. *Science* 332(6034): 1196–1201 (2011).

17. Yan, H., Zhang, X., Shen, Z., Seeman, N.C., A robust DNA mechanical device controlled by hybridization topology. *Nature* 415(6867): 62–65 (2002).

18. Yin, P., Yan, H., Daniell, X.G., Turberfield, A.J., Reif, J.H., A unidirectional DNA walker that moves autonomously along a track. *Angew. Chem. Int. Ed.* 43(37): 4906–4911 (2004).

19. Shin, J.S., Pierce, N.A., A synthetic DNA walker for molecular transport. *J. Am. Chem. Soc.* 126(35): 10834–10835 (2004).

20. Wickham, S.F., Endo, M., Katsuda, Y., Hidaka, K., Bath, J., Sugiyama, H., Turberfield, A.J., Direct observation of stepwise movement of a synthetic molecular transporter. *Nat. Nanotech*. 6(3): 166–169 (2011).

21. Sherman, W.B., Seeman, N.C., A precisely controlled DNA biped walking device. *Nano Lett.* 4(7): 1203–1207 (2004).

22. Lund, K., Manzo, A.J., Dabby, N., Michelotti, N., Johnson-Buck, A., Nangreave, J., Taylor, S., Pei, R., Stojanovic, M.N., Walter, N.G., Winfree, E., Yan, H., Molecular robots guided by prescriptive landscapes. *Nature* 465(7295): 206–210 (2010).

23. Venkataraman, S., Dirks, R.M., Rothemund, P.W., Winfree, E., Pierce, N.A., An autonomous polymerization motor powered by DNA hybridization. *Nat. Nanotech.* 2(8): 490–494 (2007).

24. Yin, P., Choi, H.M.T., Calvert, C.R., Pierce, N.A., Programming biomolecular self-assembly pathways. *Nature* 451(7176): 318–U314 (2008).

25. Soskine, M., Biesemans, A., Moeyaert, B., Cheley, S., Bayley, H., Maglia, G., An engineered ClyA nanopore detects folded target proteins by selective external association and pore entry. *Nano Lett.* 12(9): 4895–4900 (2012).

26. Mueller, M., Grauschopf, U., Maier, T., Glockshuber, R., Ban, N., The structure of a cytolytic alpha-helical toxin pore reveals its assembly mechanism. *Nature* 459(7247): 726–730 (2009).

27. Maglia, G., Henricus, M., Wyss, R. Li, Q., Cheley, S., Bayley, H., DNAstrands from denatured duplexes are translocated through engineered protein nanopores at alkaline pH. *Nano Lett.* 9(11): 3831–3836 (2009).

28. Franceschini, L., Mikhailova, E., Bayley, H., Maglia, G., Nucleobase recognition at alkaline pH and apparent pKa of single DNA bases immobilised within a biological nanopore. *Chem. Commun. (Camb)* 48(10): 1520–1522 (2012).

29. Pease, A.R., Jeppesen, J.O., Stoddart, J.F., Luo, Y., Collier, C.P., Heath, J.R., Switching devices based on interlocked molecules. *Acc. Chem. Res.* 34(6): 433–444 (2001).

30. Balzani, V.V., Credi, A., Raymo, F.M., Stoddart, J.F., Artificial molecular machines. *Angew. Chem. Int. Ed. Engl.* 39(19): 3348–3391 (2000).

31. Ackermann, D., Schmidt, T.L., Hannam, J.S., Purohit, C.S., Heckel, A., Famulok, M., A double-stranded DNA rotaxane. *Nat. Nanotech.* 5(6): 436–442 (2010).

32. Sánchez-Quesada, J., Saghatelian, A., Cheley, S., Bayley, H., Ghadiri, M.R. Single DNA rotaxanes of a transmembrane pore protein. *Angew. Chem. Int. Ed. Engl.* 43(23), 3063–3067 (2004).

33. Meller, A., Nivon, L., Branton, D., Voltage-driven DNA translocations through a nanopore. *Phys. Rev. Lett.* 86(15): 3435–3438 (2001).

34. Henrickson, S.E., Misakian, M., Robertson, B., Kasianowicz, J.J., Driven DNA transport into an asymmetric nanometer-scale pore. *Phys. Rev. Lett.* 85(14): 3057–3060 (2000).

35. Maglia, G., Restrepo, M.R., Mikhailova, E., Bayley, H., Enhanced translocation of single DNA molecules through a-hemolysin nanopores by manipulation of internal charge. *Proc. Natl Acad. Sci. USA* 105(50): 19720–19725 (2008).

36. Butler, T.Z., Pavlenok, M., Derrington, I.M., Niederweis, M., Gundlach, J.H., Single-molecule DNA detection with an engineered MspA protein nanopore. *Proc. Natl Acad. Sci. USA* 105(52), 20647–20652 (2008).

37. Liu, Q., Wu, H., Wu, L., Xie, X., Kong, J., Ye, X., Liu, L., Voltage-driven translocation of DNA through a high throughput conical solid-state nanopore. *PLoS One* 7(9): e46014 (2012).

38. Heng, J.B., Aksimentiev, A., Ho, C., Marks, P., Grinkova, Y.V., Sligar, S., Schulten, K., Timp, G., Stretching DNA using the electric field in a synthetic nanopore. *Nano. Lett.* 5(10): 1883–1888 (2005).

39. Wanunu, M., Morrison, W., Rabin, Y., Grosberg, A.Y., Meller, A., Electrostatic focusing of unlabelled DNA into nanoscale pores using a salt gradient. *Nat. Nanotech.* 5(2): 160–165 (2010).

40. Murphy, M.C., Rasnik, I., Cheng, W., Lohman, T.M., Ha, T., Probing singlestranded DNA conformational flexibility using fluorescence spectroscopy. *Biophys. J.* 86(4): 2530–2537 (2004).

41. Kowalczyk, S.W., Tuijtel, M.W., Donkers, S.P., Dekker, C., Unraveling singlestranded DNA in a solid-state nanopore. *Nano Lett.* 10(4): 1414–1420 (2010).

42. Cracknell, J.A., Japrung, D., Bayley, H., Translocating kilobase RNA through the Staphylococcal alpha-hemolysin nanopore. *Nano Lett.* 13(6): 2500–2505 (2013).

43. Zhang, Y., Zhou, H., Ou-Yang, Z.C., Stretching single-stranded DNA: interplay of electrostatic, base-pairing, and base-pair stacking interactions. *Biophys. J.* 81(2): 1133–1143 (2001).

44. Baumann, C.G., Smith, S.B., Bloomfield, V.A., Bustamante, C., Ionic effects on the elasticity of single DNA molecules. *Proc. Natl Acad. Sci. USA* 94(12): 6185–6190 (1997).

45. Movileanu, L., Howorka, S., Braha, O., Bayley, H., Detecting protein analytes that modulate transmembrane movement of a polymer chain within a single protein pore. *Nat. Biotechnol.* 18(10): 1091–1095 (2000).

46. Zhang, D.Y., Winfree, E., Control of DNA strand displacement kinetics using toehold exchange. *J. Am. Chem. Soc.* 131(47): 17303–17314 (2009).

47. Miyazaki, K., MEGAWHOP cloning: a method of creating random mutagenesis libraries via megaprimer PCR of whole plasmids. *Methods Enzymol.* 498: 399–406 (2011).

48. Maglia, G., Heron, A.J., Stoddart, D., Japrung, D., Bayley, H., Analysis of single nucleic acid molecules with protein nanopores. *Methods Enzymol.* 474: 591–623 (2010).

3.9 Supplementary Information

A nanopore machine promotes the vectorial transport of DNA across membrane

Table 3-S1 DNA molecules used in this work.

Name		DNA sequence
1†	1a	5′-/Bio/TAATACGACTCACTATAGGGAGACCACAACGGTTTCCCTCTAGAAATAATTTTG TTTAACTTTAAGAAGGAGATATACATATGACGGGTATCTTTGCGGAACAGACGGTGGAAGTT GTGAAAAGTGCGATTGAAACGGCTGACGGTGCGCTGGACCTGTATAATAAATATCTGGATCA GGTCATCCCGTGGAAAACCTTTGACGAAACGATTAAAGAACTGAGCCGTTTCAAACAGGAAT ACAGTCAAGAAGCGTCCGTCCTGGTGGGCGATATCAAAGTGCTGCTGATG-3′
	1b	5′-*CATCAGCAGCACTTTGATATCGCCCACCAGGACGGACGCTTCTTGACTGTATTCCTGTT TGAAACGGCTCAGTTCTTTAATCGTTTCGTCAAAGGTTTTCCACGGGATGACCTGATCCAGA TATTTATTATACAGGTCCAGCGCACCGTCAGCCGTTTCAATCGCACTTTTCACAACTTCCAC CGTCTGTTCCGCAAAGATACCCGTCATATGTATATCTCCTTCTTAAAGTTAAACAAAATTAT TTCTAGAGGGAAACCGTTGTGGTCTCCCTATAGTGAGTCGTATTA*-3′
2		5′-TTTTTTTTTATCTACGAATTCATCAGGGCTAAAGAGTGCAGAGTTACTTAG-3′
3†	3a	5′-GGATGACCTGATCCAGATATTTATTATACAGGTCCAGCGCACCGTCAGCCCAATCGCAC TTTTCACAAAAAGAGAGAGAGATCGATTACC/Bio/-3′
	3b	5′-*GGTAATCGATCTCTCTCTCTTTTTGTGAAAAGTGCGATTGGGCTGACGGTGCGCTG GAC* -3′
4		5′-AATAAATATCTGGATCAGGTCATCCCTAAGTAACTCTGCAC-3′
5a		5′-GGATGACCTGATCCAGATATTTATTATACAGGTCCAGCGCACCGTCAGCCCAATCGCAC TTTTCACAAAAAGAGAGAGAGATCGATTACC/Bio/-3′
5b		5'-GGTAATCGATCTCTCTCTCTTTTTGTGAAAAGTGCGATTGGGCTGACGGTGCGCTGGA CCTGTATAATAAATATCTGGATCAGGTCATCC-3'
6		5′-GCCCTATATTATCAGGTCATCCCTAAGTAACTCTGCA-3′
7		5′-TGCAGAGTTACTTAGGGATGACCTGATAATATAGGGC-3′

†1 & 3 were formed and purified as described in 3.6.3 DNA preparation (page 88). The complementary sequences in the two DNA strands are shown in italics. The suffix bio indicates a biotin moiety.

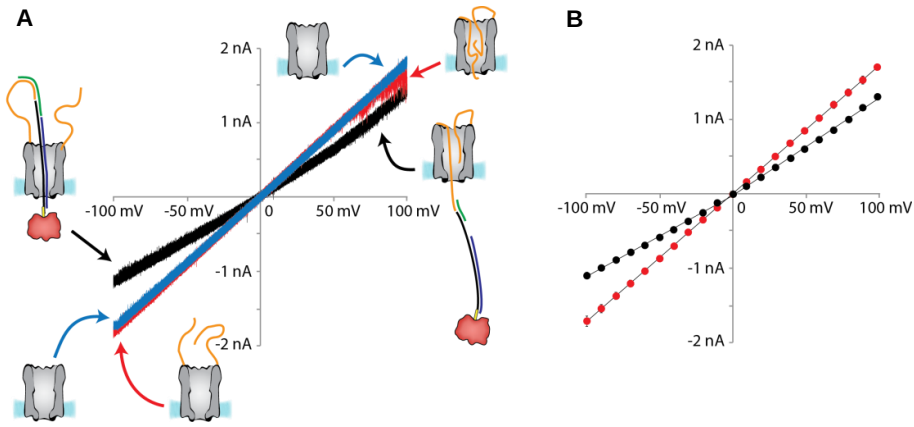

Figure 3-S1 Current versus voltage (IV) relationships for ClyA-2 nanopores.

A A typical IV curve for ClyA-**2** before (red line) and after (black line) rotaxane formation. The blue line indicates the same nanopore after the DNA molecules attached to the nanopore have been removed by the addition of DTT. The current recordings were measured by applying an automated protocol that ramped the voltage from -100 mV to +100 mV in 4 seconds. **B** I-V curves calculated from the average of four experiments showing the steady-state (1 s) ClyA-**2** open pore current levels (red spheres) and ClyA- 2 open pore current levels in a rotaxane configuration (black spheres). The unitary conductance values of the nanopores as calculated from the slopes of the I-V curves were 17.1 nS for ClyA-2 at both positive and negative bias, 10.8 nS for the rotaxane at negative bias and 13.0 nS at positive bias. The rotaxanes were prepared as described in Figure 3-3. The electrical recordings were carried out in 2.5 M NaCl, 15 mM Tris-HCl, pH 7.5, at 22 °C. Data were recorded by applying a 10 kHz low-pass Bessel filter and using a 20 μs (50 kHz) sampling rate.

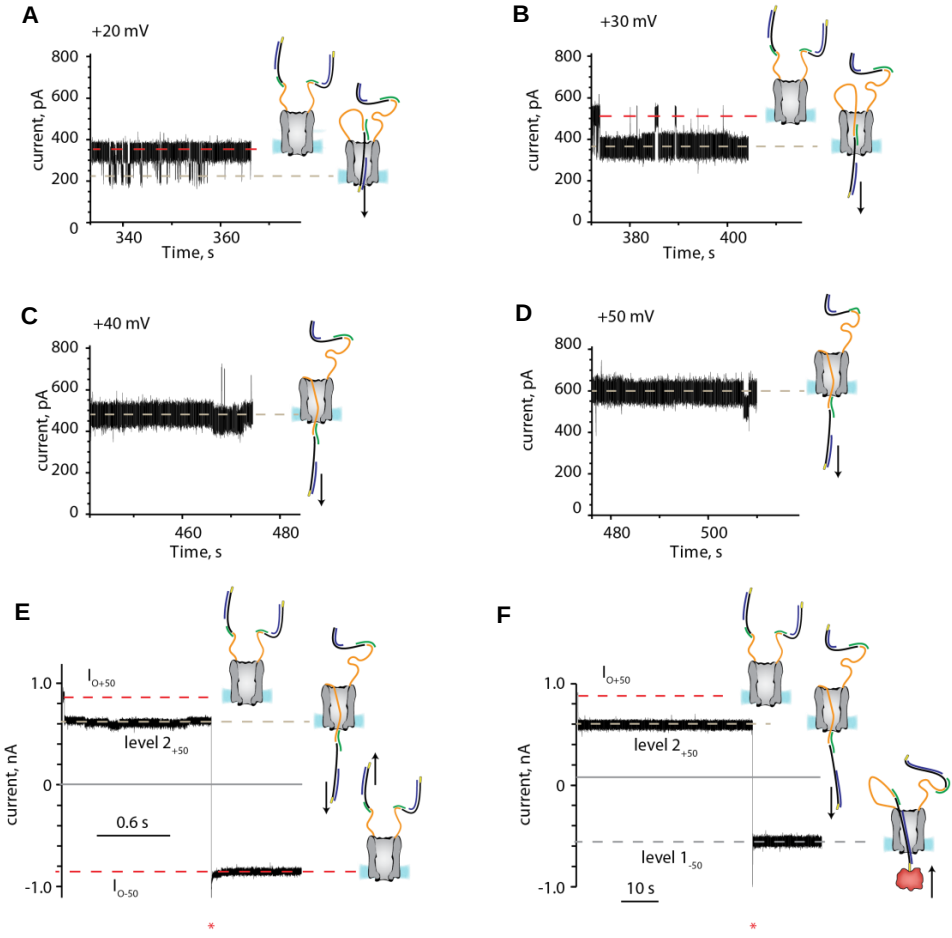

Figure 3-S2 dsDNA current blockades to ClyA-2.
On the right of each current trace the cartoon represents the physical interpretation of the current recordings. **A-D** Current recordings for ClyA-2 after hybridization with a 3•6 (green and black lines, respectively) at different applied potentials. **E** At +50 mV, upon hybridization with 6 (green strand, 40 nM) and 2 (orange strand) the DNA duplex 3 (black strand, 0.3 µM) is transported through the pore as shown by the drop in the ionic current from I_{O+50}= 0.85 ± 0.01 nA, to a level 2_{+50} block (I_{RES+50} = 0.70 ± 0.02). Reversal of the applied potential to -50 mV restored the open pore current (I_{O-50}= 0.83 ± 0.01nA). **F** The subsequent addition of 0.3 µM neutravidin (red) to the *trans* compartment locked the DNA thread within the pore as revealed after the reversal of the potential to -50 mV when a blocked pore level (I_{RES-50} = 0.67 ± 0.02) was observed. The electrical recordings were carried out in 2.5 M NaCl, 15 mM Tris-HCl, pH 7.5, at 22 °C. Data were recorded by applying a 10 kHz low-pass Bessel filter and using a 20 µs (50 kHz) sampling rate.

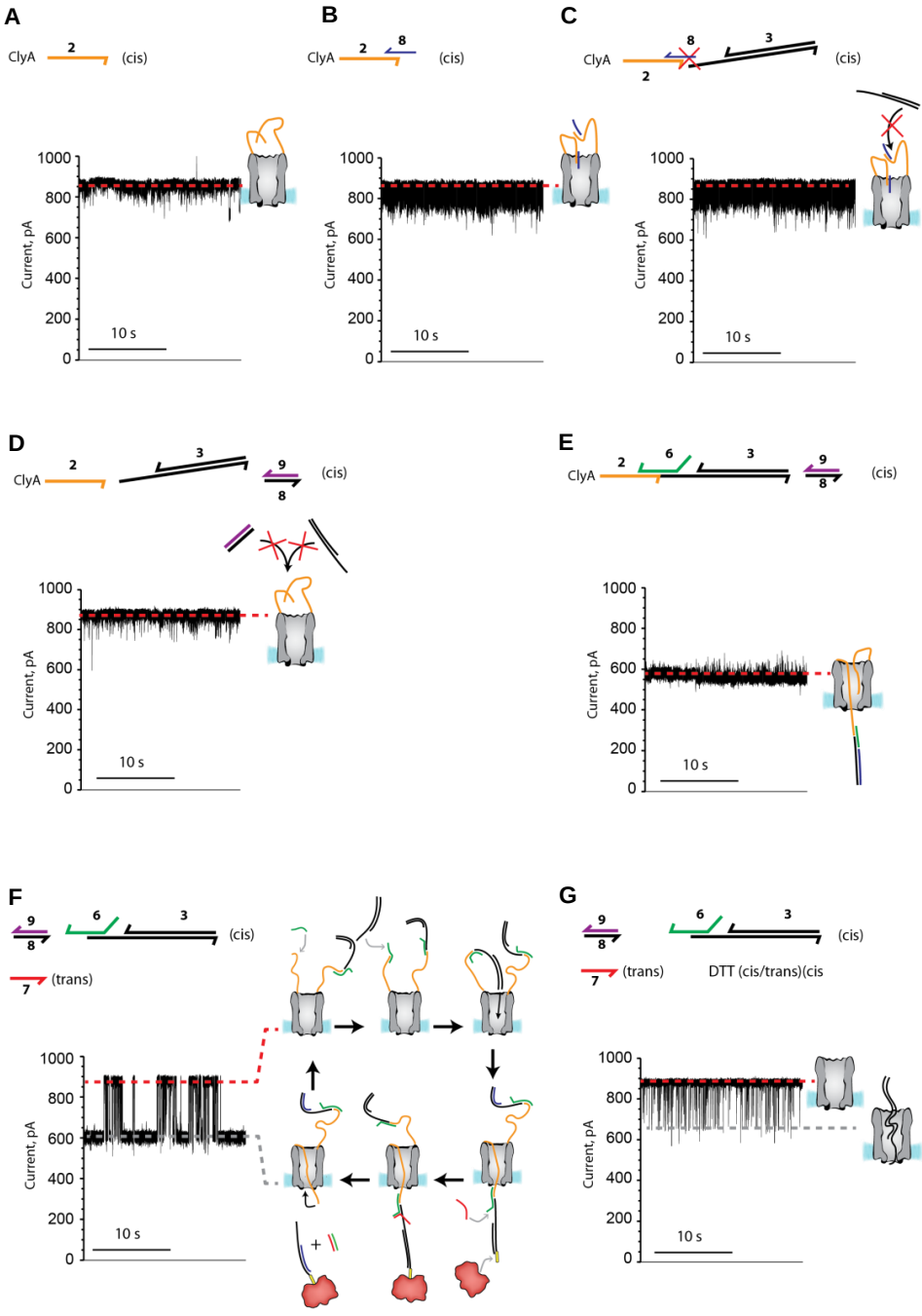
A
ClyA
2
(cis)
Current, pA
1000
800
600
400
200
0
10 s
B
ClyA
2
8
(cis)
Current, pA
10 s
C
ClyA
2
8
3
(cis)
Current, pA
10 s
D
ClyA
2
3
9
8
(cis)
Current, pA
10 s
E
ClyA
2
6
3
9
8
(cis)
Current, pA
10 s
F
9
8
6
3
(cis)
7
(trans)
Current, pA
10 s
G
9
8
6
3
(cis)
7
(trans)
DTT (cis/trans)(cis
Current, pA
10 s

Figure 3-S3 Selective DNA capture by ClyA-2 pores at +50 mV.
In all panels at the top is the depiction of the DNA molecules used in the experiment that are added in succession (from panel a to panel g). The DNA oligos were added to the *cis* compartment except for oligo **7** and neutravidin that were added to the *trans* compartment. DTT was added to both compartments. **A** Open pore current of a ClyA-2 nanopore (oligo 2 is shown in orange). The transient ionic current blockades below the open pore current indicate the transient entry of the tethered ssDNA molecules in the lumen of the pore. **B** Addition of oligo 8 (20 nM, blue, 5'-TTTTTTTTTTTT CAGGTCATCCCTAAGTAACTCTGCA-3') to the *cis* compartment. The 15 nucleotides at the 3' end of oligo 8 hybridized with the last 15 nucleotides of 2 as shown by the more frequent ionic current blockades due to the entry of the dsDNA hybrid into the pore lumen. **C** Addition of DNA duplex 3 (1 μM, black) to the *cis* compartment. The 5' end of 8 contained a stretch of poly(dT) that could not bind to the 3' ssDNA stretch of 3, which then could not enter the pore, as shown by no additional current blockades. **D** Addition of oligo 9 (60 nM, purple, 5' –TGCAGAGTT ACTTAGGGATGACCTGAAAAAAAAAAAA-3') to the *cis* compartment. Oligo 9 was complementary to oligo 8 and detached it from ClyA-2 by a strand displacement reaction and restored the open pore current typical for ClyA-2 nanopores (panel a). **E** Addition of oligo 6 (600 nM) to the *cis* compartment. Since oligo 6 was complementary to the ssDNA attached to ClyA-2 and the ssDNA overhang in the duplex 3, a dsDNA became tethered to the top of ClyA, which was then captured by the pore, as shown by a permanent current blockade. **F** Addition of oligo 7 (1 μM, red) and neutravidin (0.3 μM, tetramer) to the *trans* compartment. Oligo 7 promoted the release of the DNA duplex 3 to the *trans* compartment as shown by the cycling of the open and the blocked pore currents. **G** Addition of DTT (20 mM) to both *cis* and *trans* compartments. After DTT was added, the DNA molecules were detached from the pore entrance and the dsDNA in solution could enter the ClyA pore, as shown by the transient current blockades. The electrical recordings were carried out in 2.5 M NaCl, 15 mM Tris-HCl, pH 7.5, at 22 °C. Data were recorded by applying a 10 kHz low-pass Bessel filter and using a 20 μs (50 kHz) sampling rate.

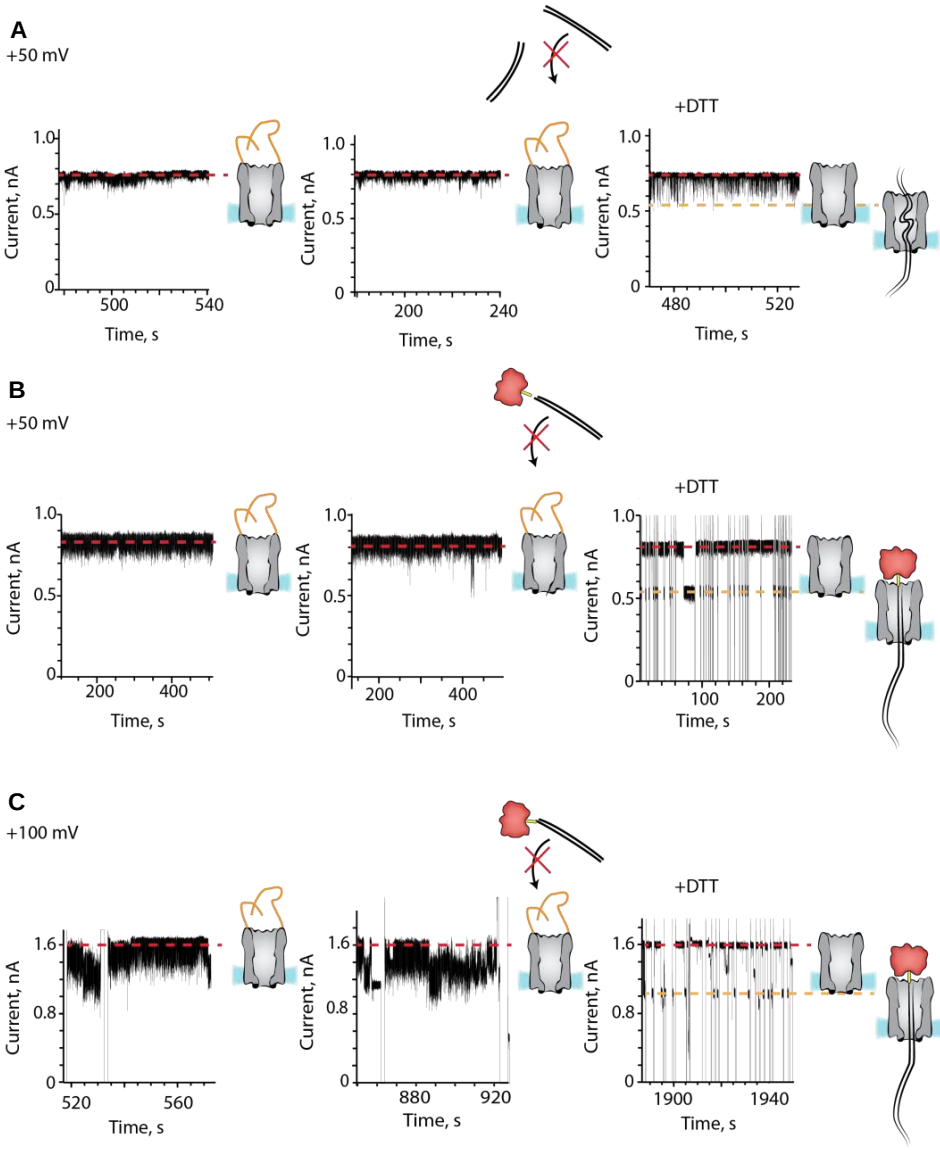

Figure 3-S4 Selective DNA threading through ClyA-2 pores.
A Left, at +50 mV the ionic current through ClyA-2 nanopores showed fast and shallow current blockades, suggesting that the ssDNA molecules attached at the *cis* entrance of ClyA-2 transiently occupy the lumen of the pore. Middle, after dsDNA strand 1 (50 nM) was added to the *cis* compartment the current signals did not change, indicating that dsDNA did not enter ClyA-2. Right, 20 minutes after the addition of 20 mM DTT to the *cis* compartment the DNA molecules atop the ClyA pore were removed and the DNA could translocate through the pore. **B** Same experiment as described in panel a, but in the presence of 1 µM of neutravidin in the *cis* compartment resulting in pseudorotaxane formation as shown by the permanent ionic current blockades due to the threading of

DNA through the pore. The open pore current was restored by reversing the potential to -100 mV and the stepping back to +100 mV. Spikes above and below the open pore current level represent capacitive transients that followed the reversing of the bias that was applied after each DNA threading event. **C** Same as in panel b, but at +100 mV. The electrical recordings were carried out in 2.5 M NaCl, 15 mM Tris.HCl, pH 7.5, at 22 °C. Data were recorded by applying a 10 kHz low-pass Bessel filter and using a 20 μs (50 kHz) sampling rate.

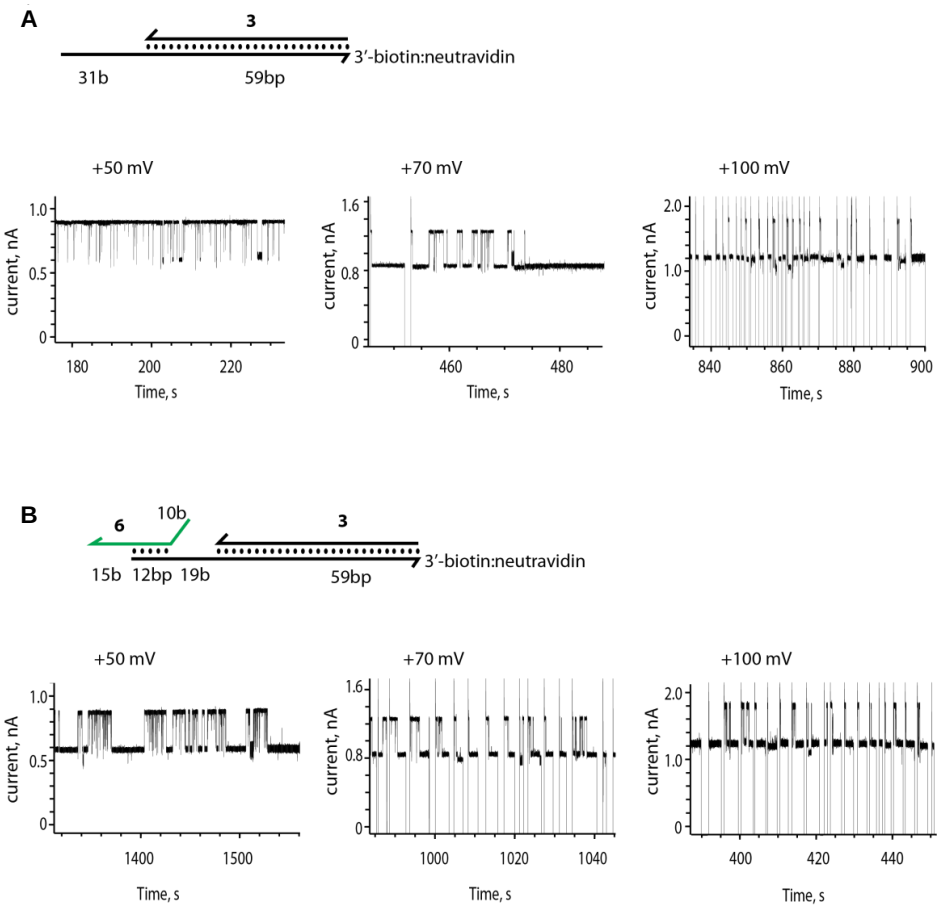

Figure 3-S5 Voltage dependence of the interaction of a ssDNA-dsDNA hybrid construct with ClyA-CS pores.

The DNA molecules used in each experiment are depicted above the current recordings. **A** Current blockades of the DNA hybrid 3 (1.0 µM) in complex with neutravidin (0.3 µM) at +50 mV (left), +70 mV (middle) and +100 mV (right). **B** Current blockades of the DNA hybrid 3•6 in complex with neutravidin at +50 mV (left), +70 mV (middle) and +100 mV (right). After each DNA threading event, the open pore was regenerated by manual switching the potential to -/+100 mV. Spikes above and below the open pore current level represent capacitive transients. The electrical recordings were carried out in 2.5 M NaCl, 15 mM Tris-HCl, pH 7.5, at 22 °C. Data were recorded by applying a 10 kHz low-pass Bessel filter and using a 20 µs (50 kHz) sampling rate.

Chapter 4

The precise engineering of the ClyA nanopore is required to observe ssDNA and dsDNA translocation at physiological ionic strength

Lorenzo Franceschini[1], Tine Brouns[1] and Giovanni Maglia[1&2]

Manuscript in preparation

L. F. and G. M. designed the research,
L. F. and T. B. performed the research,
G. M. and L. F. wrote the paper.

[1]University of Leuven, Leuven, Belgium

[2]University of Groningen, Groningen, The Netherlands

4.1 Abstract

The transport of DNA molecules across nano-scale pores is an important biological process and is under intense investigation for the development of rapid DNA analysis and biomarker detection. Many of such applications require observing the translocation of DNA at near physiological ionic strengths, at which condition the majority of biological nanopores do not perform well. Here we engineered the ClyA, a biological nanopore with a 3.3 nm constriction, to electrophoretically translocate double and single-stranded DNA molecules at physiological salt concentration. We found that the exact distribution of the internal surface charges in the nanopore, it is crucial for observing DNA translocation events. The resulting engineered ClyA nanopore demonstrated by DNA rotaxane formation the translocation and detection of both ssDNA and dsDNA molecules at physiological salt concentration (0.15 M NaCl). Further, the results obtained from the electrophoretical translocation of DNA molecules tested at different ionic strengths, suggest that the precise engineering of the nanopore is important to overcome the electrostatic and entropic barriers that regulate the translocation of DNA molecules through narrow nanopores.

4.2 Introduction

Nucleic acid analysis with nano-scale pores is an advantageous process that has received strong interest for the many possible applications that can be exploited such as fast and inexpensive DNA sequencing[1-3]. When a biological nanopore is reconstituted in an artificial lipid membrane, in aqueous solution and under an electrical applied potential, ions are conducted through the nanopore generating an ionic current. A DNA molecule can enter the pore and provide a characteristic current blockade event, which amplitude and duration time can be used to identify the molecule, while the frequency of events can be used to determine its concentration in solution[1]. Notably, the biological nanopores alpha haemolysin (αHL) and porin A (MspA) have been extensively used for single-stranded DNA analyses, allowing the identification of homopolymer strands[4], detection of different ssDNA lengths[5], discrimination of nucleo-bases[2,6] and their epigenetic modifications[7] and the investigation of intra-molecular ssDNA/dsDNA assemblies such as rotaxanes[8] and hairpins[9]. However, direct dsDNA readings with these pores are not possible, because of their narrow inner pore constriction[1,8], which allows only the translocation of ssDNA molecules. Enabling dsDNA translocation with biological nanopores could be particularly advantageous for the development of genomic applications such as DNA mapping analysis[9]. The bacteriophage connector φ29[10] and more recently the Cytolysin A (ClyA) pore[11] have shown DNA translocation through their large inner pore diameter (> 3 nm), allowing the direct passage and detection of dsDNA molecules (2 nm B form[12]). Although in both pores, the numerous negatively charged residues lining the inner pore lumen limited DNA translocation to high ionic strengths only (1 and 2.5 M NaCl respectively for φ29 connector and ClyA pore)[10,11]. The electrostatic repulsions generated between the negatively charged DNA molecules and the pore inner negative charges hamper the passage of DNA molecules through the pore, especially at low ionic strengths where the pore internal charges are not screened by the counterions of the electrolyte buffer solution[11]. Nevertheless, allowing DNA translocation at low ionic strengths could be advantageous for the detection with

biological nanopores of drugs and biological markers, which can specifically bind to DNA molecules only at low-salt concentrations[13,14]. Furthermore, nanopores could be used to investigate the mechanism of action of biological systems such as enzymes that process nucleic acids in real-time and required low salt concentration for their activity[15–17]. In the present work we engineered the ClyA pore to translocate DNA at low ionic strengths. The resulting ClyA mutant demonstrated the ability to translocate and detect both ssDNA and dsDNA molecules at physiological salt concentration (0.15 M NaCl).

4.3 Results

4.3.1 Engineering ClyA nanopores to favor the capture of DNA

In this work we used an engineered *Salmonella* Typhi ClyA nanopore (ClyA-AS), selected for its favorable proprieties such as high-applied voltage stability in planar lipid bilayer recording as previously described[14]. ClyA-AS contains the following mutations relative to the *S.* Typhi ClyA-WT gene: C87A, L99Q, E103G, C285S, F166Y, I203V, K294R, H307Y. DNA molecules do not enter ClyA-AS nanopores at low ionic strengths [11]. Inspired by previous works with the αHL and MspA nanopores[8,18], we rearranged the internal charge of ClyA-AS to induce the capture of DNA by the nanopore at physiological ionic strengths (Figure 4-1A and Table 4-1). In Figure 4-1A at the left side of ClyA-AS pore are indicated the positions for each single amino acid substitution tested in the present work. The resulting ClyA- AS variants showed a transient reduction of the open pore conductance (gating) at constant applied voltage. Although the nanopore gating frequency is voltage dependent, we use the gating-voltage (V_G) as measurement of gating to define the applied voltage at which an engineered nanopore remained open (no gating) for a 30 seconds timespan (Table 4-1). The translocation of DNA through each modified nanopore was tested at the respective applied V_G by adding

1 μM of a 90mer 3'- biotinylated ssDNA molecule (1a, Table 4-S1) followed by its complementary strand at equimolar concentration (1b, Table 4-S1) and finally neutravidin (NA 1.2 μM, Figure 4-S1 and Table 4-1).

Initially, we introduced a single arginine ring at the *cis* entrance of ClyA-AS (position 110, Figure 4-1A). ClyA-AS-S110R (ClyA-R) showed no DNA translocation events in 150 mM NaCl solutions and additional modifications were implemented on this variant (Table 4-1). We then made amino acid substitutions in three sections of the ClyA-R nanopore: the *cis* entry, the mid-section and the *trans* entry (Figure 4-1A). Additional positive charges in ClyA-R at the *cis* opening showed either no channel insertion into planar lipid bilayers (as for variants ClyA- R-E106R and ClyA-R-D114R) or no DNA translocation at 150 mM NaCl (as for variants ClyA- R-D122R and ClyA-R-D129R). The addition of an arginine ring in the mid-section of the ClyA- R nanopore induced DNA translocation only when the negatively charged residues at position 64 were replaced by arginines (ClyA-R-D64R). The substitution of either glutamine residues at nearby position (Q56R) or negatively charged residues in the transmembrane region of ClyA-R (E7S or E11S) showed no DNA translocation events in 150 mM NaCl solutions. Surprisingly, the combined addition of positively charged residues in both the mid-section and *trans* entry (as for variant ClyA-R-Q56R-Q8K) also did not induce DNA translocation events. All tested mutations except for D129R in ClyA-R (ClyA- R- D129R) reduced the pore gating voltage (V_G, Table 4-1). ClyA-R-D64R (ClyA-RR) was the only ClyA mutant that showed DNA induced current events following the addition of either 1 μM ssDNA or dsDNA to the *cis* side of the nanopore in 150 mM NaCl under applied V_G (Figure 4-1C-D). Interestingly ClyA-AS, ClyA- R and ClyA-RR showed the same ion selectivity (P_{Na+}/P_{Cl-}= 1.91±0.9, 1.97±1.6 and 1.92±0.7 respectively, Table 4-S2) indicating that, as shown before with the αHL nanopore[19] the ion selectivity of the nanopore is dominated by the charge distribution of the nanopore transmembrane region.

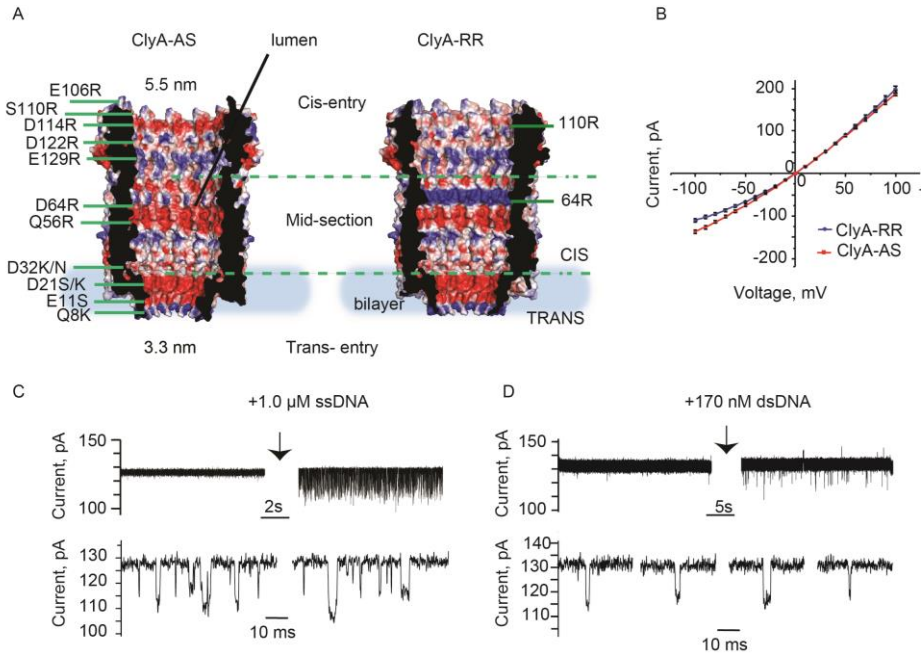

Figure 4-1 Engineering ClyA nanopore for DNA translocation.
A Cross section for ClyA-AS and ClyA-RR nanopores imbedded into a lipid bilayer (light blue) constructed by homology modeling from the *E. coli* ClyA structure (PDB: 2WCD, 90% sequence identity). At the left side of ClyA-AS pore are indicated each amino acid substitution tested in the present study.ClyA-AS inner pore lumen is shown as surface representation and colored according to the 'in vacuo' electrostatics (red for negative regions, and blue for positive regions, Pymol). ClyA-RR pores contain two additional arginine residues per protomer at positions 110 and 64 (right). **B** Current versus voltage relationship for ClyA-AS (red line) and ClyA-RR (blue line). (C-D) DNA translocation through ClyA-RR nanopore at physiological salt concentration (150 mM NaCl, 15 mM Tris HCl, pH 7.5, at 22 °C). **C** Current traces observed before and after adding 1 µM ssDNA (1a, Table 4-S1) at +70 mV. The bottom current traces show a magnification of the DNA translocation events. The average residual current for ssDNA blockades was 0.92 ± 0.00, the τ_{OFF} = 0.5 ± 0.3 ms and the τ_{ON} = 8.5 ± 1.1 ms, average ± s.d., n = 3). **D** Current traces showing the blockades induced by dsDNA (1, Table 4-S1, 170 nM) at +70 mV. The Lower traces show selected current blockades induced by dsDNA translocation (I_{RES+70} = 0.92 ± 0.00, τ_{OFF} = 0.3 ± 0.1 ms and τ_{ON} = 0.24 ± 0.07 s, average ± s.d., n = 3). The current signal is acquired sampling at 100 µs (10kHz) with at 2kHz low-pass Bessel filter in 0.15 M NaCl, 15 mM Tris HCl, pH 7.5 and at 22 °C.

Table 4-1 Electrical properties of engineered ClyA nanopore variants for *cis* DNA translocation at physiological salt concentration

Pore variants[a]	Bilayer activity	I_O±100mV (pA)	Rectification ratio[b]	V_G (mV) [c]	DNA Translocation[d]
ClyA-AS	+	+190±13 -138±6	1.4±0.1	+100	-
ClyA-AS-S110R (ClyA-R)	+	+198±1 -127±2	1.6±0.0	+100	-
ClyA-R-E106R	-	-	-	-	-
ClyA-R-D114R	-	-	-	-	-
ClyA-R-D122R	+	+207±2 -99.8±2	2.1±0.1	+50	-
ClyA-R-E129R	+	+171±25 -161±24	1.1±0.2	+100	-
ClyA-R-D64R (ClyA-RR)	+	+198±8 -110±4	1.8±0.1	+70	*+ (cis)*
ClyA-R-Q56R	+	+202±8 -128±3	1.6±0.1	+50	-
ClyA-R-Q8K	+	+202±15 -147±18	1.4±0.2	+50	-
ClyA-R-E11S	+	+194±4 -154±0	1.3±0.03	+70	-
ClyA-R-Q56R-Q8K	+	+207±20 -150±15	1.4±0.2	+50	-

(a) The activities of the nanopores were tested by adding ~0.1 ng of oligomeric proteins to the *cis* chamber. A negative activity (-) indicates that no channel insertions were observed. ***(b)*** Rectification ratio refers to the ratio of the open pore current measured at + and –100 mV. ***(c)*** The gating voltage (V_G) represents the maximum applied voltage at which no gating events were observed within a 30 s timespan. ***(d)*** DNA translocation indicates that a dsDNA rotaxane could be formed. Each data point is the average of at least three experiments and the error is the standard deviation. Experiments were carried out in 0.15 M NaCl, 15 mM Tris HCl, pH 7.5 solutions.

4.3.2 A DNA rotaxane proves the translocation of DNA through ClyA-RR nanopores

A rotaxane is a dumbbell shaped molecule formed by a macrocycle that encircles a thread locked by two stoppers. Here we formed two nanopore/ DNA rotaxanes to prove the translocation of both ssDNA and dsDNA through ClyA-RR nanopores (Figure 4-2). The first rotaxane was formed by using a 100mer 5'-biotinylated ssDNA molecule as the initial thread (2a, Table 4-S1) added to the *cis* compartment. The second rotaxane was formed by using a 3'-biotinylated 59 base pairs dsDNA molecule containing a 31 nucleotides overhang (1a:1c, Table 4-S1). The rotaxanes were locked by adding on the opposite side of the nanopore a second biotinylated ssDNA molecule: 2b (50mer, 5'-biotinylated) or 1d (31mer, 3'- biotinylated), designed to hybridize with the overhangs of 2a or 1a:1c, respectively. Both *cis* and *trans* solutions contained neutravidin (NA, 1.2 µM monomer), which complexed with biotin prevented the full translocation of the DNA strand across the nanopore (rotaxane stoppers). In 150 mM NaCl and at +50 mV, both thread ssDNA 2a and dsDNA/ ssDNA 1a:1c entered the nanopore (I_{RES+50} 0.92 ± 0.00, and 0.84 ± 0.07 respectively, average ± s.d., n = 3) and were ejected from the pore when the applied potential was reversed to -50 mV (Figure 4- 2A-C). The subsequent addition of the DNA:neutravidin stoppers to the trans solutions induced a permanent blockade at both positive and negative applied potential, indicating the assembly of a DNA rotaxane, and confirming that both threads translocated through the nanopore. Interestingly, as observed before for solid-state nanopores at low ionic strengths[20] at negative applied potentials the blocked ionic current was higher than the open pore current for both rotaxanes (I_{RES-50} = 1.16 ± 0.03 and 1.11 ± 0.06, for ssDNA 2a and dsDNA / ssDNA 1a:1c threads respectively, n = 3, Figure 4-2B- D). By contrast, at positive applied potential the open pore current was higher than the blocked current, suggesting that at the pore top side neutravidin might interact with the pore inner lumen further blocking the residual ionic current.

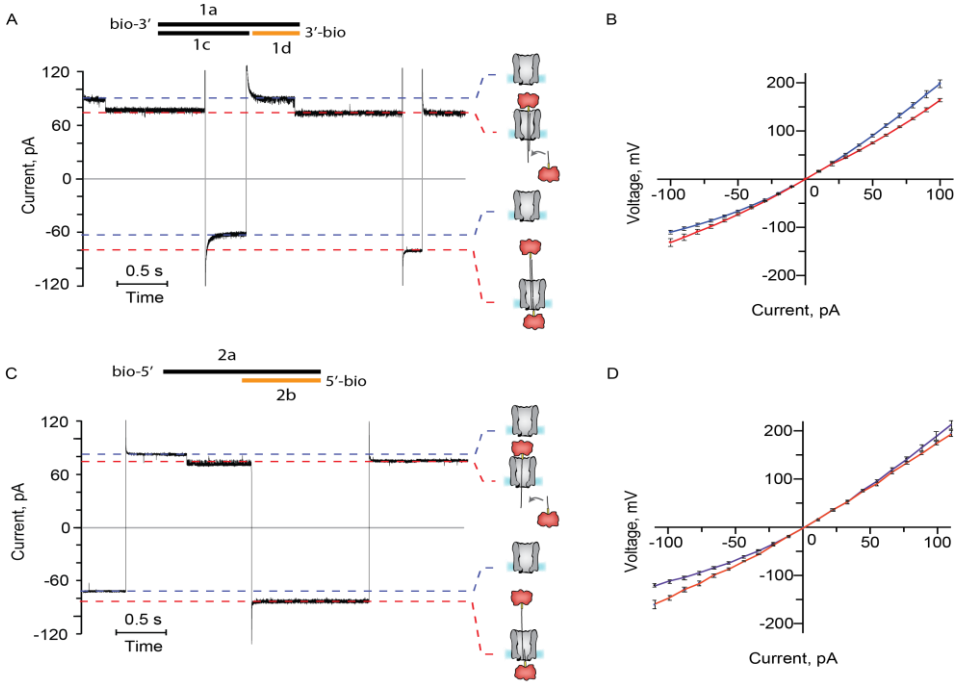

Figure 4-2 DNA rotaxane formation at 150 mM NaCl.
A A dsDNA rotaxane was formed at +50 mV by adding a hybrid dsDNA/ssDNA thread 1a:1c (1.0 µM Table 4-S1) complexed with neutravidin (1.2 µM, monomer) to the cis compartment. 1a:1c contained a 31 nucleotides single stranded overhang at the 5' that was used to hybridize with 1d (1.0 µM Table 4-S1), a biotinylated ssDNA molecule complementary to the ssDNA overhang of 1a:1c added to the *trans* compartment. Thus, a nanopore / DNA rotaxane is formed only if 1a:1c translocates the nanopore. **B** Current voltage relationship (IV curve) for free ClyA-RR (blue line) and ClyA-RR in a rotaxane configuration (red line). When DNA occupied the lumen of ClyA- RR pore the open pore current was reduced at positive applied potentials (I_{RES+50} = 0.84 ±0.07, average ± s.d., n = 3) and enhanced at negative applied potentials (I_{RES-50} = 1.11 ± 0.06, average ± s.d., n = 3). **C** A ssDNA/dsDNA hybrid rotaxane was formed at +50 mV by adding a 5' biotinylated ssDNA thread 2a (1.0 µM, Table 4-S1) complexed with neutravidin (1.2 µM, monomer) to the cis compartment of a ClyA-RR nanopore (I_{RES+50} = 0.92 ± 0.00, average ± s.d., n = 3). A second 5' biotinylated ssDNA molecule 2b (1.0 µM, Table 4-S1) complementary to the 2a 3' end complexed with neutravidin (1.2 µM, monomer) was added to the *trans* compartment. Upon rotaxane formation, the reversal of the applied potential to -50 mV induced a current enhancement (I_{RES-50} = 1.16 ± 0.03, average ± s.d., n = 3), indicating that the hybrid ssDNA/dsDNA is assembled. **D** Current voltage relationship (IV curve) for free ClyA-RR (blue line) and ClyA-RR in a rotaxane configuration (red line). The black and orange lines above figure A and C indicate the DNA configuration of the two rotaxanes. The buffer used was 15 mM Tris-HCl, pH 7.5, and the temperature 22 °C.

4.3.3 DNA threading and translocation depends on the solution ionic strength

We used the Debye length of the solution as a measure of the net electrostatic effect of the pore inner charges on the entry of DNA molecules into ClyA pores. The Debye length (K^{-1}, expressed in nm) refers to the maximum distance at which a charged particle (*e.g.* DNA) will be still influenced by the electric field of another charged particle (*e.g.* pore inner charges) at the molar concentration of the electrolyte solution[21]. For aqueous symmetric monovalent electrolyte solutions the Debye length is given by the equation:

$$K^{-1} = \sqrt{\frac{\varepsilon^o \varepsilon^r RT}{2F^2 C_o}}$$

Where ε^o is the permittivity of free space, ε^r is the water dielectric constant, R is the universal gas constant: 8.314 472 J K^{-1} mol^{-1}, T is the absolute temperature on the kelvin scale (+ 273.15°C), F is the Faraday constant: 9.64853399×10^4 C mol^{-1} and C_o mol L^{-1} is the molar concentration of the electrolyte solution[21].

The frequency of dsDNA translocation, from the *cis* to the *trans* side of the pore**,** increased linearly with the Debye length of the solution (+70 mV, Figure 4-3A and Figure 4-S4), suggesting that the electrostatic interactions between the DNA and the nanopore are important for DNA entry and translocation. As reported before with solid-state nanopores[20], the residual current increased as the ionic strength of the solution decreased (*e.g.* from 0.78 ± 0.09 in 2.5 M NaCl to 0.92 ± 0.00 in 150 mM NaCl, Table 4-S6). Interestingly, we found a linear relationship between the I_{RES} of the DNA blockades and the Debye length of the solution (Figure 4-3B). For dsDNA in complex with neutravidin the residual current was 10 % lower than for free DNA, suggesting that neutravidin reduced the overall ionic current of the blockade, most likely by interacting with the *cis* nanopore lumen. The frequency of ssDNA translocation increased exponentially (R^2 = 0.99) rather than linearly (R^2 = 0.78) with the Debye length of the solution (Figure 4-3C and Figure 4-S3), suggesting that additional factors (*e.g.* the polymer coiling) other than the

interaction between the engineered positive charges in the ClyA lumen and ssDNA play an important role for the nanopore entry and/ or translocation. At 150 mM NaCl, ssDNA molecules in complex with neutravidin threaded permanently inside ClyA-RR, while at 1 M NaCl or higher, the threading was transient (Figure 4-3D). A likely explanation to this data is that at high ionic strengths ssDNA entered and escaped the pore from the *cis* side. Confirming this interpretation, at ionic strengths $\geq$ 1 M the I_{RES} values for ssDNA in the presence and absence of neutravidin were the same, suggesting that under these conditions ssDNA might not fully thread the nanopore, preventing neutravidin from interacting with the lumen of ClyA.

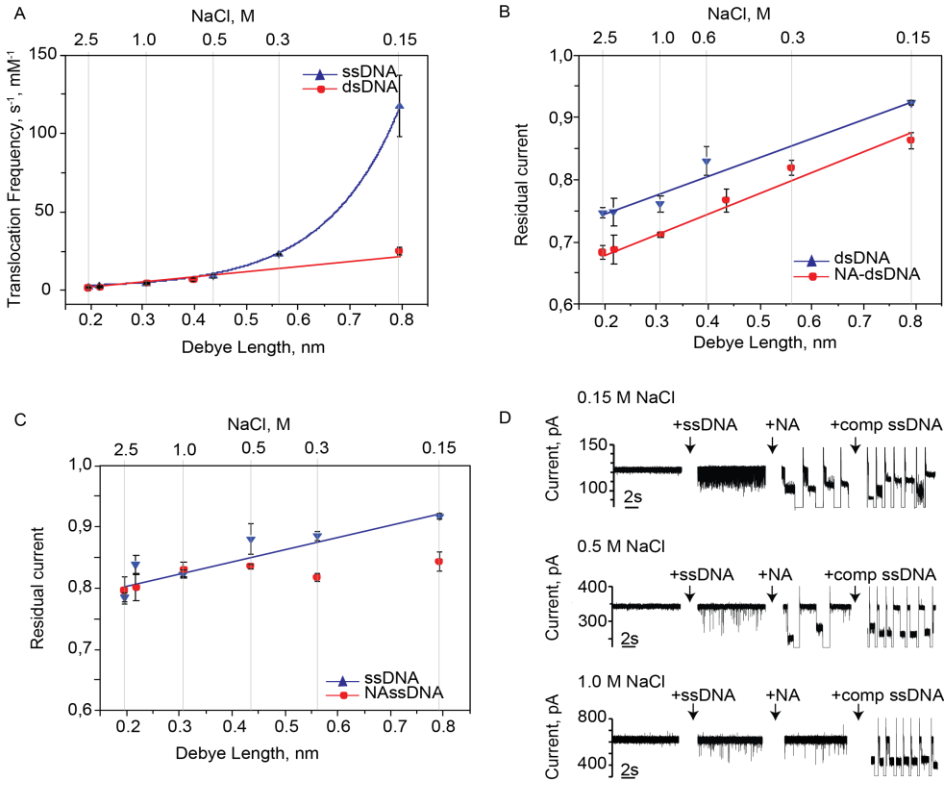

Figure 4-3 Ionic strength dependency of DNA translocation and threading. **A** Debye length dependency of the frequency of translocation for dsDNA (red circles) and ssDNA (blue triangles). The frequency of dsDNA translocation events fitted well to a linear regression (red line, $R^2 = 0.98$), while the frequency of ssDNA fitted better to a single exponential fit (blue line, $R^2 = 0.99$) than a linear regression ($R^2 = 0.78$, Table 4- S6). **B** Dependency of the residual current of dsDNA (red circles) and neutravidin:dsDNA complex (red circles) blockades on the solution Debye length. The lines represent linear regressions, (Table 4-S6). **C** Same as in B but for ssDNA. **D** Ionic strength dependency of DNA threading. Under +70 mV applied potential, the initial addition of ssDNA (1a, 1 µM) to the *cis* side of ClyA-RR induced fast current blockades to ClyA-RR open pore current. The subsequent addition of neutravidin (1.2 µM, *cis*, Table 4-S6) induced long lasting current blockades in 150 and 300 mM NaCl solutions, which are most likely due to the threading of ssDNA. This was not observed in 1 M NaCl solution (or higher), where the blockades remained transient. Further addition of the complimentary ssDNA (1a**,** 1 µM, *cis*, Table 4-S6) induced permanent blockades at all ionic strengths due to the threading of dsDNA. After each permanent DNA capture event, the open pore was regenerated by manual reversal of the potential to −70 mV. Spikes above and below the open pore current level represent capacitive transients following the potential reversal. The electrical recordings were carried out in 15 mM Tris-HCl, pH 7.5, at 22 °C. Data were recorded by applying a 10-kHz low-pass Bessel filter and using a 20 µs (50 kHz) sampling rate. At 150 mM NaCl and additional digital 2-kHz low-pass Bessel filter was applied to the current traces.

4.3.4 **Unidirectional entry of DNA into ClyA nanopores**

In 150 mM NaCl solutions and under negative applied potentials (up to -100 mV), the addition of 1 µM of ssDNA or dsDNA to the *trans* compartment of ClyA-RR did not induce DNA blockades, suggesting that DNA cannot enter the nanopore from the *trans* entrance of the nanopore (Figure 4-4A). Under a positive applied bias, the current blockades appeared at potentials higher than approximately +50 mV, suggesting the existence of a voltage threshold for the translocation of ssDNA from the *cis* side of the nanopore. The entry and further translocation of DNA from the *trans* compartment was observed in 1 M NaCl solution (Figure 4-4B and Figure 4-S5). In the attempt of observing the entry of DNA from the *trans* compartment under physiological ionic strengths, we remodeled the charges of the transmembrane region of ClyA-RR nanopores (Table 4-S3). We found that an additional arginine ring at the N-terminal end of the protein (ClyA- 3R) combined with the substitution of negatively charged residues at position 7 (ClyA- 3R-E7S) sufficed to observe current blockades upon the addition of 1µM of dsDNA 1* (1a:1b, Table 4-S1) to the *trans* chamber at negatively applied potential (Table 4- S3 and Figure 4-S2). Interestingly, similar substitutions (negative charges knocked out) at positions deeper inside the nanopore: 11, 21 and 32 (Figure 4-1A) did not have the same effect, suggesting that, as observed for the translocation of DNA from the *cis* side, the exact location of the charges inside the nanopore is important for initiating DNA translocation. Surprisingly, despite DNA added to the *trans* entry of ClyA- 3R- E7S nanopores showed transient current blockades, a rotaxane could not be formed.

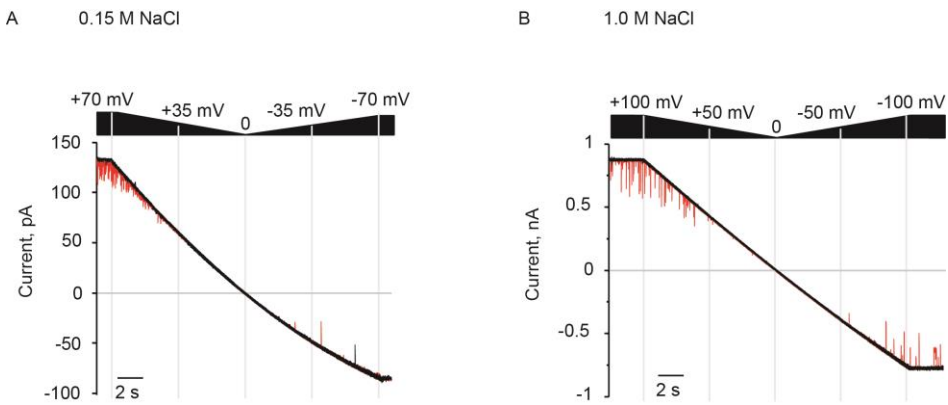

Figure 4-4 Unidirectional DNA translocation through ClyA-RR at 0.15 M NaCl.
A In 150 mM NaCl solutions, the addition of 3 µM of dsDNA 1* (1a:1b, Table 4-S1) to both the *cis* and *trans* sides of a ClyA-RR nanopores induced transient current blockades (red lines) only under positive applied potentials. **B** In 1.0 M NaCl solutions the DNA blockades are observed under both applied potentials. DNA induced blockades are shown in red. The applied potential was automatically changed from +70 to -70 mV (A) or from +100 to -100 mV (B) in 21 seconds. The electrical recordings were carried out in 15 mM Tris HCl, pH 7.5, at 22 °C. Data were recorded by applying a 2-kHz low-pass Bessel filter and using a 100 µs (10 kHz) sampling rate.

4.3.5 Mechanism of ssDNA and dsDNA translocation through ClyA nanopores

ClyA can be approximated by a cylindrical *cis* lumen (5.5 nm diameter and 10 nm length) followed by a smaller and negatively charged *trans* constriction (3.3 nm diameter and 3.0 nm length, Figure 4-1A). The latter forms the main barrier for DNA translocation. We propose a model where the translocation through the *trans* constriction at physiological ionic strengths is obtained when the dsDNA strand is pre-aligned by the *cis* lumen (Figure 4-5.A2). In this view, the dsDNA initially interacts with the charges at the *cis* entry to then enter the lumen where it further interacts with the arginine residues at the mid-section of the nanopore (Figure 4- 5A). At low ionic strength, these electrostatic interactions prevent the exit of the DNA back to the *cis* solution. In this configuration, the dsDNA is aligned

to enter the *trans* constriction, where the electrophoretic force is the strongest, allowing the translocation through the nanopore under applied potential (Figure 4- 5A3). The frequency of dsDNA translocation increased linearly with the Debye length of the solution (Figure 4-3A), suggesting that the electrostatic interactions of dsDNA with the engineered charges in ClyA-RR are important for the translocation process (Figure 4-5.A).

By contrast, the Debye length dependency of ssDNA blockades fitted well to an exponential regression, suggesting that additional factors as the polymer coiling at high ionic strengths influence the translocation of ssDNA through ClyA-RR nanopores. In our experiments, the dsDNA maximum length (when it is stretched completely) is lower than its persistence length (dsDNA persistence length 50 nm)[22], indicating that the dsDNA molecules translocate as a rigid rod (Figure 4- 5.A). By contrast, ssDNA (persistence length 1.5 nm)[23] have a coiled structure with a gyration radius, which is the average squared distance of any point in the polymer coil from its center of mass, of approximately 6 nm[24]. Since the gyration radius is similar to the diameter of the nanopore (Figure 4-5.B1), ssDNA most likely enters the *cis* side of the nanopore as a partially coiled structure (Figure 4-5.B2). Then, as the ssDNA moves from the *cis* reservoir to the *trans* side, it must gradually uncoil in order to navigate through the *trans* constriction of the nanopore and then recoil on the opposite side (Figure 4- 5B3-4). This entropic uncoiling/ recoiling force, which together with the hydrodynamic viscous drag force, induces the *cis* ejection of ssDNA from the nanopore at high ionic strengths. It decreases with the ionic strength, augmenting the efficiency of DNA translocation as the ionic strength of the solution decreased[20,22,24–27].

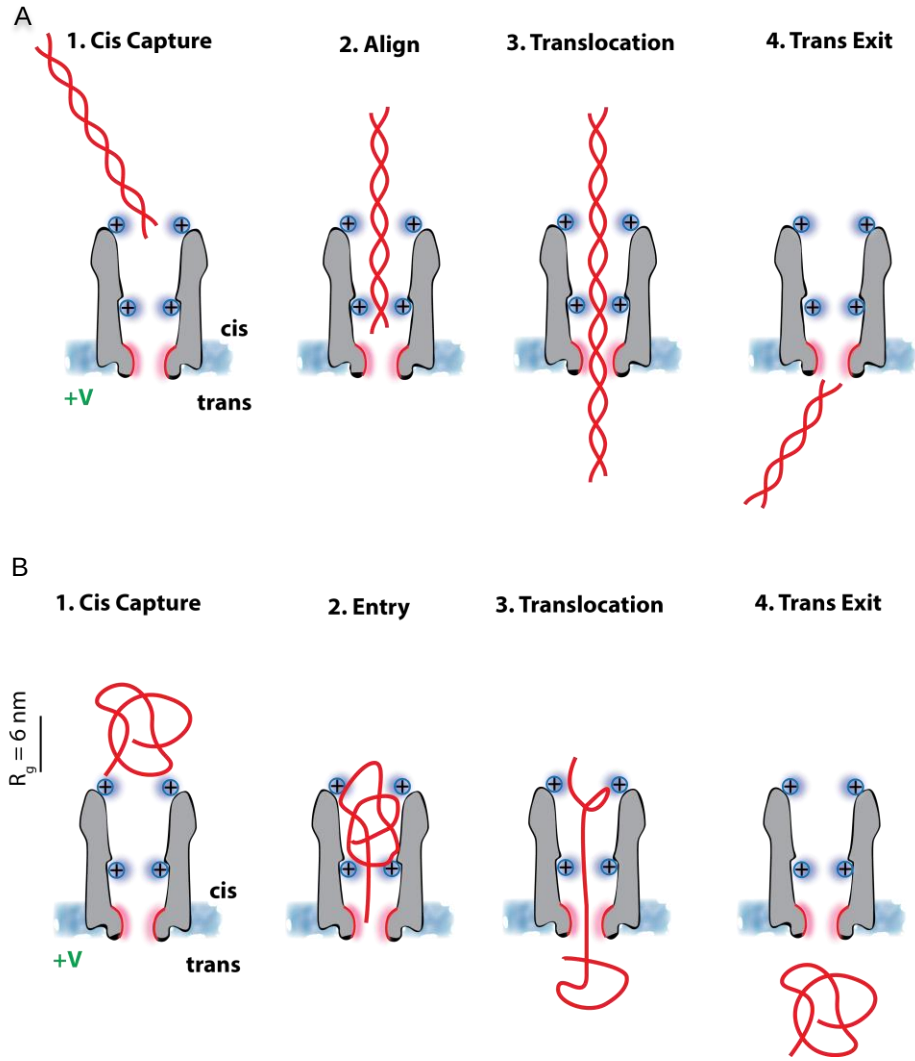

Figure 4-5 Mechanism of dsDNA and ssDNA translocation through ClyA pores.

A dsDNA translocate through the nanopore as a rigid rod. Following the initial interaction with the nanopore (1). dsDNA penetrates inside the nanopore where it interacts with the pore mid-section engineered charges (2). The latter charges are important to align the DNA rod for productive translocation through the negatively charged *trans* constriction. The dsDNA can then translocate (3) and exit the pore (4). **B** The additional charges at the pore *cis* entrance mediate the efficient capture of the ssDNA inside the nanopore (1). ssDNA enters the *cis* lumen most likely as a coiled structure (2). In order to translocate the *trans* constriction, ssDNA needs to uncoil (3) to then recoil outside the nanopore (4). The DNA molecules and the nanopore are drawn in scale. Under the experimental condition dsDNA is a rigid rod and ssDNA is a coiled structure. R_g indicates the gyration radius of ssDNA[24].

4.3.6 **Biological significance**

In bacteriophages, DNA is transferred through the procapsid by packing proteins that align and push the DNA across portal proteins that have similar dimensions and internal surface charge compared to ClyA[28]. A negative internal surface charge appears to be important for the smooth translocation of DNA across the portal proteins[28,29] and it is observed in other proteins that encircle and slide along DNA such as β clamp proteins[30]. Portal proteins also have positively charged rings that have been proposed to play a direct role in genomic DNA packaging by interacting with the negatively charged phosphate backbone of the translocating DNA[28,29,31]. In this work we showed that the electrophoretic translocation of DNA through ClyA nanopores could be observed when two rings of positively charged residues were introduced at the *cis* entrance and mid-section of the nanopore (ClyA-RR, Figure 4-1A). Most likely, such residues strongly interact with phosphate groups of DNA aligning the DNA for the passage through the narrow and electronegative constriction. In the absence of such interactions, for example during the translocation from the *trans* to the *cis* side, DNA translocation is not observed. Our results suggest, therefore, that in connector proteins such rings of positive charges might be important to initiate the ejection of the DNA out of the capsid into the infected cell.

4.4 Discussion

DNA molecule translocating through a nanopore is subjected to the electrical driving force and the hydrodynamic viscous drag force arising from the electroosmotic flow (EOF) inside the nanopore that opposes the translocation of DNA[32–34]. ClyA and most solid-state nanopores have a negatively charged surface that is electrostatically balanced by a layer of cations in the immediate contact with the surface, which is usually called electric double layers (EDL)[35–38]. Under the applied electric field, the movement of the ions in the EDLs induces the preferential translocation of the counterions, which in turn generates an EOF and makes the nanopore ion selective (e.g. ClyA-AS P_{Na+}/P_{Cl-} =1.9, Table 4-S2). Due to the screening by the electrolyte, the EDL force decays in an exponential fashion over the diffuse layer[37]. The range of this force is given by the Debye length and its strength by the surface potential. In narrow nanopores, especially in the regime of low salt concentrations, the thickness of the EDLs including the diffuse layer, can be comparable to the size of the nanopores, yielding overlapped EDLs[39]. Under this regime a DNA molecule (diameter 2.2 nm) approaching such nanopores will experience a strong surface potential that for nanopores with negative surface charge will oppose the entry of DNA into the nanopore.[25,37]. In this work, to induce the translocation of ssDNA and dsDNA at physiological ionic strength, we systematically introduced rings of positively charged residues in the lumen of the nanopore. We found that DNA translocation was observed only when two arginine rings were added at precise locations inside the ClyA-AS nanopore: one arginine ring at the *cis* entrance and one arginine ring in the mid-section of the nanopore (ClyA-RR, Figure 4-1A and Table 4-1). Further, DNA translocation could be observed only when initiated from the *cis* to the *trans* side of the nanopore. This is surprising, because ClyA-RR has the same negative surface charge at the constriction, conferring also the same ionic selectivity as ClyA-AS (Table 4-S2). Therefore, our results indicate that other than the surface charge of the nanopore the precise location of the introduced positive rings in ClyA-RR allows a strong

interaction with DNA molecules, assisting the passage of the DNA through the narrow and electronegative constriction of the nanopore.

4.5 Conclusion

In this work we have engineered the ClyA nanopore to translocate single-stranded and double-stranded DNA molecules at physiological salt concentration (0.15 M NaCl). The resulting engineered ClyA nanopore (ClyA-RR) might be used to study protein DNA interactions at the single-molecule level and it could be employed in DNA mapping and sequencing applications, where an enzyme controls the translocation of the nucleic acid through the nanopore at physiological ionic strengths[16,17]. Throughout our work we found that the number and the exact distribution of internal charges in the nanopore lumen is crucial to induce the passage of DNA molecules through the pore. In addition, the results obtained from the electrophoretical DNA translocation tested at different ionic strengths, helped to understand the electrostatic and entropic barriers that regulate the transport of DNA molecules through the biological nanopore ClyA and might be useful to design new applications for nucleic acid analyses with nanopore-based biosensors.

4.6 Materials and Methods

4.6.1 DNA oligos and reagents

DNA was purchased from Integrated DNA Technologies (IDT). Neutravidin was acquired from Thermo Fisher and 1, 2-diphytanoyl-sn-glycero -3-phosphocholine from Avanti Polar Lipids. β-Dodecyl maltoside (DDM) was purchased from GLYCON Biochemicals GmbH. Enzymes were bought from Fermentas and all other materials from Sigma, unless otherwise specified.

4.6.2 **Protein preparation**

We used an engineered *Salmonella enterica* serovar Typhi ClyA nanopore (ClyA- AS)[14] containing the following mutations relative to the ClyA-WT gene: C87A, L99Q, E103G, C285S, F166Y, I203V, K294R, H307Y. Additional single point mutations were added to the ClyA-AS gene by PCR. Typically, two PCR were performed to prepare a new DNA construct: The first PCR was performed following the "mega primer" method[40]. The plasmid DNA was amplified with two primers: a first oligo 20-30 nucleotides in length carried the residue substitution and the second primer was either T7 promoter or T7 terminator as forward or reverse primer respectively. For mutations at the transmembrane region, we used a reverse primer, which was a 25mer oligo complementary to the middle protein sequence. The PCR product, containing the template and 200-300 bp (mega primers), was loaded into an electrophoresis gel (2 % agarose/ TAE and crystal violet). The megaprimer was cut out and purified using a PCR quick purification kit (QIAGEN). 5 µL of purified mega primers were loaded on 2% agarose/ TAE gel to check for purity and 5-10 µL of the megaprimer were employed for a second PCR. The second PCR product was first digested with DpnI (incubated 1-2 h at 37 °C, fast digest DpnI, Fermenthas) to eliminate the template DNA (ClyA-AS or ClyA-RR) and then ~1 µL used for transformation with *E. coli* electro-competent cells (E. Cloni-10G, Lucigen).

4.6.3 **Protein purification**

Monomers (containing a C-terminal end oligo-histidine tag) were expressed in *E. coli* BL 21 cells (E. Cloni, BL21 DE3 chem.comp cells, Lucigen) and the soluble fraction purified using Ni-NTA affinity chromatography as described elsewhere[14] (see 2.1.2 Nanopore purification.). ClyA dodecamers were formed by the addition of 0.2% DDM and were separated from monomers (1 mg/ mL) using blue native polyacrylamide gel electrophoresis. The thickest and lowest

oligomerization band was extracted by simple diffusion in extraction buffer (150 mM NaCl, 15 mM Tris-HCl, pH 7.5, 0.2 % DDM and 1 mM EDTA) and stored at 4 °C.

4.6.4 **DNA preparation**

dsDNA 1 was formed by incubating 1a, 3' biotinylated ssDNA molecule (5'-GGA TGACCTGATCCAGATATTTATTATACAGGTCCAGCGCACCGTCAGCCC AATCGCACTTTTCACAAAAAGAGAGAGATCGATTACC-3'-bio), with a 20% excess of complementary ssDNA 1b (5'-GGTAATCGATCTCTCTCTCTT TTTGTGAAAAGTGCGATTGGGCTGACGGTGCGCTGGAC-3', Table 4-S1). The temperature was brought to 95 °C for 1 min and then decreased stepwise to room temperature. At around the estimated annealing temperature of 70 °C, the temperature was decreased in 2 °C steps to 21°C. Each step lasted for 1 min. The DNA was then purified from the excess of ssDNA with affinity chromatography using a biotin-binding column containing monomeric avidin immobilized on agarose beads (Thermo Scientific Pierce). dsDNA 1 was eluted in biotin blocking/ elution buffer according to the protocol. The elution fraction was further concentrated and biotin purified by using PCR quick purification kit (QIAGEN). Typically, a DNA concentration of 0.2 µg/ mL (NanoDrop) was obtained. The size and purity of the dsDNA was checked by using a 2 % agarose gel in TAE buffer. The purified dsDNA was stored at -20 °C in the presence of 1 mM EDTA. dsDNA 1* was formed by hybridization of 1a with equal molar concentration of 1b (Table 4-S1). The rotaxane thread 1a:1c was formed by incubation of 1a with equal molar concentration of a partially complementary ssDNA (5'- GGTAATCGATCTCTC TCTCTTTTTGTGAAAAGTGCGATTGGGCTGACGGTGCGCTGGAC-3', 1c, Table 4-S1). The temperature was brought to 95 °C for 1min and then decreased stepwise to room temperature. At around the estimated annealing temperature 70 °C, the temperature was decreased in 2 °C steps, each held for 1 min.

4.6.5 Electrical recordings and data analysis

Artificial planar lipid bilayers were prepared as previously described[41]. If not otherwise specified, the signal was recorded by applying a 10-kHz low-pass Bessel filter and using a 20 μs (50 kHz) sampling rate. The lipid bilayer was formed by pretreating a small aperture (~ 100 μm) on a Teflon film (Goodfellow, UK) with 1–2 μL of a 10% v/ v solution of 1,2-diphytanoylsn-glycero-3-phosphocholine in pentane. The electrical potential was applied by using Ag / AgCl electrodes submerged in agar bridges (3 % w/v low melt agarose in 2.5 M NaCl buffer). The applied potential refers to the potential of the working electrode connected to the *trans* compartment of the apparatus. ClyA nanopore solutions (0.01–0.1 ng / mL) were added to the *cis* compartment, which was connected to the ground electrode. After the insertion of a single pore, excess protein was removed by several cycles of perfusion. Electrical recordings were carried out in 0.15-2.5 M NaCl, 15 mM Tris-HCl, pH 8.0, at 22 °C. In 0.15 M NaCl data were recorded by applying a 2 kHz low-pass Bessel filter and using a 10 kHz sampling rate. While at higher salt concentration a 10-kHz low-pass Bessel filter and 50 kHz sampling rate. Current traces at 0.3 and 0.5 M NaCl were extra filtered with a 4-kHz Bessel filter for accurate event detection. Current blockade events were collected individually by using the "single channel search" function of Clampfit (Molecular devices) using a data acquisition threshold of 0.05 ms. I_O and I_B values were calculated from Gaussian fitting to all-point histograms of the open pore and blocked pore currents, respectively. The DNA translocation dwell time τ_{off} was calculated by fitting the τ_{off} of the blocked pore current level (I_B) to a single exponential standard from a cumulative histogram, thus the inter-event time τ_{on} was measured by fitting the τ_{on} of the blocked pore current level (I_B) to a single exponential (logarithmic binning, 10 bin per decade). The errors indicate the standard deviation from the average for at least three independent repeats, the number of which is indicated by 'n'. Pores inserted from the *cis* chamber showed higher conductance at positive applied potential, helping to assess the orientation of the inserted channel. Single channels

were characterized by measuring the current versus applied voltage relationship, (I-V curve, the potential was applied in 10 mV steps from -100 to +100 mV in 21 s). The pore rectification was obtained from the ratio of the open pore current at +100 mV and that at -100 mV ($I_{0+100mV}/I_{0-100mV}$ 1). The propensity for gating of the nanopores was assessed by the continuous measurement of the open pore current at a given applied potential. V_G was then given by the applied potential at which no gating events were observed within a 30 s timespan. Spontaneous fast and reversible fluctuations of the ionic current were observed at applied voltages higher than V_G. Ultimately DNA translocation through the pore was tested by adding 1 µM of 3'-biotinylated ssDNA 1a (90mer, Table 4-S1) to the *cis* and *trans* chamber under an applied potential equal to V_G. For nanopores that showed DNA induced blockades, the addition of equimolar concentration of the complementary ssDNA 1b (Table 4-S1) and 1.2 µM of neutravidin (monomer), to the opposite side of the lipid bilayer assessed the ability of the DNA to translocate through the nanopore.

4.6.6 **Ionic permeability**

We calculated the permeability ratio (P_{Na+}/P_{Cl}) for ClyA engineered nanopores by measurement of the reversal potential in asymmetric salt condition: 150 mM NaCl *trans*, 1 M NaCl *cis.* The protein nanopores were added to the *cis* chamber and a single channel was first characterized in a symmetric condition (150 mM NaCl, 15 mM Tris-HCl pH 7.5 in both *cis* and *trans* solutions). After the electrodes were balanced, the electrolyte concentration in *cis* was increased up to 1 M, by adding aliquots of 5 M NaCl stock solution to the *cis* compartment. The volume of the *trans* chamber was adjusted by adding the same volume added to the *cis* side using the same buffer of the *cis* solution (150 mM, NaCl). The reversal potential (V_r), which is the electrical potential used to obtain a zero current, was obtained by current-voltage (IV) curve (Table 4-S2 and Table 4-S5). Ion selectivity (P_{Na+}/P_{Cl})

was calculated from the V_r by using the Goldman-Hodgkin-Kats (GHK) equation. According both to the GHK equation positive value for V_r observed for the ClyA nanopores show a preferential movement of the cations through the pore, indicating that the pores are cationic selective channels. The *cis* chamber was at ground and Ag/AgCl electrodes with 2.5 % agarose bridges containing 2.5 M NaCl were used to perform all the experiments[17,19,42]. The permeability ratio (P_{Na+}/P_{Cl}) is given by the Goldman-Hodgkin-Kats (GHK) equation:

$$V_r = \frac{RT}{F} ln\left(\frac{p_{Na}[Na^+]_{cis} + p_{Cl}[Cl^-]_{trans}}{p_{Na}[Na^+]_{trans} + p_{Cl}[Cl^-]_{cis}}\right)$$

$$\frac{P_{Na^+}}{P_{Cl^-}} = \frac{[a_{Cl^-}]_{trans} - [a_{Cl^-}]_{cis}\, e^{\frac{V_r F}{RT}}}{[a_{Na^+}]_{trans}\, e^{\frac{V_r F}{RT}} - [a_{Na^+}]_{cis}}$$

Where V_r is the membrane potential, R the universal gas constant (8.314 $J.K^{-1}.mol^{-1}$), T the temperature in Kelvin, F the Faraday constant (96485 $C.mol^{-1}$), P_x the relative membrane permeability for Na^+ and Cl^-, $[X]_{cis}$ the concentration of Na^+ and Cl^- in the *cis* compartment, $[X]_{trans}$ the concentration of Na^+ and Cl^- in the *trans* compartment, and a_x the activity of Na^+ and Cl ions[42]

4.7 Acknowledgements

We thank Prof. Marc De Maeyer for helping with the ClyA-RR PDB modeling and the European Research Council (European Commission's Seventh Framework Programme, project no. 260884) for funding. LF is funded by a PhD grant from the Agency for Innovation by Science and Technology (IWT) Flanders.

4.8 References

1. Kasianowicz, J.J., Brandin, E., Branton, D., Deamer, D.W., Characterization of individual polynucleotide molecules using a membrane channel. *Proc. Natl. Acad. Sci. USA*. 93(24): 13770–13773 (1996).

2. Ashkenasy, N., Sánchez-Quesada, J., Ghadiri, M.R., Bayley, H., Recognizing a single base in an individual DNA strand: a step toward nanopore DNA sequencing. *Angew. Chem. Int. Ed. Engl.* 44(9): 1401–1404 (2005).

3. Howorka, S., Cheley, S., Bayley, H., Sequence-specific detection of individual DNA strands using engineered nanopores. *Nat. Biotechnol.* 19(7): 636–639 (2001).

4. Akeson, M., Branton, D., Kasianowicz, J.J., Brandin, E., Deamer, D.W., Microsecond time-scale discrimination among polycytidylic acid, polyadenylic acid, and polyuridylic acid as homopolymers or as segments within single RNA molecules. *Biophys. J.* 77(6): 3227–3233 (1999).

5. Meller, A., Nivon, L., Brandin, E., Golovchenko, J., Branton, D., Rapid nanopore discrimination between single polynucleotide molecules. *Proc. Natl. Acad. Sci. USA*. 97(3): 1079–1084 (2000).

6. Sánchez-Quesada, J., Saghatelian, A., Cheley, S., Bayley, H., Ghadiri, M.R., Single DNA Rotaxanes of a transmembrane pore protein. *Angew. Chem. Int. Ed. Engl.* 43(23): 3063–3067 (2004).

7. Vercoutere, W.A., Winters-Hilt, S., DeGuzman, V.S., Deamer, D., Ridino, S.E., Rodgers, J.T., Olsen, H.E., Marziali, A., Akeson, M., Discrimination among individual Watson–Crick base pairs at the termini of single DNA hairpin molecules. *Nucleic Acids Res.* 31(4): 1311–1318 (2003).

8. Butler, T.Z., Pavlenok, M., Derrington, I.M., Niederweis, M., Gundlach, J. H., Single-molecule DNA detection with an engineered MspA protein nanopore. *Proc. Natl. Acad. Sci. USA*. 105(52): 20647–20652 (2008).

9. Neely, R.K., Deen, J., Hofkens, J., Optical mapping of DNA: single-molecule-based methods for mapping genomes. *Biopolymers* 95(5): 298–311 (2011).

10. Wendell, D., Jing, P., Geng, J., Subramaniam, V., Lee, T.J., Montemagno, C., Guo, P., Translocation of double-stranded DNA through membrane-adapted phi29 motor protein nanopores. *Nat. Nanotechnol.* 4(11): 765–772 (2009).

11. Franceschini, L., Soskine, M., Biesemans, A., Maglia, G., A nanopore machine promotes the vectorial transport of DNA across membranes. *Nat. Commun.* 4: 2415 (2013).

12. Mandelkern, M., Elias, J.G., Eden, D., Crothers, D.M., The dimensions of DNA in solution. *J. Mol. Biol.* 152(1): 153–161 (1981).

13. Wolfe, A.J., Mohammad, M.M., Cheley, S., Bayley, H., Movileanu, L., Catalyzing the translocation of polypeptides through attractive interactions. *J. Am. Chem. Soc.* 129(45): 14034–14041 (2007).

14. Soskine, M., Biesemans, A., Maglia, G., Single-molecule analyte recognition with ClyA nanopores equipped with internal protein adaptors. *J. Am. Chem. Soc.* 137(17): 5793–5797 (2015).

15. Astier, Y., Braha, O., Bayley, H., Toward single molecule DNA sequencing: Direct identification of ribonucleoside and deoxyribonucleoside 5'-monophosphates by using an engineered protein nanopore equipped with a molecular adapter. *J. Am. Chem. Soc.* 128(5): 1705–1710 (2006).

16. Cockroft, S.L., Chu, J., Amorin, M., Bayley, H., Ghadiri, M.R., A single-molecule nanopore device detects DNA polymerase activity with single-nucleotide resolution. *J. Am. Chem. Soc.* 130(3): 818–820 (2008).

17. Benner, S., Chen, R.J., Wilson, N.A., Abu-Shumays, R., Hurt, N., Lieberman, K.R., Deamer, D.W., Dunbar, W.B., Akeson, M., Sequence-specific detection of individual DNA polymerase complexes in real time using a nanopore. *Nat. Nanotechnol.* 2(11): 718–724 (2007).

18. Maglia, G., Restrepo, M.R., Mikhailova, E., Bayley, H., Enhanced translocation of single DNA molecules through alpha-hemolysin nanopores by manipulation of internal charge. *Proc. Natl. Acad. Sci. USA.* 105(50):, 19720–19725 (2008).

19. Gu, L.Q., Dalla Serra, M., Vincent, J.B., Vigh, G., Cheley, S., Braha, O., Bayley, H., Reversal of charge selectivity in transmembrane protein pores by using noncovalent molecular adapters. *Proc. Natl. Acad. Sci. USA.* 97(8): 3959–3964 (2000).

20. Smeets, R.M., Keyser, U.F., Krapf, D., Wu, M.Y., Dekker, N.H., Dekker, C., Salt-dependence of ion transport and DNA translocation through solid-state nanopores. *Nano Lett.* 6(1): 89–95 (2006).

21. Israelachvili, J.N., "Electrostatic forces between surfaces in liquids" in Intermolecular and Surface Forces, 2nd Ed. Academic Press, London, 312 (1991).

22. Long, D., Viovy, J.L., Ajdari, A., Stretching DNA with electric fields revisited. *Biopolymers* 39(6): 755–759 (1996).

23. Chi, Q., Wang, G., Jiang, J., The persistence length and length per base of single-stranded DNA obtained from fluorescence correlation spectroscopy measurements using mean field theory. *Physica A* 392(5): 1072–1079 (2013).

24. Murphy, M.C., Rasnik, I., Cheng, W., Lohman, T.M., Ha, T., Probing single-stranded DNA conformational flexibility using fluorescence spectroscopy. *Biophys. J.* 86(4): 2530–2537 (2004).

25. Chen, L., Conlisk, A.T., Forces affecting double-stranded DNA translocation through synthetic nanopores. *Biomed. Microdevices* 13(2): 403–414 (2011).

26. Ghosal, S., The effect of salt concentration on the electrophoretic speed of a polyelectrolyte through a nanopore. *Phys. Rev. Lett.* 98(23): 238104 (2007).

27. Levy, S., Mannion, J., Cheng, J., Reccius, C., Craighead, H., Entropic unfolding of DNA molecules in nanofluidic channels. *Nano Lett.* 8(11): 3839–3844 (2008).

28. Rao, V.B., Feiss, M., Mechanisms of DNA Packaging by Large Double-Stranded DNA Viruses. *Annu. Rev. Virol.* 2: 351-378 (2015).

29. Guasch, A., Pous, J., Ibarra, B., Gomis-Rüth, F.X., Valpuesta, J.M., Sousa, N., Carrascosa, J.L., Coll, M., Detailed architecture of a DNA translocating machine: the high-resolution structure of the bacteriophage phi29 connector particle. *J. Mol. Biol.* 315(4): 663–676 (2002).

30. Georgescu, R.E., Kim, S.S., Yurieva, O., Kuriyan, J., Kong, X.P., O'Donnell, M., Structure of a sliding clamp on DNA. *Cell* 132(1): 43–54 (2008).

31. Casjens, S.R., The DNA-packaging nanomotor of tailed bacteriophages. *Nat. Rev. Microbiol.* 9(9): 647–657 (2011).

32. Viovy, J.L., Electrophoresis of DNA and other polyelectrolytes: physical mechanisms. *Rev. Mod. Phys.* 72: 813–822 (2000).

33. Ghosal, S., Electrokinetic-flow-induced viscous drag on a tethered DNA inside a nanopore. *Phys. Rev. E* 76(6 Pt 1): 61916 (2007).

34. Ghosal, S. Electrophoresis of a polyelectrolyte through a nanopore. *Phys. Rev. E* 74(4 Pt 1): 41901 (2006).

35. Wanunu, M., Sutin, J., McNally, B., Chow, A., Meller, A., DNA translocation governed by interactions with solid state nanopores. *Biophys. J.* 95(10): 4716–4725 (2008).

36. Luan, B., Aksimentiev, A., Effective screening of the DNA charge in a nanopore. *Phys. Rev. E* 78(2 Pt 1): 21912 (2008).

37. Van Dorp, S., Keyser, U.F., Dekker, N.H., Dekker, C., Lemay, S.G., Origin of the electrophoretic force on DNA in solid-state nanopores. *Nature Physics* 5(5): 347–351 (2009).

38. Behrens, S., Grier, D., The charge of glass and silica surfaces. *J. Chem. Phys.* 115: 6716–6721 (2001).

39. Huang, M.J., Mei, L., Yeh, L.H., Qian, S., pH-Regulated nanopore conductance with overlapped electric double layers. *Electrochem. Commun.* 55: 60-63, (2015).

40. Ke, S.H., Madison, E.L., Rapid and efficient site-directed mutagenesis by single-tube 'megaprimer' PCR method. *Nucleic Acids Res.* 25(16): 3371–3372 (1997).

41. Soskine, M., Biesemans, A., Moeyaert, B., Cheley, S., Bayley, H., Maglia, G., An engineered ClyA nanopore detects folded target proteins by selective external association and pore entry. *Nano Lett.* 12(9): 4895–4900 (2012).

42. Zemaitis, J.F., Clark, D.M., Rafal, M., Scrivner, N.C., "Activity coefficients of single strong electrolytes" in Handbook of aqueous electrolyte thermodynamics: theory and application. Wiley, New York 45-204 (1986).

4.9 Supplementary Information

The precise engineering of the ClyA nanopore is required for ssDNA and dsDNA translocation at physiological ionic strength

Table 4-S1 DNA molecules used in this work.

Name	DNA sequence
1a	5′-GGATGACCTGATCCAGATATTTATTATACAGGTCCAGCGCACCGTCAGCCCAATCGCACTTTTCACAAAAAGAGAGAGAGATCGATTACC/Bio/-3′
1b	5′-GGTAATCGATCTCTCTCTCTTTTTGTGAAAAGTGCGATTGGGCTGACGGTGCGCTGGACCTGTATAATAAATATCTGGATCAGGTCATCC-3′
1c	5′- GGTAATCGATCTCTCTCTCTTTTTGTGAAAAGTGCGATTGGGCTGACGGTGCGCTGGAC/Bio/-3′
1d	5′-CTGTATAATAAATATCTGGATCAGGTCATCC/Bio/-3′
2a	5′-/Bio/CCGTAGTTTGGGATGACCTGATCCAGATATTTATTATACAGGTCCAGCGCACCGTCAGCCCAATCGCACTTTTCACAAAAAAGAGAGAGAGATCGATTACC-3′
2b	5′-/Bio/GGTAATCGATCTCTCTCTCTTTTTGTGAAAAGTGCGATTGGGCTGACGGT-3′

See DNA preparation (4.6.1 Materials and Methods, page 124) for oligos hybridization and purification.

Table 4-S2 ClyA nanopores ionic permeability.

Pore variants[a]	V_r (mV)[b]	P_{Na+}/P_{Cl-} [c]
ClyA-AS	+11.5±0.7	1.92±0.08
ClyA-R	+11.9±1.6	1.97±0.08
ClyA-RR	+11.4±0.9	1.91±0.10

(a) Four or more single channel experiments were measured to calculate ***(b)*** the reversal potential (V_r) and ***(c)*** the permeability ratio (P_{Na+}/ P_{Cl^-}). Data are reported as the average ± standard deviation at the stated conditions: 15 mM TRIS-HCl pH 7.5 with 1 M NaCl in the *cis* chamber and 150 mM in the *trans* chamber.

Table 4-S3 Pore engineering for *trans* DNA translocation.

Pore variants[a]	I_o ±100 mV (pA)	Rectification ratio[b]	V_G (mV) [c]	DNA Capture[d]	DNA Translocation[e]
ClyA-RR-E7S	+186±2 -110±2	1.7±0.0	- 70	-	-
ClyA-RR-E11S	+214±27 -124±14	1.7±0.3	- 100	-	-
ClyA-RR-D21S	+193±9 -113±9	1.7±0.2	- 70	-	-
ClyA-RR-D21K	+149±0 -112±0	1.3±0.0	- 50	-	-
ClyA-RR-D32N	+196±5 -104±5	1.9±0.1	-150	-	-
ClyA-RR-E7S-D32N	+182±4 -104±6	1.8±0.1	- 70	-	-
ClyA-RR-E7S-D21S	+182±5 -121±3	1.5±0.1	- 70	-	-
ClyA-RR-E129R	-	-	-	-	-
ClyA-RR-1'R (ClyA-3R)	+184±8 -101±3	1.8±0.1	-150	-	-
ClyA-3R-E7S	+176±5 -109±3	1.6±0.1	- 50	+	-
ClyA-3R-D21S	+179±9 -108±5	1.7±0.1	- 50	-	-

(a) The activity of each nanopore was tested by adding 0.01- 0.1 ng oligomeric protein to the *trans* chamber. A negative activity (-) indicates that no channel insertions were observed. Each data point is the average of at least three experiments and the error is the standard deviation. Experiments were carried out in 0.15 M NaCl, 15 mM Tris-HCl, pH 7.5 solutions. ***(b)*** Rectification ratio refers to the ratio of the open pore current measured at ±100 mV. ***(c)*** V_G represents the maximum applied voltage at which no gating events were observed within 30 s. ***(d)*** DNA capture indicates that only transient current blockades were observed upon the addition of biotinylated dsDNA in complex with neutravidin. ***(e)*** DNA translocation indicates that a DNA rotaxane could be formed. (← See previous table)

Table 4-S4 ClyA variants IV curves.

Voltage (mV)	ClyA−AS	ClyA−AS −S110R (ClyA−R)	ClyA−R-D56R	ClyA−R−Q8K	ClyA−R−D64R (ClyA-RR)
-100	-138±6	-128±2	-128±2	-147±18	-111±2
-90	-126±6	-118±1	-119±2	-134±15	-104±2
-80	-115±5	-107±1	-108±2	-120±12	-96.2±1.8
-70	-102±5	-96.2±1.3	-97.3±1.3	-107±10	-87.5±1.4
-60	-89.1±4.3	-84.6±1.1	-85.9±0.9	-93.2±7.9	-78.1±1.3
-50	-75.8±3.6	-72.4±0.9	-73.2±0.3	-78.1±4.9	-67.4±1.1
-40	-61.8±2.9	-59.3±0.9	-60.4±0.4	-63.9±4.2	-56±1
-30	-47.1±2.2	-45.6±0.6	-46.2±0.2	-48.6±2.8	-43.6±0.7
-20	-31.9±1.5	-31.2±0.4	-31.7±0.3	-32.3±2	-30±1
-10	-16.2±0.7	-15.9±0.2	-16.2±0.3	-16.7±0.9	-15.4±0.2
0	0	0	0	0	0
+10	16.8±0.9	16.8±0.1	17.1±0.1	17±2	16.5±0.1
+20	34.2±1.7	34.4±0.3	35.2±0.3	35.3±3.1	34±1
+30	52.1±2.5	52.5±0.6	53.5±0.9	54.4±4.3	52.3±0.3
+40	70.5±3.4	71.6±0.7	72.9±1.1	73.8±5.7	71.5±0.3
+50	89.0±4.5	91.3±0.8	93±2	94.3±6.8	91.8±0.5
+60	108±5	112±1	114±3	115±8	112±1
+70	128±7	132±1	135±4	137±10	13±1
+80	148±8	154±1	157±5	157±12	156±1
+90	168±10	175±2	179±6	181 ±14	179±1
+100	190±13	198±1	202±8	202±16	202±1
Voltage (mV)	**ClyA−R E11S**	**ClyA−R−D122R**	**ClyA−R−E129R**	**ClyA−R−D56R-Q8K**	
-100	-165±19	-99.8±2.1	-161±24	-150±15	
-90	-150±17	-93.8±2.1	-145±23	-135±14	
-80	-136±15	-87.3±1.8	-130±20	-123±13	
-70	-120±13	-78.8±2.6	-114±18	-110±11	
-60	-105±11	-70.7±2.2	-98.3±15.1	-94.9±10.8	
-50	-88.7±9.3	-62.5±1.3	-81.2±11	-81±9	
-40	-71.9±7.3	-52.3±0.9	-65.4±8.9	-65.3±7.9	
-30	-54.6±5.3	-41.1±0.5	-49.2±6.5	-49.9±6.4	
-20	-36.9±3.6	-28.6±0.4	-32.9±4.4	-33±5	
-10	-18.6±1.8	-14.9±0.2	-16.6±2.4	-16.5±2.5	
0	0	0	0	0	
+10	19±2	16±0	16.8±2.5	17.9±2.3	
+20	38.4±3.4	33.3±0.5	33.8±5.1	35.4±5.6	
+30	58±5	51.6±0.5	50.7±7.6	54±9	
+40	77.7±6.9	71.1±0.8	67.6±10.2	72.5±12.5	
+50	97.8±8.2	91.6±0.8	84.6±12.6	91.7±15.9	
+60	119±10	113±1	101±15	114±17	
+70	140±11	135±1	118±18	133±20	
+80	159 ±13	158±2	136±20	154±23	
+90	181 ±15	182±2	153±23	182±20	
+100	201±13	207±2	171±26	207±20	

Table 4-S4 Continued

Voltage (mV)	ClyA-RR-E7S	ClyA-RR-E11S	ClyA-RR-D21S	ClyA-RR-D21K	ClyA-RR-D32N
-100	-111±4	-128±11	-113±9	-120±1	-108±1
-90	-103±3	-119±10	-106±8	-109±0	-101±1
-80	-95.4±3.4	-109±9	-96.6±7.9	-99.1±0.3	-93.2±0.9
-70	-87±3	-98.9±8.2	-87.6±6.5	-88.1±0.1	-84.7±0.7
-60	-77.3±2.8	-87.9±7.5	-77.9±5.4	-76.6±0.2	-75.5±0.6
-50	-66.3±2.2	-75.5±6.2	-67.1±4.5	-65±0	-65.2±0.5
-40	-54.7±1.9	-62.5±5.2	-55.2±3.8	-53.2±0.1	-54.2±0.5
-30	-42.3±1.4	-48.3±4	-42.3±3.3	-40.5±0.1	-42.1±0.4
-20	-28.9±1	-33.2±2.8	-29±2	-27.5±0	-29±0
-10	-15±0	-17±1	-15.1±0.9	-13.9±0	-15±0
0	0	0	0	0	0
+10	15±1	18±1	16±1	14.3±0	15.6±0.6
+20	31.2±2.4	36.8±3.1	32.5±2.2	29.2±0	32.2±1.3
+30	49.1±2	56.3±4.6	50.1±3.1	44.3±0.1	49.6±2.1
+40	66.2±3.7	76.8±6.6	67.2±5.1	60±0	67.9±2.8
+50	85.7±3.3	98±8	87.3±5.5	75.6±0.5	87±4
+60	105±4	120±11	107±6	92.2±0.1	107±5
+70	125±4	142±13	127±7	109±0	127±5
+80	145±5	165±15	148±8	125±0	149±6
+90	166±5	189±17	170±9	142±0	171±7
+100	188±6	214±19	193±11	160±0	198±4
Voltage (mV)	**ClyA-RR-E7S –D21S**	**ClyA-RR-E7S- D32N**	**ClyA-RR-1R (ClyA-3R)**	**ClyA-3R-E7S**	**ClyA-3R-D21S**
-100	-120±4	-104±6	-112±9	-109±3	-108±5
-90	-109±1	-96.9±5.6	-103±12	-101±2	-101±4
-80	-99.9±2.1	-89.2±4.7	-93.5±11.8	-93.2±2.9	-93.1±4
-70	-88.6±1	-80.9±4.2	-86±10	-84.8±1.1	-83.4±2
-60	-80.4±1.7	-71.9±3.5	-77.6±8.2	-74.3±0.9	-73.2±1.3
-50	-67.4±2.7	-62±3	-65.9±7.1	-63.7±1	-63.3±1
-40	-56.2±2	-51.4±2.3	-54.6±5.6	-52.8±1	-52.3±0.8
-30	-43.4±1.1	-39.8±1.7	-42.5±3.6	-40.6±1	-40.6±0.6
-20	-28.9±1.6	-27.4±1.2	-30±3	-28.1±0.5	-28±0
-10	-13.5±1	-14.2±0.5	-14.9±1.7	-14.3±0.3	-14.4±0.2
0	0	0	0	0	0
+10	16.4±2.4	15±0	16.1±0.8	15.1±0.5	15.3±0.3
+20	32.2±1.4	30.7±1	32.4±2.1	30.9±1.1	31.5±1.1
+30	50.3±2.1	47.4±1.5	50±2	47.5±1.5	48.3±1.8
+40	68±2	64.7±1.9	68.7±2.7	64.5±2	65.8±2.4
+50	85.8±1.1	82.7±2.4	88±3	81.7±2.5	83.7±3.3
+60	103±1	101±3	106±5	99.5±2.9	102±4
+70	122±4	121±3	126±5	118±3	121±6
+80	143±0	140±3	149±9	137±4	140±6
+90	163±2	160±3	170±5	156±4	160±7
+100	184±0	182±4	191±11	176±5	179±9

The electrical recordings were carried out in 0.15 M NaCl, 15 mM Tri-HCl, pH 7.5, at 22 °C. Each data point is the average of at least three experiments and the error is the standard deviation

Table 4-S5 IV curves of ClyA variants under asymmetric salt concentrations.

IV	ClyA Ionic permeability Open pore current, pA (average ± standard deviation)		
Voltage (mV)	ClyA-AS	ClyA−R	ClyA−RR
20	26.5±0.7	36.7±14.1	32.4±4.3
19	23.1±0.9	32.5±13	28.6±2.7
18	19.8±0.5	27.6±12.8	25.2±2.5
17	16.6±0.9	23.4±10.8	21.3±1.8
16	13.6±1.8	17.9±10.7	16.6±1.2
15	9.9±1.9	14.4±9.7	12.8±1.9
14	7.2±1.2	7.8±9.3	10.2±1.2
13	4.4±1.1	2.9±8.9	7.2±1.4
12	2.5±1.4	-1.7±9.4	1.8±1.3
11	-0.7±2.5	-5.6±8.6	-0.8±1.9
10	-3.8±2.7	-12.7±7.3	-4±1
9	-7.3±2.7	-15.6±8	-9.3±3.1
8	-10.7±1.5	-22.3±6.3	-11.9±0.5
7	-13.4±4.3	-24.5±5.9	-15.5±2.6
6	-16.2±0.9	-31.2±5.8	-19.8±3.2
5	-18±2	-35.2±4.5	-23.1±3.1
4	-22.3±2.5	-40.4±5.2	-25.7±1.7
3	-25±2	-43.7±3.5	-30.1±2.9
2	-27.8±3.1	-51.2±4.1	-33.8±4.5
1	-30.5±3.1	-55.6±2.1	-36.9±4.8
0	-34.9±2.7	-60.7±2	-40.7±5
-1	-37.1±3.5	-65.1±2.6	-44.4±3.8
-2	-41±3	-68.8±3.8	-48.2±4.2
-3	-42.1±3.9	-74.8±3.6	-51.3±6.5
-4	-46.2±4.2	-79.8±2.1	-54.8±7.9
-5	-48.8±4.2	-85.2±2.5	-57.8±6.5
-6	-51.5±3.5	-90±3	-61.2±7.8
-7	-55.1±6.3	-94±4	-66.2±7.3
-8	-57.8±5.5	-100±3	-68.6±10.7
-9	-61±4	-103±3	-73.1±8.3
-10	-62.8±4.9	-109±4	-76.5±7.9
-11	-66.2±5	-114±4	-80.1±9.1
-12	-69.7±6	-117±4	-83.6±9.9
-13	-74.7±5.5	-123±4	-86.6±8.7
-14	-74.8±6.1	-129±5	-91.1±11.2
-15	-78.3±5.7	-134±7	-93.5±10.7
-16	-80.2±6.2	-137±8	-96.7±9.7
-17	-84.2±6.4	-144±7	-100±13
-18	-87.6±7.6	-148±8	-104±12
-19	-90.4±7.7	-153±8	-108±12
-20	-92.4±7.3	-158±8	-112±11

Four or more single channels were measured for each variant. Each data point is the average of at least three experiments and the error is the standard deviation. The buffer used was 15 mM TRIS.HCl pH 7.5, while the *cis* chamber contained 1 M NaCl and the *trans* chamber 150 mM. The electrical recordings were carried out in 15mM Tris HCl, pH 7.5 at 22 °C. Data were recorded by applying a 2-kHz low-pass Bessel filter and using a 100 μs (10 kHz) sampling rate.

(← See previous table)

Table 4-S6 DNA analysis with ClyA-RR nanopores.

ssDNA (1a)			
[NaCl] (M)	I_{RES}	τ_{off} (ms)	τ_{on} (ms)
0.15	0.92±0.00	0.54±0.28	8.5±1.1
0.3	0.89±0.01	0.18±0.04	44±1
0.5	0.88±0.02	0.12±0.02	112±14
1	0.82±0.01	0.13±0.01	232±36
2	0.84±0.01	0.12±0.02	393±17
2.5	0.78±0.01	0.18±0.02	500±50
dsDNA (1)			
[NaCl] (M)	I_{RES}	τ_{off} (ms)	τ_{on} (ms)
0.15	0.92±0.00	0.29±0.07	40±13
0.6	0.83±0.03	0.26±0.09	162±31
1	0.76±0.01	0.26±0.09	214±18
2	0.75±0.04	0.33±0.07	532±52
2.5	0.75±0.01	0.60±0.48	641±37
NA:ssDNA (1a)			
[NaCl] (M)	I_{RES}	τ_{off} (ms)	τ_{on} (ms)
0.15	0.84±0.02	-	-
0.3	0.82±0.01	-	-
0.5	0.83±0.00	-	-
1	0.83±0.01	0.14±0.03	450±41
2	0.80±0.02	0.15±0.01	593±204
2.5	0.80±0.02	0.16±0.03	929±306
NA:dsDNA (1*)			
[NaCl] (M)	I_{RES}	τ_{off} (ms)	τ_{on} (ms)
0.15	0.86±0.01	-	-
0.3	0.82±0.01	-	-
0.5	0.77±0.02	-	-
1	0.71±0.00	-	-
2	0.69±0.02	-	-
2.5	0.68±0.01	-	-

(-) indicates a NA:DNA permanent capture event. Each data point is the average of at least three experiments and the error is the standard deviation

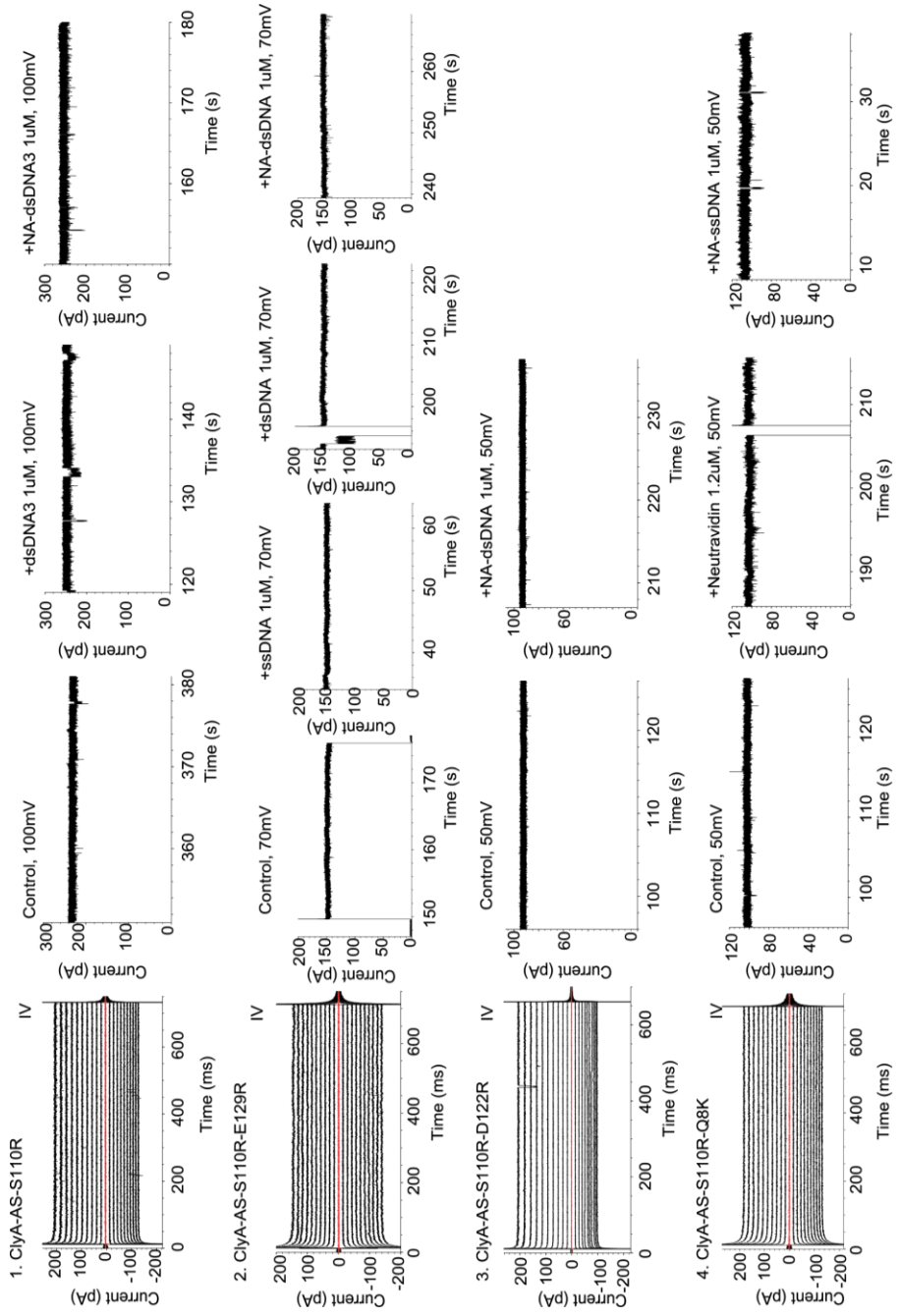
1. ClyA-AS-S110R
IV
Current (pA)
Time (ms)
Control, 100mV
+dsDNA3 1uM, 100mV
+NA-dsDNA3 1uM, 100mV
2. ClyA-AS-S110R-E129R
Control, 70mV
+ssDNA 1uM, 70mV
+dsDNA 1uM, 70mV
+NA-dsDNA 1uM, 70mV
3. ClyA-AS-S110R-D122R
Control, 50mV
+NA-dsDNA 1uM, 50mV
4. ClyA-AS-S110R-Q8K
+Neutravidin 1.2uM, 50mV
+NA-ssDNA 1uM, 50mV
Time (s)

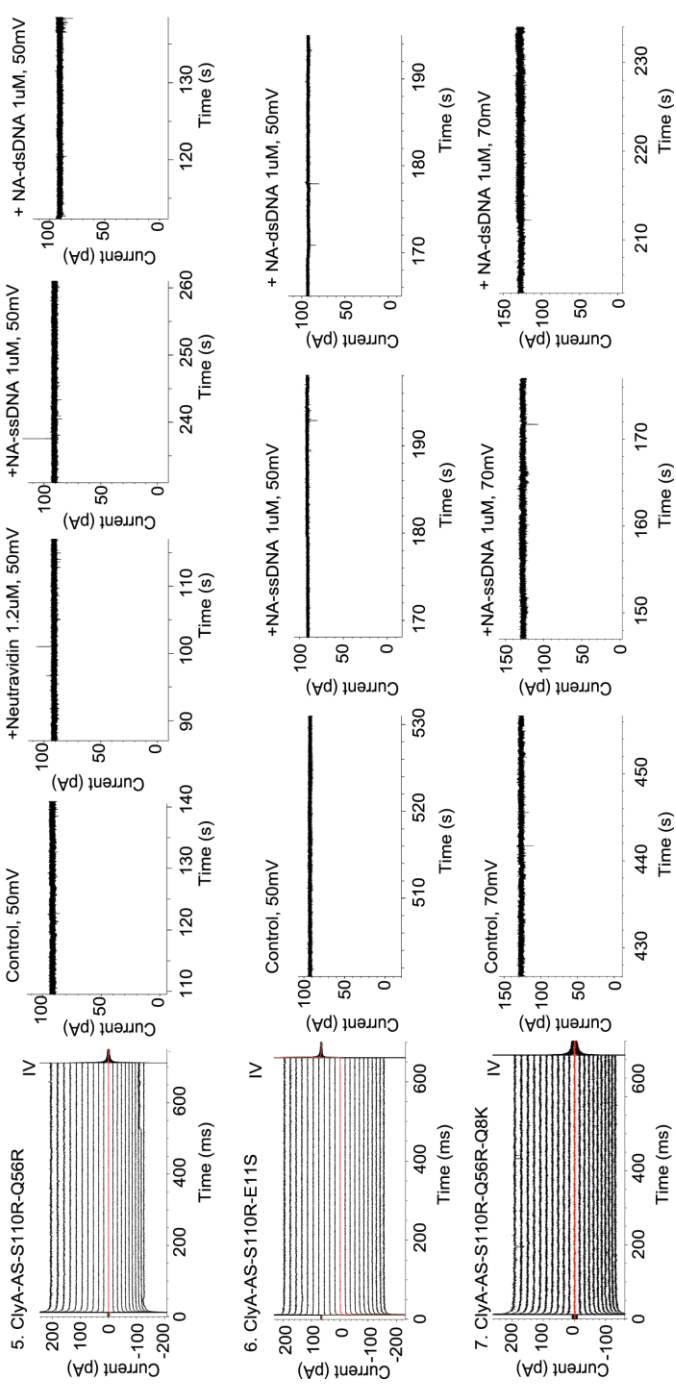

Figure 4-S1 *Cis* DNA translocation through ClyA variants.
DNA translocation from the *cis* side of ClyA nanopores in 0.15 M NaCl solutions. For each mutant it is reported: the IV relationship (voltage ramp from +100 to -100 mV in 21 s and 10 mV voltage steps) and a representative current trace under positive V_G applied potential before and after adding 1 µM of a biotinylated ssDNA (1a, Table 4-S1) to the *cis* compartment. A variety of current traces is also shown after the subsequent addition of 1.2 µM neutravidin (monomer) and 1 µM of the complementary ssDNA (1b, Table 4-S1) to the *cis* solution. The electrical recordings were carried out in 0.15 M NaCl, 15 mM Tris-HCl. pH 7.5 at 22 °C. Data were recorded by applying 2-kHz low-pass Bessel filter and using a 100 µs (10 kHz) sampling rate.

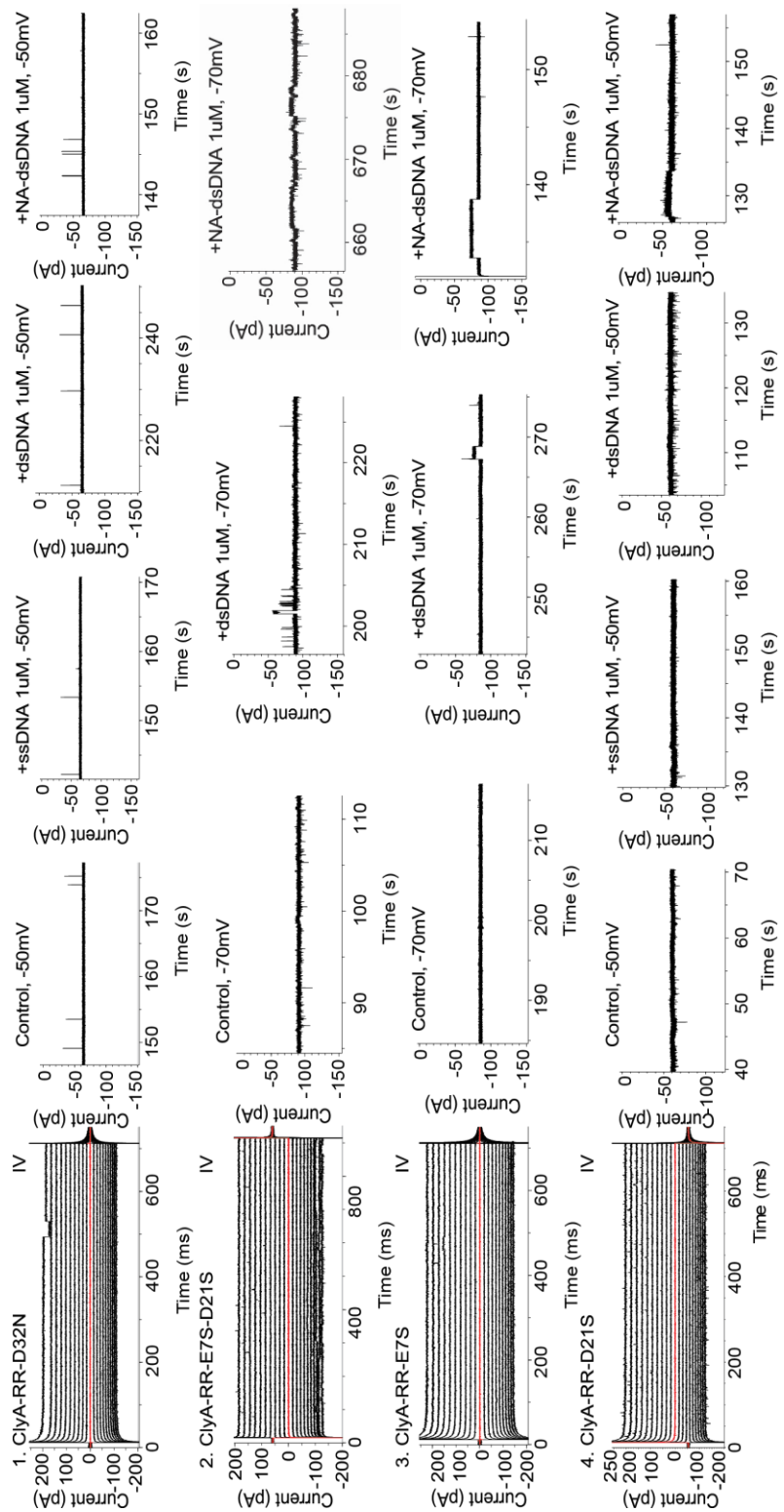

Figure 4-S2 Part 1

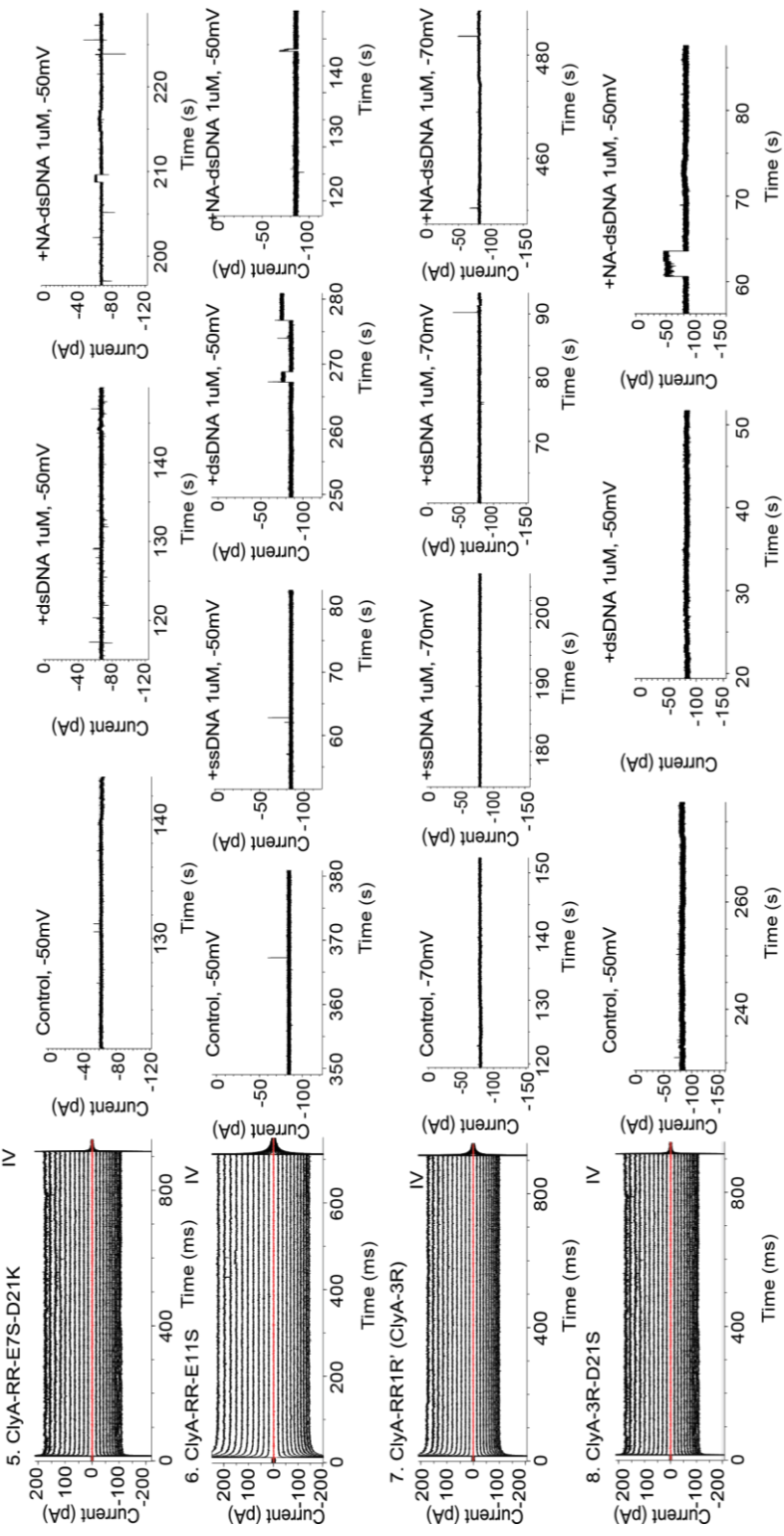
5. ClyA-RR-E7S-D21K
6. ClyA-RR-E11S
7. ClyA-RR1R' (ClyA-3R)
8. ClyA-3R-D21S
IV
Time (ms)
Current (pA)
Control, -50mV
Control, -70mV
+dsDNA 1uM, -50mV
+dsDNA 1uM, -70mV
+ssDNA 1uM, -50mV
+ssDNA 1uM, -70mV
+NA-dsDNA 1uM, -50mV
+NA-dsDNA 1uM, -70mV
Time (s)

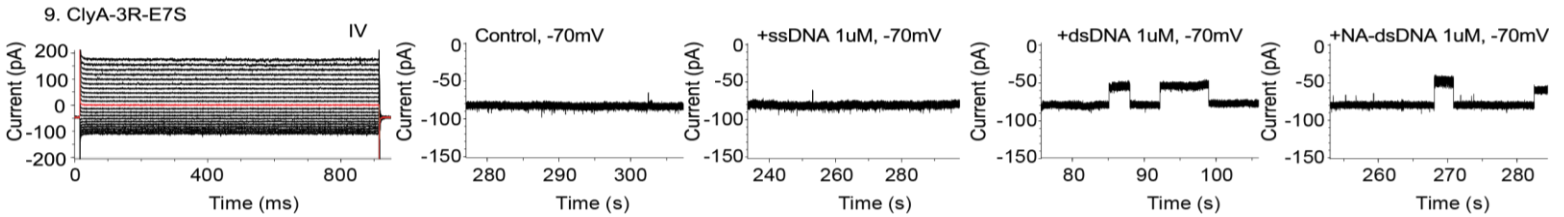

Figure 4-S2 *Trans* DNA translocation through ClyA variants.

DNA translocation initiated from the ClyA mutants *trans* side in 0.15 M NaCl solutions. For each mutant it is reported: the IV relationship (voltage ramp from +100 to -100 mV in 21 s and 10 mV voltage steps) and a representative current trace under negative V_G applied potential before and after adding 1 μM of a biotinylated ssDNA (1a, Table 4-S1) to the *trans* compartment. A variety of current traces is also shown after the subsequent addition of 1.2 μM neutravidin (monomer) and 1 μM of the complementary ssDNA (1b, Table 4-S1) to the *trans* solution. The electrical recordings were carried out in 0.15 M NaCl, 15 mM Tris-HCl. pH 7.5 at 22 °C. Data were recorded by applying a 2-kHz low-pass Bessel filter and using a 100 μs (10 kHz) sampling rate.

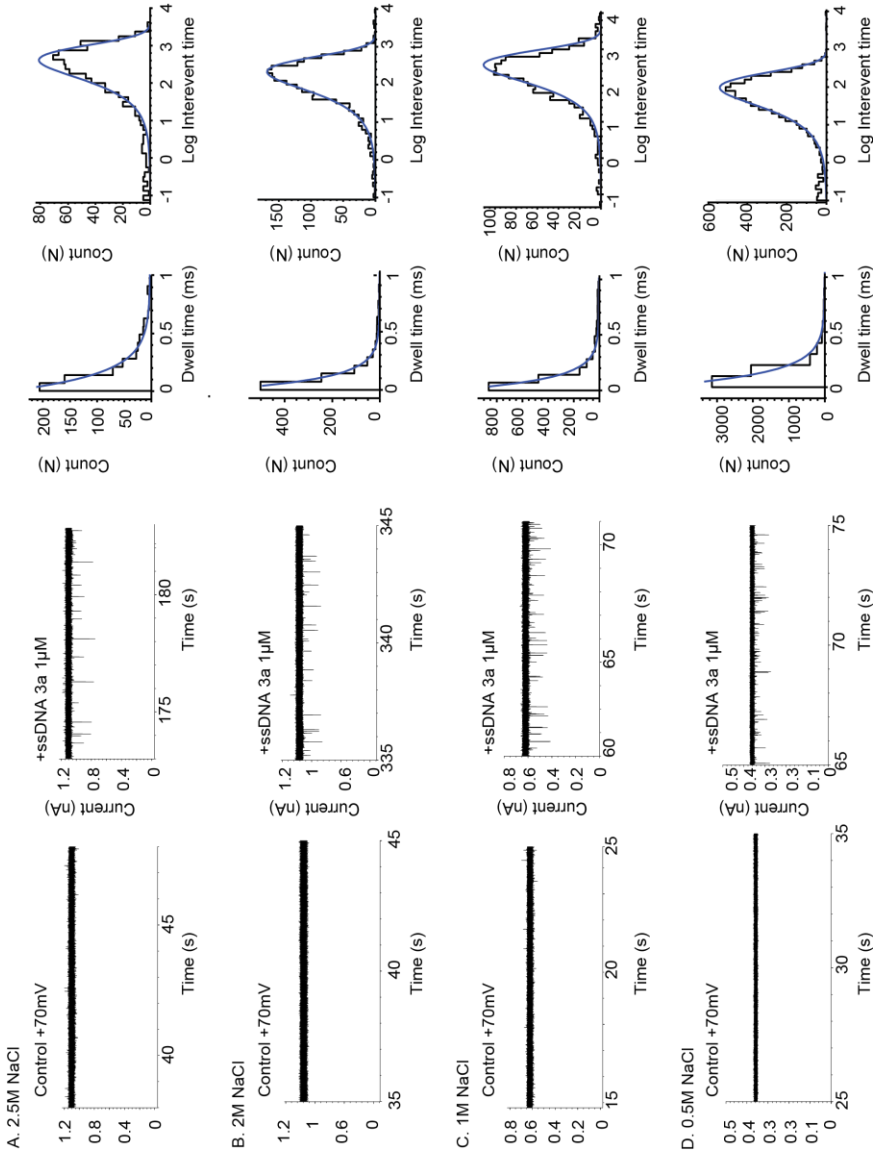
A. 2.5M NaCl
Control +70mV
+ssDNA 3a 1µM
Current (nA)
Time (s)
Count (N)
Dwell time (ms)
Log Interevent time
B. 2M NaCl
C. 1M NaCl
D. 0.5M NaCl

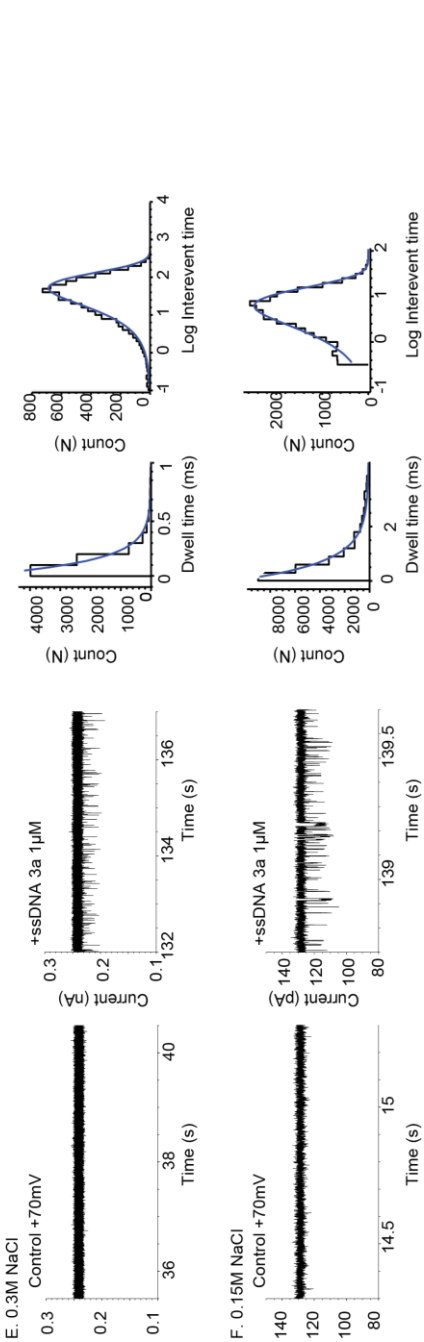

Figure 4-S3 Ionic strength dependency of ssDNA translocation through ClyA-RR nanopores.
(Left side) Representative current trace showing the open pore current of ClyA-RR nanopores before and after adding 1 µM of a biotinylated ssDNA (1a, Table 4-S1) to the *cis* side of the pore under + 70 mV at different NaCl concentrations. The histograms on the right side represent the dwell times (t_{OFF}, left histogram) and inter-event time (t_{ON}, right histogram) of individual ssDNA translocation events. Individual t_{OFF} and inter-event time t_{ON} events were collected individually by using the "single channel search" function in the Clampfit Software (Molecular devices) using a data acquisition threshold of 0.05 ms. The average DNA translocation dwell times τ_{OFF} were calculated from single exponential fits from cumulative histograms. The inter-event times τ_{ON} were calculated from exponential logarithmic probability fitting from histograms using logarithmic bins (base 10). The electrical recordings were carried out in 15 mM Tris-HCl. pH 7.5 at 22 °C. Data were recorded by applying a 10-kHz low-pass Bessel filter and using a 20 µs (50 kHz) sampling rate. An additional 2-kHz low-pass Bessel filter was used for the data collected at 0.15 M NaCl solutions.

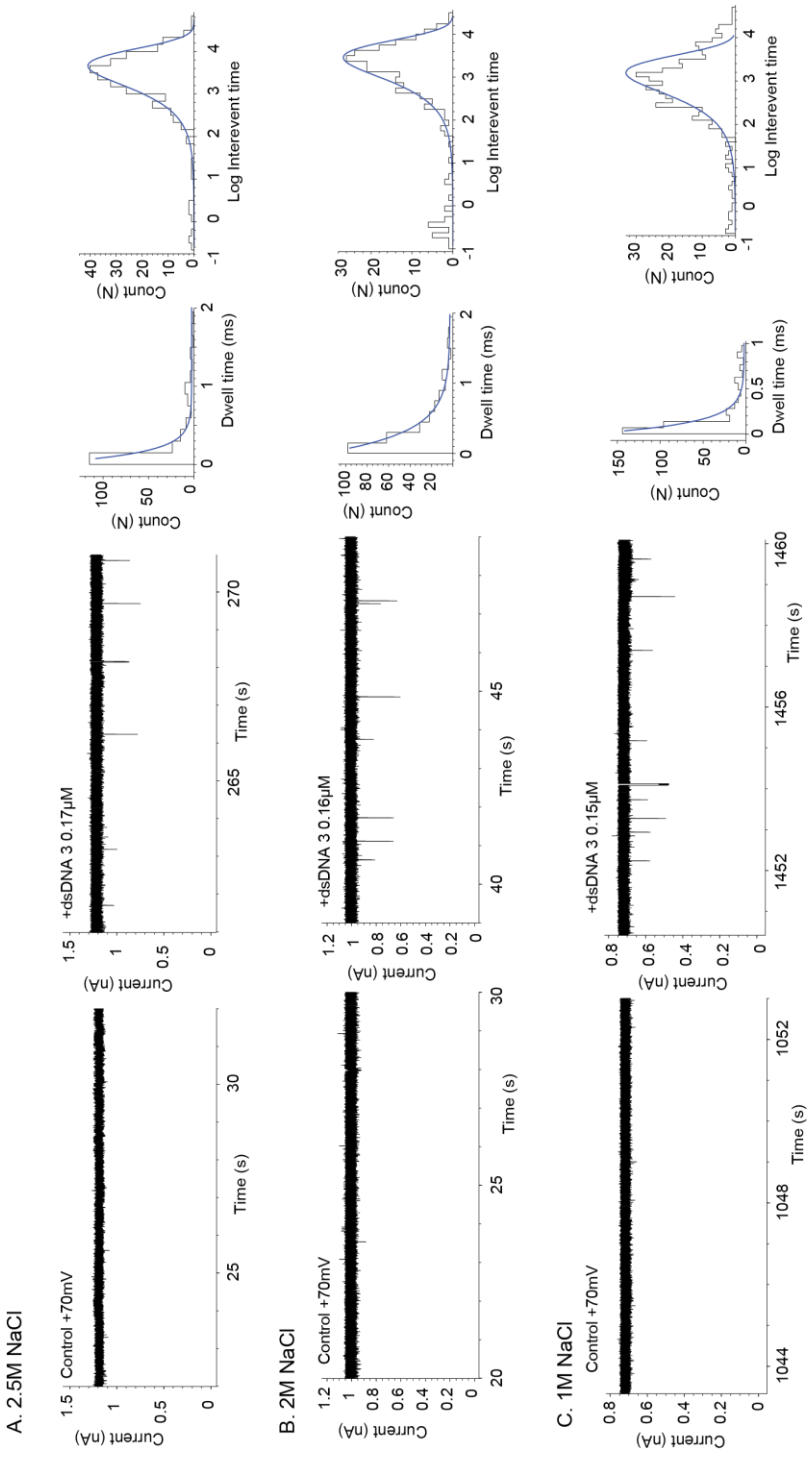
A. 2.5M NaCl
Control +70mV
Current (nA)
Time (s)
+dsDNA 3 0.17µM
Count (N)
Dwell time (ms)
Log Interevent time
B. 2M NaCl
Control +70mV
+dsDNA 3 0.16µM
C. 1M NaCl
Control +70mV
+dsDNA 3 0.15µM

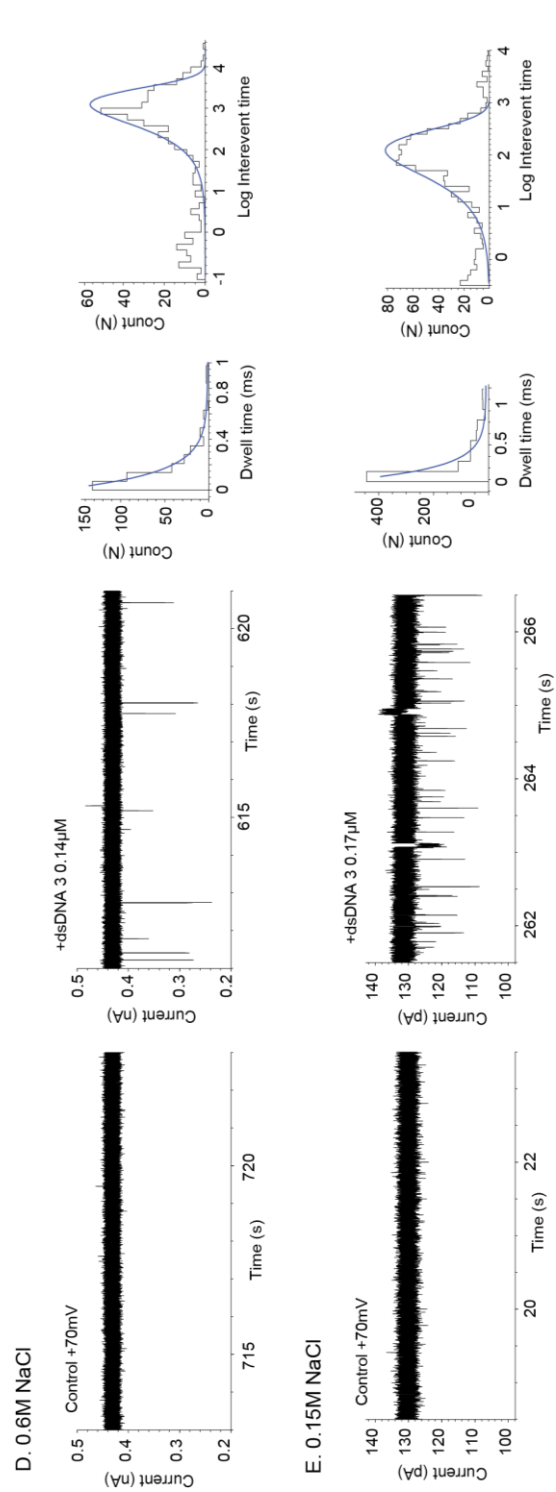

Figure 4-S4 Ionic strength dependency of dsDNA translocation through ClyA-RR nanopores.
The current traces show the open pore current of ClyA-RR nanopores before (left) and after (right) the addition of 170 nM dsDNA (1, Table 4-S1) added to the *cis* side of the pore under + 70 mV and at indicated NaCl concentrations. The histograms on the right side represent the dwell times (t_{OFF}, left histogram) and inter-event time (t_{ON}, right histogram) of individual ssDNA translocation events. Individual t_{OFF} and inter-event time t_{ON} events were collected individually by using the "single channel search" function in the Clampfit Software (Molecular devices) using a data acquisition threshold of 0.05 ms. The average DNA translocation dwell times τ_{OFF} were calculated from single exponential fits from cumulative histograms. The inter-event times τ_{ON} were calculated from exponential logarithmic probability fitting from histograms using logarithmic bins (base 10). The electrical recordings were carried out in 15 mM Tris-HCl. pH 7.5 at 22 °C. Data were recorded by applying a 10-kHz low-pass Bessel filter and using a 20 µs (50 kHz) sampling rate. An additional 2-kHz low-pass Bessel filter was used for the data collected at 0.15 M NaCl solutions.

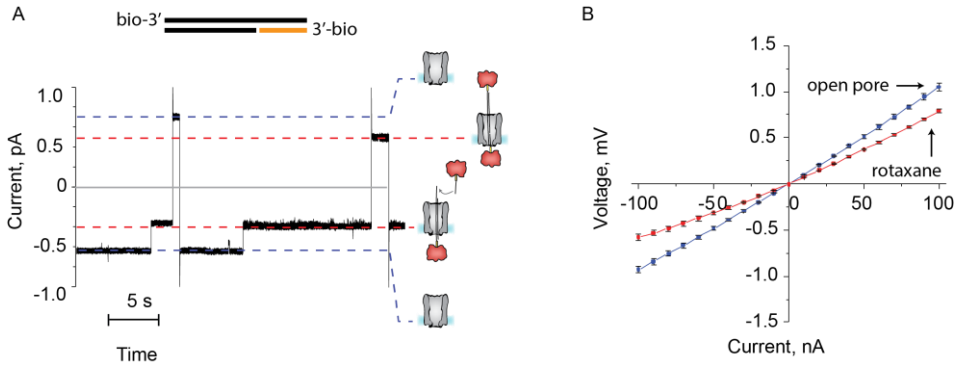

Figure 4-S5 Formation of a DNA rotaxane initiated from the ClyA-RR pore *trans* side at 1 M NaCl.

A dsDNA rotaxane was formed under -70mV applied potential by adding a hybrid dsDNA/ssDNA thread (1a and 1c, 1.0 µM, Table 4-S1, shown as a black line above the current trace) complexed with neutravidin (1.2 µM, monomer) to the *trans* nanopore compartment. A 3' biotinylated ssDNA molecule, 1d (1.0 µM, Table 4-S1, corresponding to the orange line above the current trace) complementary to the overhang of 1a:1c was added to the *cis* compartment. Since the nanopore/ DNA rotaxane can only formed if 1a:1c translocates through the nanopore to hybridize with 1d, this experiments proves the translocation of DNA through ClyA from *trans* to *cis.* At -70 mV the blocked pore current of the threaded DNA was 64 ± 2.0, average ± s.d., n = 3. After rotaxane formation, the reversal of the applied potential to +70 mV showed a blocked pore current (I_{RES+70} = 73 ± 0.5, average ± s.d., n=3), indicating that dsDNA occupied the nanopore. **B** IV current/ voltage relationship for ClyA-RR (blue line) and ClyA-RR in a rotaxane configuration (red line).

Chapter 5

Conclusions and future perspectives

Conclusions

In the present work we employed the membrane nanopore Cytolysin A (ClyA) from *Salmonella enterica* serovar Typhi, to study the electrophoretic translocation of nucleic acids through the nanopore. The internal diameter of ClyA[1] is larger than the diameter of single or double-stranded DNA molecules[2,3], indicating that DNA should readily translocate through the pore when driven by an electrical potential[1]. However, we found that DNA translocation is hampered at low ionic strengths, due to the many negatively charged residues lining inside the pore lumen. We observed that DNA molecules could thread through the pore only at high salt concentration (2.5 M NaCl, Figure 3-2, page 72), where the pore internal negative charges were screened by the counterions from the concentrated electrolyte buffer solution. At this condition, we found a different result for the capture of ssDNA and dsDNA molecules inside the ClyA pore (Figure 3-5, page 79). While dsDNA molecules (complexed with neutravidin throughout a biotin linkage) could be permanently immobilized inside the pore under constant applied potential, ssDNA showed only transient capture events. ssDNA molecules could enter the pore but only transiently, they were entropically constrained to promptly exit the pore inner lumen (Figure 3-5, page 79). This different behavior between ssDNA and dsDNA molecules could be most likely associated with the different polymer conformation of ssDNA molecules at high salt concentrations, where the molecules undergo a coiled-conformation[4–9]. We thought to use this finding as an advantage to build a membrane-embedded DNA transporter that was able to selectively shuttle DNA molecules across a phospholipid membrane. ClyA nanopores were engineered with ssDNA molecules chemically attached at the pore *cis* entrance (Figure 3-6, page 82) As observed, at fixed applied potential the ssDNA molecules attached to ClyA *cis* entry did not enter the pore permanently (Figure 3- 4, page 76) but when they hybridized with a complementary ssDNA molecule added in solution, the following DNA duplex formation promoted a permanent capture inside the pore. The DNA duplex was translocated through the nanopore to the opposite compartment of the lipid membrane, where it was released by a strand-

displacement reaction (Figure 3-6, page 82). Then the ssDNA attached to the ClyA moved back to the *cis* compartment through the nanopore against the applied potential and start a new transportation cycle. Notably, the ssDNA covalently attached atop the nanopore produced a steric and / or electrostatic impediment that prevented or drastically reduced the translocation of dsDNA and also non-specific ssDNA added in solution (Figure 3-6, page 82). This molecular machine worked at constant transmembrane potential without external intervention and it was modulated by two single-stranded DNA molecules: one attached to the pore *cis* entry that promoted the capture of DNA and the other in the *trans* solution that promoted the release of the captured DNA cargo functioning as 'fuel' (Figure 3-6, page 82).

In the future, this nanopore-based DNA transporter might be further developed to identify, purify, separate or concentrate nucleic acids for laboratory applications[10]. An array of engineered ClyA pores could be inserted into a platform as the GridION or MinION system from Oxford Nanopore Technologies and be used for high-throughput DNA analyses[11]. Moreover the transport of genetic information across biological membranes is also a very attractive application[12], that could have important implications in gene therapy[12]. However, at the present there are some important limitations such as the inverse cell polarization or the low ionic strength in the cellular fluids[13]. The negatively charged intracellular environment hampers DNA entry from the outside, due to the negative charge nature of DNA molecules. A possible solution could be the use of artificial polymers like peptide nucleic acids (PNA) to carry decoding information instead of DNA[14]. PNA oligos are not negatively charged and should be a suitable alternative to DNA[14], although their synthesis cost is at the moment more expensive than DNA. Regarding the physiological low ionic strength of the cellular environment[13], the transport of DNA molecules at low salt concentrations is important for future applications of nanopores into biological systems. Although most of biological nanopores show numerous negatively charged residues in the pore inner lumen, that limit the passage of DNA molecules at physiological salt concentration. In particular

biological nanopores can be engineered to overcome this limitation. One of the most important advantages of biological nanopores is that their structure can be controllably modified by single residue modifications, targeted to favor the transport of nucleic acids through the nanopores at low-salt concentrations.

In the second part of this work we engineered the ClyA nanopore by rearranging the inner pore charge distribution to allow DNA translocation through the pore at physiological salt concentration. The numerous negatively charged residues coating the ClyA lumen prevent DNA translocation at low ionic strengths. Encouraged by the successful results obtained in previous works with the αHL[15] and MspA[16], we introduced positively charged residues or/ and removed negatively charged residues in the pore inner lumen to favor DNA interactions with the ClyA pore. Residue substitutions were probed from the pore *cis* entrance to the *trans* transmembrane side (Figure 4-1 page 109). We found that the number and the exact distribution of charges in the nanopore lumen was crucial for observing DNA translocation events. The most challenging part of this project was to find residues in the pore lumen, which substitution did not compromise the ClyA pore favorable proprieties in planar lipid bilayer recording. Although, most of the introduced mutations reduced pore high-applied voltage stability by increasing pore gating or limiting pore insertion into the lipid membrane (Table 4-1, page 110). We found that an engineered ClyA pore (ClyA-RR), presenting two arginine rings, one at the top *cis* entrance and one at the mid-section pore, could translocate both single and double-stranded DNA molecules at low ionic strengths (0.15- 0.5 M NaCl, Figure 4- 1, page 109).

In addition, we tested the translocation of both ssDNA and dsDNA molecules in a broad range of salt concentration (0.15 - 2.5 M NaCl). We found that the frequency of DNA translocation decreased with the ionic strength of the solution, confirming that the electrostatic interactions between DNA and the nanopore are important to observe the entry of DNA through the nanopore (Figure 4-3, page 115). We used the Debye length of the solution as a measure of the net electrostatic effect of the

pore inner charges on the entry of DNA molecules into ClyA pores. The Debye length (K^{-1}, expressed in nm) refers to the maximum distance at which a charged particle (*e.g.* DNA) will be still influenced by the electric field of another charged particle (*e.g.* pore inner charges) at the molar concentration of the electrolyte solution (see page 113). The frequency of dsDNA translocation showed a linear dependence with the Debye length of the solution, thus the frequency of ssDNA translocation decreased exponentially rather than linearly with the Debye length of the solution (Figure 4-3A, page 115). Indeed the persistence length of ssDNA, which gives a measure of the stiffness of the ssDNA molecule, decreases strongly with increasing the ionic strength of the solution[4–9]. Therefore, ssDNA molecules might adopt a coiled-conformation at high ionic strengths (≥ 0.5 M NaCl), which further reduces ssDNA capturing frequency by preventing one of the polymer end to thread through the pore. Further, at 0.5 M NaCl or lower, ssDNA molecules in complex with neutravidin could be immobilized permanently under constant-applied potential inside the pore, while at 1 M NaCl or higher, the capture was only transient. Also, at ionic strengths ≥ 1M the I_{RES} measured for free ssDNA or complexed with neutravidin was similar and was not dependent on the ionic strength of the solution (Figure 4- 3, page 115). These results indicate that at high ionic strengths the ssDNA coiled-confirmation might limit not only the frequency rate of translocation events but also the entry of the molecules inside the nanopore.

In another implementation we studied DNA translocation from the *trans* to the *cis* side of the ClyA-RR pore: DNA trans-translocation. Surprisingly, DNA translocation events were not observed when DNA was added to the ClyA-RR pore *trans* side at low salt concentrations. The many negatively charged residues at the ClyA- RR pore *trans* entrance might prevent the entry of DNA molecules from this side of the pore. Supporting this assumption, by increasing the ionic strength of the solution (≥ 1M NaCl), trans-translocation events were observed and dsDNA translocation was probed by a *trans* dsDNA/ protein rotaxane formation at 1 M NaCl (Figure 4-S5, page 152).

In the attempt to induce the entry of DNA molecules from the *trans* entry at low ionic strengths (≤ 1 M NaCl), we introduced an additional arginine ring at the N- terminal end of the ClyA-RR construct (ClyA-3R) combined with the substitution of negatively charged residues at position 7 (ClyA- 3R- E7S, 1 set of negatively charged residues knocked out). Despite DNA added to the *trans* entry of ClyA- 3R- E7S nanopores showed transient current blockades, a *trans* DNA/ neutravidin rotaxane could not be formed. Additional nanopore engineering could be exploited to induce DNA trans-translocation. This could be advantageous during analyses, because ClyA pores showed high-voltage stability at the *trans* pore side (fewer gating events, $V_{G-} > V_{G+}$, Table 4-S3). Apply high-voltages during analyses can favor DNA capture frequency[17] and could allow the detection of long DNA molecules (few kilo bases length), which might need high-applied voltage for their translocation through small nanopores[17–19].

In summary, in this research work we demonstrated single molecule detection of both single and double-stranded DNA with the biological nanopore ClyA at physiological salt concentration. DNA translocation at low ionic strengths is advantageous for the investigation with biological nanopores of biomarkers or other biological systems that can bind and process DNA molecules only at low ionic strengths[20–22]. Throughout our work we extensively engineered the ClyA pore to favor DNA translocation, which was limited by the numerous negatively charged residues in the pore inner cavity. We found that the number and the exact distribution of charges in the nanopore lumen was crucial for observing the passage of DNA molecules through the pore. The results obtained helped to understand the electrostatic and entropic barriers that regulate the transport of DNA molecules through the biological nanopore ClyA and can be useful for the future design of new applications for nucleic acid analyses with nanopore-based biosensors.

Future Perspectives

For the future continuation of this research ClyA pore could be further engineered to reduce the residual inner pore electrostatic repulsions, which are still limiting DNA translocation through the pore (*e.g.* from the *trans* pore side). At the same time, reducing electrostatic repulsions could be advantageous not only for DNA translocation but also for precise single DNA molecule detection. Reducing charge repulsions by single residue substitutions might stabilize a captured DNA molecule inside the pore. When DNA is captured inside the pore electrostatic repulsions might constrain the DNA molecule to continuously move, compromising the precise ionic current reading. This effect is even more accentuated at low ionic strengths, where all the residual inner pore charges are unscreened. We expect that removing negative charges or introducing additional positive charges in the pore cavity might improve both sensing and detection of DNA molecules.

Another important challenge could be the investigation of the ability for ClyA pores to discriminate between different DNA molecules. The precise identification of DNA molecules based on their base composition or modifications, length, structure and sequence could have useful applications[10]. On this direction, it would be interesting for the continuation of this work to introduce new modifications aimed to improve the ionic current resolution for DNA detection analyses with ClyA pores. Many encouraging results show that a recognition region can be engineered or better developed inside a biological nanopore. As for the alpha haemolysin pore, the introduction of charged cyclodextrins as molecular adapters to the pore inner constriction provided detection among freely translocating nucleotides[21]. Moreover, also less invasive modifications to the pore as residue side-chain substitutions showed improved nucleo-bases discrimination with the αHL pore[25]. This could be maybe a better approach, considering that in this work nanopore engineering with ClyA pores proved to be not that well tolerated, though most of the constructed mutants showed low-applied voltage stability (Table 4-1, page 110).

In addition, ClyA nanopores could be used for the investigation of drugs or biological markers, which can specifically bind to DNA molecules at low ionic strengths[25]. The inner pore cavity is large enough to host small peptides or chemical compounds, which can be precisely identified[20] and further, their association with specific DNA sequences could be exploited for drawing genomic maps useful for the identification of physiological disorders, denovo and viral genome profiling[26].

Moreover, the ionic current resolution for small nanopores is highly affected from the concentration of ions in solution[10,24,27,28]. ClyA large inner pore size, on the other hand allows a consistent ionic flow, which is still preserved at low ionic strengths. This might be advantageous for analyses with biological systems that only perform at near physiological salt concentrations. For example ClyA pores could be integrated into high-throughput DNA analysis systems as the GridION or MinION (Oxford Nanopore Technologies), where during analysis DNA samples are processed by enzymes at low-salt concentration[11,21,22,29].

5.1 References

1. Ludwig, A., Bauer, S., Benz, R., Bergmann, B., Goebel, W., Analysis of the SlyA-controlled expression, subcellular localization and pore-forming activity of a 34 kDa haemolysin (ClyA) from Escherichia coli K-12. *Mol Microbiol.* 31(2): 557-567 (1999).

2. Watson, J.D., Crick, F.H., Molecular structure of nucleic acids: a structure for deoxyribose nucleic acid. *Nature* 171(4356): 737-738 (1953).

3. Mandelkern, M., Elias, J.G., Eden, D., Crothers, D.M., The dimensions of DNA in solution. *J. Mol. Biol.* 152(1): 153–161 (1981).

4. Chi, Q., Wang, G., Jiang, J., The persistence length and length per base of single-stranded DNA obtained from fluorescence correlation spectroscopy measurements using mean field theory. *Physica A* 392(5): 1072–1079 (2013).

5. Smeets, R.M., Keyser, U.F., Krapf, D., Wu, M.Y., Dekker, N.H., Dekker, C., Salt-dependence of ion transport and DNA translocation through solid-state nanopores. *Nano Lett.* 6(1): 89–95 (2006).

6. Tinland, B., Pluen, A., Sturm, J., Weill, G., Persistence length of single-stranded DNA. *Macromolecules* 9297(97): 5763–5765 (1997).

7. Wanunu, M., Morrison, W., Rabin, Y., Grosberg, A.Y., Meller, A., Electrostatic focusing of unlabelled DNA into nanoscale pores using a salt gradient. *Nat. Nanotech.* 5(2): 160–165 (2010).

8. Murphy, M.C., Rasnik, I., Cheng, W., Lohman, T.M., Ha, T., Probing single-stranded DNA conformational flexibility using fluorescence spectroscopy. *Biophys. J.* 86(4): 2530–2537 (2004).

9. Baumann, C.G., Smith, S.B., Bloomfield, V.A., Bustamante, C., Ionic effects on the elasticity of single DNA molecules. *Proc. Natl Acad. Sci. USA* 94(12): 6185–6190 (1997).

10. Kasianowicz, J.J., Brandin, E., Branton, D., Deamer, D.W., Characterization of individual polynucleotide molecules using a membrane channel. *Proc. Natl. Acad. Sci. USA.* 93(24): 13770–13773 (1996).

11. Mikheyev, A.S., Tin, M.M., A first look at the Oxford Nanopore MinION sequencer. *Mol. Ecol. Resour.* 14(6): 1097–1102 (2014).

12. Gurnev, P., Nestorovich, E., Channel-forming bacterial toxins in biosensing and macromolecule delivery. *Toxins* 6(8): 2483-2540 (2014).

13. Lang, F., Ritter, M., Völkl, H., Haussinger, D., The biological significance of cell volume. *Ren. Physiol. Biochem.* 16(1-2): 48–65 (1993).

14. Nielsen, P.E., Peptide nucleic acid (PNA) from DNA recognition to antisense and DNA structure. *Biophys. Chem.* 68(1-3), 103–108 (1997).

15. Maglia, G., Restrepo, M.R., Mikhailova, E., Bayley, H., Enhanced translocation of single DNA molecules through alpha-hemolysin nanopores by manipulation of internal charge. *Proc. Natl. Acad. Sci. USA.* 105(50): 19720–19725 (2008).

16. Butler, T.Z., Pavlenok, M., Derrington, I.M., Niederweis, M., Gundlach, J. H., Single-molecule DNA detection with an engineered MspA protein nanopore. *Proc. Natl. Acad. Sci. USA.* 105(52): 20647–20652 (2008).

17. Meller, A., Nivon, L., Branton, D., Voltage-driven DNA translocations through a nanopore. *Phys. Rev. Lett.* 86(15): 3435–3438 (2001).

18. Deamer, D.W., Branton, D., Characterization of nucleic acids by nanopore analysis. *Acc. Chem. Res.* 35(10): 817–825 (2002).

19. Meller, A., Branton, D., Single molecule measurements of DNA transport through a nanopore. *Electrophoresis* 23(16): 2583–2591 (2002).

20. Soskine, M., Biesemans, A., Maglia, G., Single-molecule analyte recognition with ClyA nanopores equipped with internal protein adaptors. *J. Am. Chem. Soc.* 137(17): 5793–5797 (2015).

21. Cockroft, S.L., Chu, J., Amorin, M., Bayley, H., Ghadiri, M.R., A single-molecule nanopore device detects DNA polymerase activity with single-nucleotide resolution. *J. Am. Chem. Soc.* 130(3): 818–820 (2008).

22. Benner, S., Chen, R.J., Wilson, N.A., Abu-Shumays, R., Hurt, N., Lieberman, K.R., Deamer, D.W., Dunbar, W.B., Akeson, M., Sequence-specific detection of individual DNA polymerase complexes in real time using a nanopore. *Nat. Nanotechnol.* 2(11): 718–724 (2007).

23. Stoddart, D., Heron, A. J., Mikhailova, E., Maglia, G., Bayley, H., Single-nucleotide discrimination in immobilized DNA oligonucleotides with a biological nanopore. *Proc. Natl. Acad. Sci. USA.* 106(19): 7702–7707 (2009).

24. Stoddart, D., Heron, A.J., Klingelhoefer, J., Mikhailova, E., Maglia, G, Bayley, H., Nucleobase recognition in ssDNA at the central constriction of the αhemolysin pore. *Nano Lett.* 10(9): 3633–3637 (2010).

25. Spiering, A., Getfert, S., Sischka, A., Reimann, P., Anselmetti, D., Nanopore translocation dynamics of a single DNA-bound protein. *Nano Lett.* 11(7): 2978–2982 (2011).

26. Neely, R.K., Deen, J., Hofkens, J., Optical mapping of DNA: single-molecule-based methods for mapping genomes. *Biopolymers* 95(5): 298–311 (2011).

27. Maglia, G., Heron, A.J., Stoddart, D., Japrung, D., Bayley, H., Analysis of single nucleic acid molecules with protein nanopores. *Methods Enzymol.* 475: 591–623 (2010).

28. He, Y., Tsutsui, M., Scheicher, R.H., Fan, C., Taniguchi, M., Kawai, T., Mechanism of how salt-gradient-induced charges affect the translocation of DNA molecules through a nanopore. *Biophys. J.* 105(3): 776–782 (2013).

29. Ashton, P.M., Nair, S., Dallman, T., Rubino, S., Rabsch, W., Mwaigwisya, S., Wain, J., O'Grady, J., MinION nanopore sequencing identifies the position and structure of a bacterial antibiotic resistance island. *Nat. Biotechnol.* 33(3): 296–300 (2015).

FACULTY OF SCIENCE
DEPARTMENT OF CHEMISTRY
Biochemistry, Molecular and Structural Biology Section
Celestijnenlaan 200G box 2413
B-3001 HEVERLEE, BELGIUM
Lorenzo.Franceschini@chem.kuleuven.be